(1)

Stereochemistry and Reactions of Pentacoordinate Organophosphorus Compounds with Martin Ligands

(マーチンリガンドを有する 5配位有機リン化合物の 立体化学と反応)

Thesis Submitted to Hiroshima University
for the Degree of Doctor of Science

Kazumasa Kajiyama

January, 1997

Contents

Chapter 1

General Introduction

A. General introduction

Phosphorus is required by all biological systems and holds an important role in biological processes in the form of phosphates. In living organisms, phosphates are important parts of large molecules or molecular assemblies such as DNA, RNA, and membranes, a carrier of substrates as shown in glucose phosphates and coenzymes, and transportation of chemical energy (ATP).[1] These phosphate esters easily undergo hydrolysis and phosphoryl transfer in biological processes due to the ease of attaining the pentacoordinate state as a transition state or an intermediate.

The chemistry of pentacoordinate phosphorus has been developing over the past decades. PPh_5, the first organic phosphorane, was synthesised by Wittig and Reiber in 1949,[2] of which trigonal bipyramid (TBP) structure was determined 15 years later by Wheatley.[3] A large number of phosphoranes have been synthesized and characterized in conjuction with the developement of the NMR technology. Burgada and Setton have summarized attractive fundamental aspects of the chemistry of pentacoordinate phosphorus compounds into three items.[4] The first one is the discovery of their stereochemical non-rigidity, that is, the exchange of substituents (ligands) at the axial and equatorial positions in a TBP structure without bond cleavage. This was interpreted by Berry[5] based on Berry pseudorotation mechanism (stereomutation). The second one is the presence of equilibria between P (III) and P (V), P (IV) and P (V), and P (V) and P (VI), stemming from the ease of phosphorus to violate the Lewis octet rule[6]. A variety of experimental observations have been reported since the first postulation was reported by Fenton and Ingold[7] in 1929. The third one is the reports of Westheimer[8]

that the rates of hydrolysis of five-membered cyclic phosphates were significantly faster than those of acyclic phosphates. He has postulated the existence of pentacoordinate intermediates which are capable of undergoing the stereomutations described by Berry.

The basic structure of pentacoordinate phosphoranes are predicted to be trigonal bipyramid (TBP) structure (Fig. 1-1), in which there are distinctive sites, the apical and the equatorial positions, by fitting the axioms of the valence shell electron pair repulsion (VSEPR) theory of Gillespie[9]. Both experimental results and theoretical calculations[9, 10] show that the TBP structure is more favorable than square pyramid (SP) structure (Figure 1-2). In an ideal arrangement the three equatorial points would be in the same plane, the angle formed with an arbittrary equatorial site, the center, and another arbitrary equatorial site is 120°, while the length between the central atom and the apical ligand is longer than the equatorial bond and the apical bond comprising of the two sites positioned linearly with the center intersects the equatorial plane perpendicularly. This inequivalence of sites causes an abrupt increase in the possible number of isomers. Assuming all five sites are occupied by different substituents, up to 20 isomers are possible including enantiomers as compared with only 2, a pair of enantiomers, for tetrahedral molecules with four different substituents.

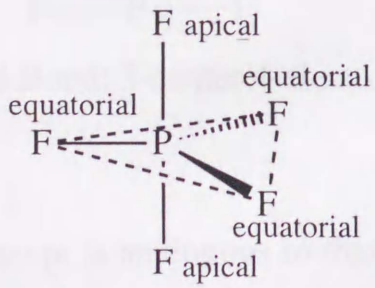

Trigonal bipyramid
(TBP)

Figure 1-1

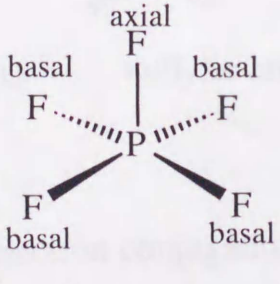

Square pyramid
(SP)

Figure 1-2

In order to explain the electronic structure of the central atom and the validity of violation of the Octet rule, Pauling[11] has proposed the conventional explanation that the lowest lying d orbital would participate in the hybridizaiton of orbitals to form a dsp^3 type combination. However, Pimental[12] and Rundle[13] have proposed an alternative explanation based on the concept of three-center four-electron (3c-4e) bond in 1951, in which the electrons are delocalized into the apical substituents to relieve the electron density upon the central atom. According to Musher's simplified bonding scheme[14] for pentacoordinate species the three equatorial bonds is described as involving sp^2 orbitals of the P atom, while the apical 3c-4e bonds can be comprised of the σ and σ_n bonds formed by the linear combination of the remaining p orbital on the central atom and one valence atomic orbital of each of the two apical atoms (Fig. 1-3).

Figure 1-3

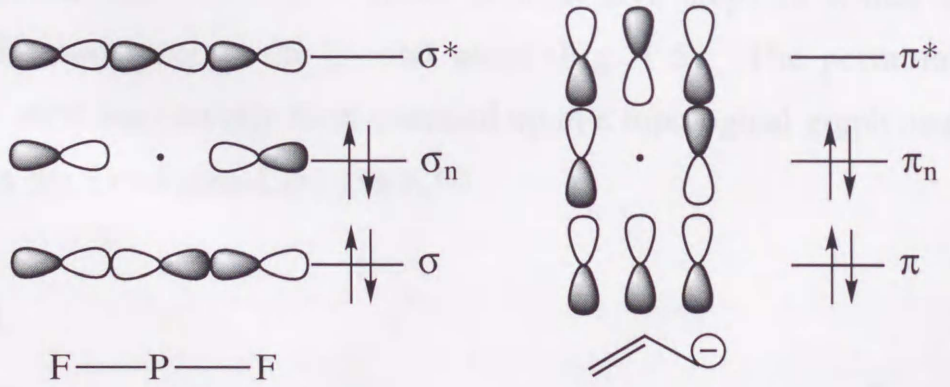

<Apical Bond: 3-center 4-electron bond> <allylic anion>

This concept is analogous to that of π electron conjugation as seen in the allylic anion. In order to alleviate the electron density upon the central atom, electron accepting substituents would be prefered in these apical positions, leading to the concept of apicophilicity. A large number of theoretical and

empirical studies on relative apicophilicity have been reported,[15] although not all of them give the same results. It is probable that the apicophilicity of a group must be attributed to the combined influences of many factors, such as electronegativity, pπ–dπ interaction, steric effects, stereoelectronic effects[16, 17] and polarizability.

The fast permutation of pentacoordinate compounds as shown in PF_5 or as postulated by Westheimer can be accounted for by the Berry pseudorotation (BPR) process which is widely accepted over other mechanisms.[18] The mechanism assumes that the pair of apical substituents bend away from a pivotal equatorial atom and the remaining two equatorial substituents bend toward this pivotal atom to proceed via a transition state of square pyramidal structure on to an isomer which has the apical atoms exchanged with the two moving equatorial atoms (Fig. 1-4). According to this mechanism when the five sites are unequally substituted the epimerization of one isomer to the enantiomer needs at least five steps in which each substituent is used once as the pivotal atom (Fig. 1-5). The permutation processes by BPR has cleverly been summed up in a topological graph usually referred to as the Desargues-Levi graph.[19]

Figure 1-4.

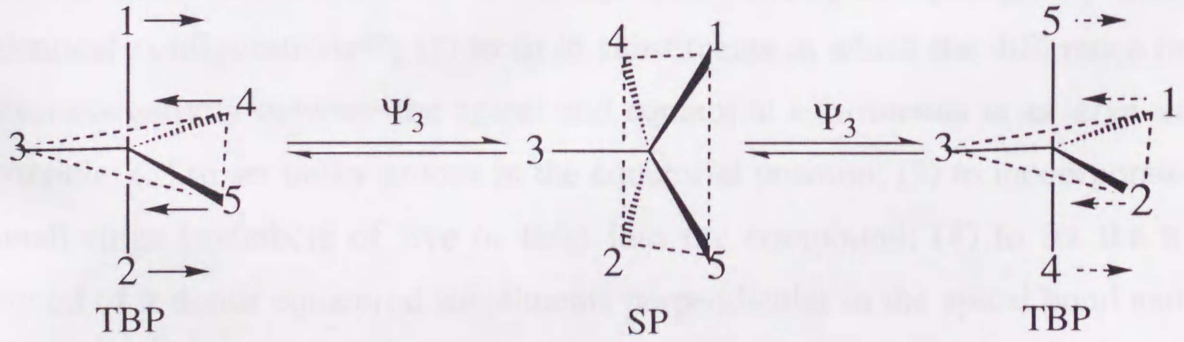

Figure 1-5. 5 Step Epimerization Process and the Desargues-Levi Graph

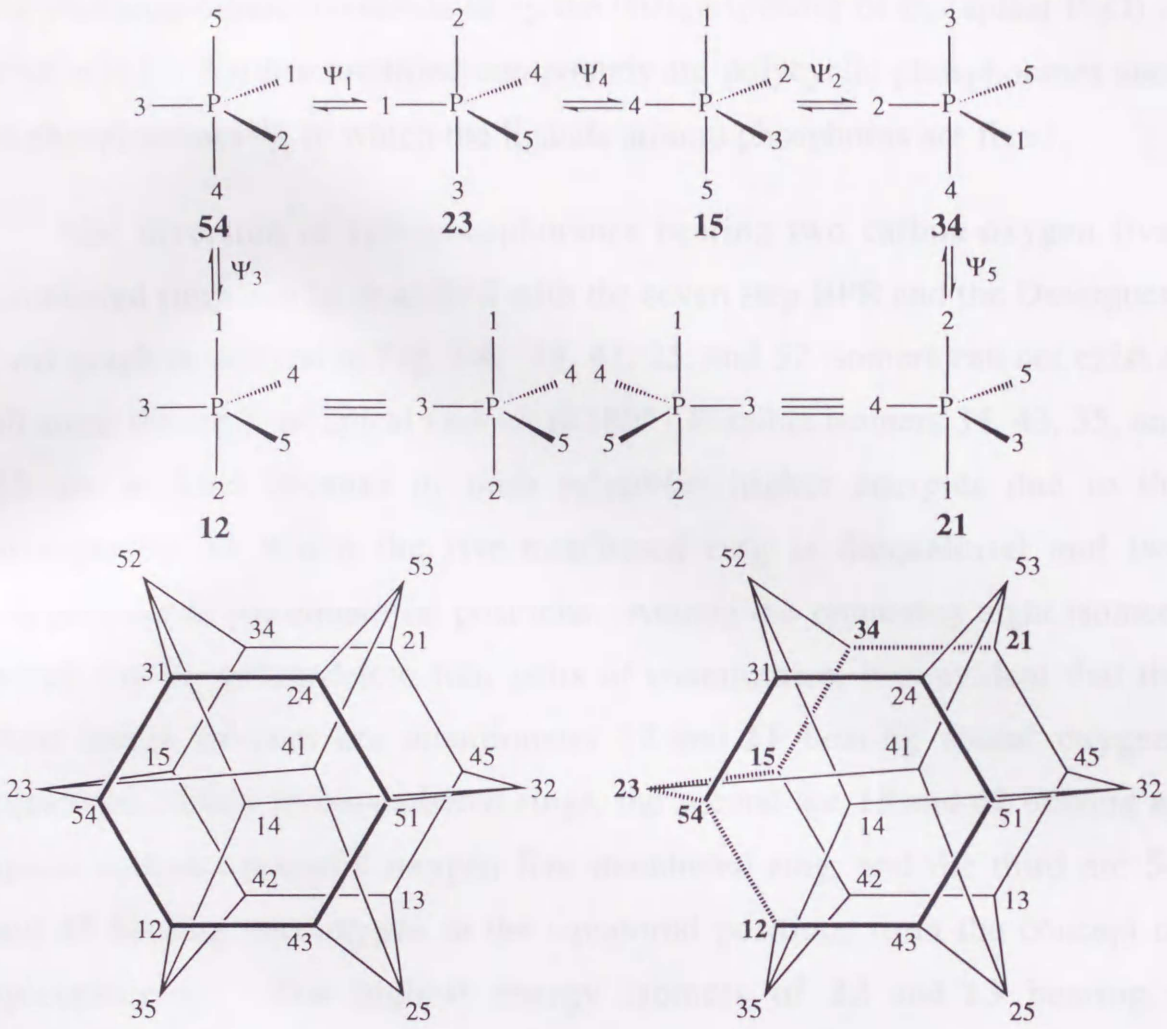

There are several guidelines for raising the permutation barrier which in principle is to differentiate the thermodynamic stability of topologically non-identical configurations[20]; (1) to fit in substituents in which the difference in electronegativity between the apical and equatorial substituents is as large as possible; (2) to set bulky groups in the equatorial position; (3) to incoorporate small rings (members of five or less) into the compound; (4) to fix the π orbital of π donor equatorial substituents perpendicular to the apical bond and π orbital of π acceptor substituents parallel to the apical bond. For example, it has been suggested that, in the hydrolysis reaction of triesters of

phosphonoformic acid, π acceptor ligand in the equatorial position stabilize the pentacoordinate intermediate by the charge transfer of σ_n (apical P–O) to π*(C=O).[17] Further modified compounds are polycyclic phosphoranes such as phosphatranes[21], in which the ligands around phosphorus are fixed.

The inversion of spirophosphoranes bearing two carbon-oxygen five-membered rings can be described with the seven step BPR and the Desargues-Levi graph is reduced to Fig. 1-6. 14, 41, 25, and 52 isomers can not exist at all since the angle of apical O–P–C is 180°. Possible isomers 34, 43, 35, and 53 are avoided because of their relatively higher energies due to the arrangement in which the five-membered ring is diequatorial and two oxygens are in the equatorial positions. Among the remaining eight isomers which can be grouped into four pairs of enantiomers, it is evident that the most stable isomers are enantiomers **12** and **21** bearing apical oxygen-equatorial carbon five-membered rings, the second are **15** and **42** bearing an apical carbon-equatorial oxygen five membered ring, and the third are **54** and **45** bearing two oxygen in the equatorial positions from the concept of apicophilicity. The highest energy isomers of **23** and **13** bearing a diequatorial five-membered ring along with one apical oxygen should be either intermediates or transition states of the inversion process of enantiomers **12** and **21**. Thus, it appears possible to isolate thermodynamically stable enantiomeric pairs of spirophosphoranes with asymmetry only at phosphorus by means of modifying the oxygen-carbon five-membered ring.

Many examples of isolations of thermodynamically stable optically active phosphoranes with chirality also in the backbone have been reported.[22] They are all diastereomers which bear more than two chiral centers including phosphorus. We are aware of only one example of an optically active

phosphorane with asymmetry only at phosphorus reported by Hellwinkel.[10b] However this optically active species exhibited residual optical activity and could not be stereochemically defined.

Figure 1-6. 7 Step Inversion Process of Spirophosphorane Bearing Two Oxygen-Carbon Five-membered Rings and the Desargues-Levi Graph

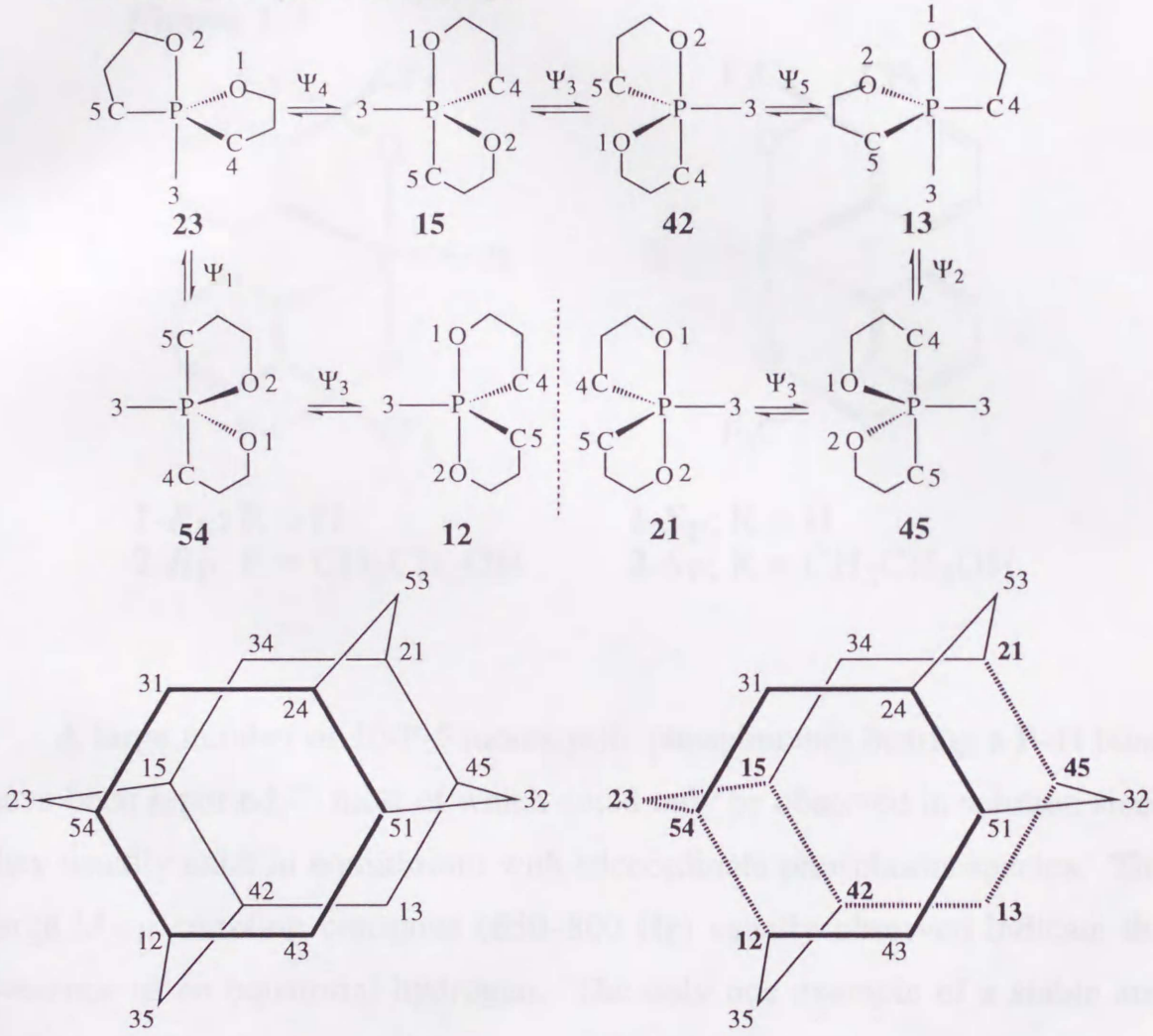

We have reported the preparation and characterization of the first enantiomeric pairs of stereochemically definable 10-P-5[23] spirophosphoranes **1**-R_P and **1**-S_P, and **2**-R_P and **2**-R_P (Figure 1-7).[24] We have utilized Martin ligand that is known to stabilize many hypervalent species.[25] The unique

features of this ligand are that the trifluoromethyl groups raise the electronegativity of the oxygen atoms attached to the phosphorus, the bidentate and the phosphorus atom together form a five-membered ring, and the trifluoromethyl groups exert Thorpe-Ingold effect[26] to favor the formation of the five-membered ring.

Figure 1-7

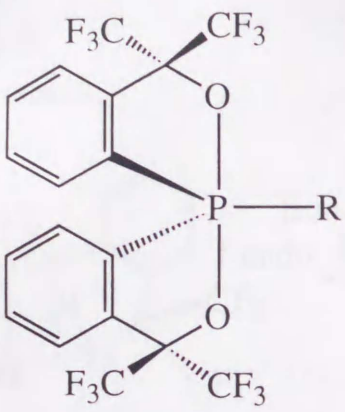

1-*R*$_P$; R = H
2-*R*$_P$; R = CH_2CH_2OH

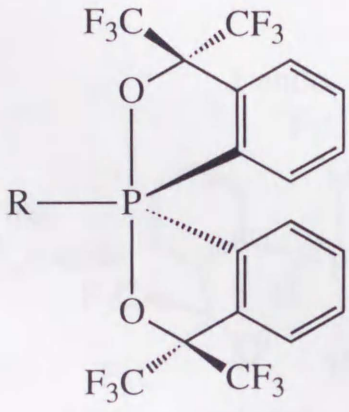

1-*S*$_P$; R = H
2-*S*$_P$; R = CH_2CH_2OH

A large number of 10-P-5 monocyclic phosphoranes bearing a P–H bond have been reported,[27] most of which could only be observed in solution since they usually exist in equilibrium with tricoordinate phosphorus species. The large $^1J_{P-H}$ coupling constants (650–800 Hz) usually observed indicate the presence of an equatorial hydrogen. The only one example of a stable and isolable P–H phosphorane bearing an apical hydrogen has been reported by M. R. Ross and J. C. Martin,[28] where the $^1J_{P-H}$ coupling constant (266 Hz) in $CDCl_3$ was much smaller than those of P–H (equatorial) phosphoranes.

In Chapter 2 the isolation and characterization of monocyclic P–H (apical) phosphoranes **6–8** bearing a hydroxy group are described (Scheme 1-

1). We have found that these P–H (apical) phosphoranes existed in solution as equilibrating mixtures of intra- and intermolecular hydrogen bonding isomers which correspond to the structures determined by X-ray analysis and observed ^{31}P NMR chemical shifts in various solvents in order to support the structure. The inversion of **6–8** turned out to be a combination of BPR and bond switching and kinetic behavior are described.

Scheme 1-1

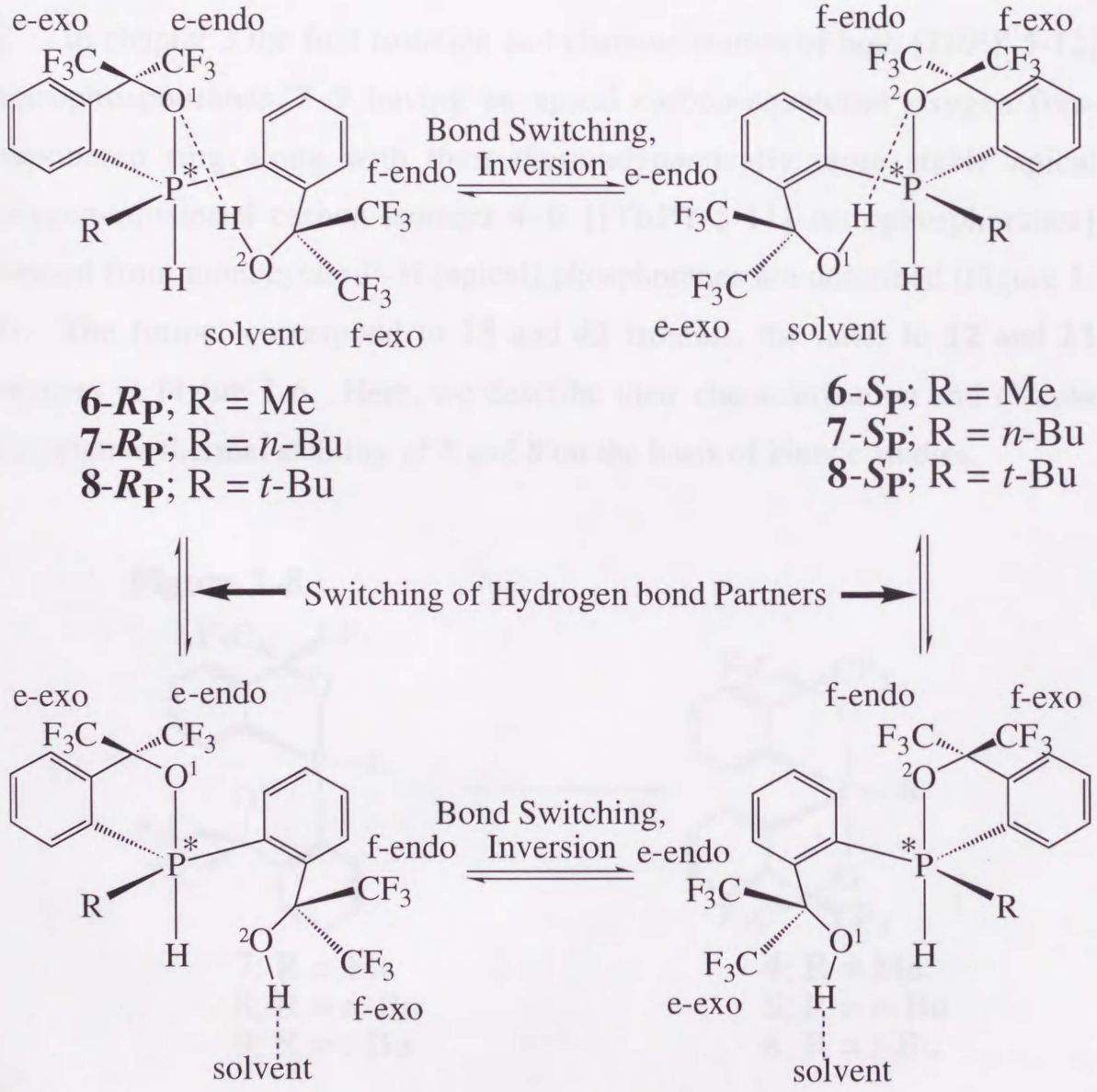

It is well-known that phosphoranes bearing oxygen and carbon substituents preferentially have oxygen atoms in the apical positions as the most stable stereoisomer according to the apicophilicity of the elements.[29] However, no example of the isolation and characterization of phosphoranes having an apical carbon-equatorial oxygen as the relatively less stable stereoisomers has been reported[24, 25c] because of the low activation energy of the permutation of pentacoordinate compounds assuming TBP structures, normally accounted for by BPR mechanism.

In chapter 3 the first isolation and characterization of both [*TBPY*-5-12] spirophosphoranes **7–9** having an apical carbon-equatorial oxygen five-membered ring along with their thermodynamically more stable apical oxygen-equatorial carbon isomers **4–6** {[TBPY-5-11] spirophosphoranes} formed from monocyclic P–H (apical) phosphoranes are described (Figure 1-8). The former correspond to **15** and **42** isomers, the latter to **12** and **21** isomers in Figure 1-6. Here, we describe their characterization and discuss the relative thermal stability of **5** and **8** on the basis of kinetic studies.

Figure 1-8

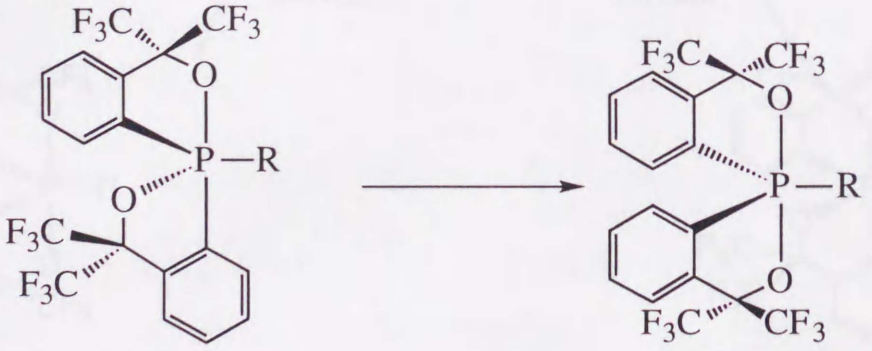

7; R = Me
8; R = *n*-Bu
9; R = *t*-Bu

4; R = Me
5; R = *n*-Bu
6; R = *t*-Bu

Monocyclic P–H (apical) phosphoranes **1–3** cyclized intramolecularly with elimination of hydrogen to form the corresponding [*TBPY*-5-11] spirophosphoranes **4–6** predominantly in nondonor solvents and the corresponding [*TBPY*-5-12] spirophosphoranes **8–10** predominantly in donor solvents on heating. In order to gain an understanding of the mechanism and the solvent effect of the thermal cyclization of **1–3**, the kinetic studies of the thermal cyclization of **1–3** (Scheme 1-2) are described in Chapter 4. On the basis of these results we propose mechanisms for formation of these phosphoranes in both nondonor and donor solvent.

Scheme 1-2

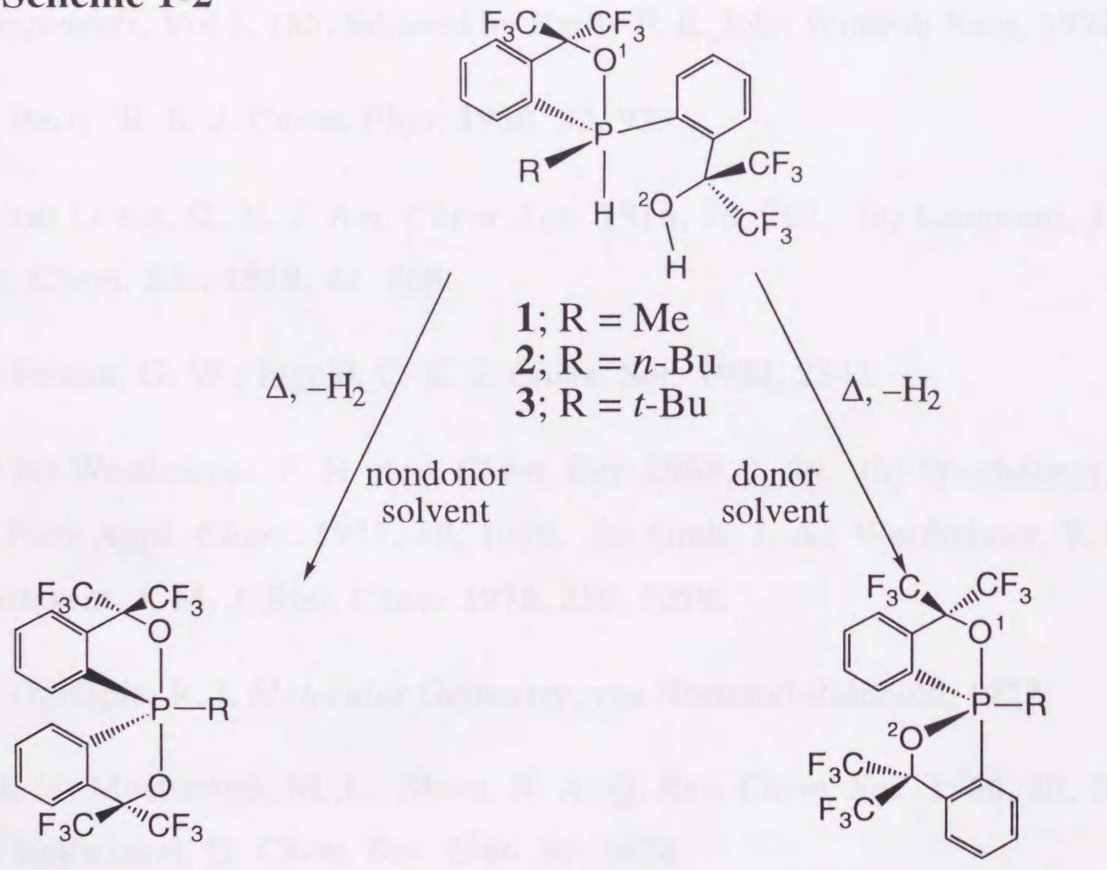

B. References

(1) Frausto da Silva, J. J. R.; Williams, R. J. P. "The Biological Chemistry of the Elements. *The Inorganic Chemistry of Life*", Clarendon Press, Oxford, 1991.

(2) Wittig, G.; Reiber, M. *Justus Liebigs Ann. Chem.* **1949**, *562*, 147.

(3) Wheatly, P. J. J. Chem. Soc. **1964**, 2206.

(4) Burgada, R.; Setton, Ralph. *The Chemistry of Organophosphorus Compounds*, Vol 3, 185, Editated by Hartly F. R. John Wiley & Sons, 1994.

(5) Berry, R. S. *J. Chem. Phys.* **1960**, *32*, 933.

(6) (a) Lewis, G. N. *J. Am. Chem. Soc.* **1916**, *38*, 762. (b) Langmuir, J. *J. Am. Chem. Soc.* **1919**, *41*, 868.

(7) Fenton, G. W.; Ingold, C. K. *J. Chem. Soc.* **1924**, 2342.

(8) (a) Westheimer, F. H. *Acc. Chem. Res.* **1968**, *1*, 70. (b) Westheimer, F. H. *Pure Appl. Chem.* **1977**, *49*, 1059. (c) Grelt, J. A.; Westheimer, F. H.; Sturtevant, J. M. *J. Biol. Chem.* **1975**, *250*, 5059.

(9) Gillespie, R. J. *Molecular Geometry*, van Nostrand-Reinhold, 1972.

(10) (a) Muetterties, M. L.; Shum, R. A. *Q. Rev. Chem. Soc.* **1966**, *20*, 245. (b) Hellwinkel, D. *Chem. Ber.* **1966**, *99*, 3628.

(11) Pauling, L. *The Nature of the Chemical Bond*, 3rd ed., Cornell: Ithaca, New York, 1960.

(12) Pimentel, G. C. *J. Chem. Phys.* **1951**, *19*, 446.

(13) Hach, R. J.; Rundle, R. E. *J. Am. Chem. Soc.* **1951**, *73*, 4321.

(14) Musher, J. I. *Angew. Chem., Int. Ed. Engl.* **1969**, *8*, 54.

(15) (a) Stewart, A. P.; Trippett, S. *J. Chem. Soc., Chem. Commun.* **1970**, 1279. (b) Cram, R. K.; Trippett, S. *J. Chem. Soc., Perkin Trans.* **1973**, *1*, 1300. (c) Duff, E.; Trippett, S.; Whittle, P. J. *J. Chem. Soc., Perkin Trans.* **1973**, *1*, 972. (d) Trippett, S.; Whittle, P. J. *J. Chem. Soc., Chem. Commun.* **1973**, 2302. (e) Dickstein, J. I.; Trippett, S. *Tetrahedron Lett.* **1973**, *24*, 2203. (f) Trippett, S. *Pure Appl. Chem.* **1974**, *40*, 595. (g) Bone, S. A.; Trippett, S.; White, M. W.; Whittle, P. J. *Tetrahedron Lett.* **1974**, *20*, 1975. (h) Bone, S. A.; Trippett, S.; White, M. W.; Whittle, P. J. *J. Chem. Soc., Perkin Trans.* **1977**, *1*, 80. (i) Brierly, J.; Trippett, S.; Whittle, P. J. *J. Chem. Soc., Perkin Trans.* **1977**, *1*, 1977. (j) Trippett, S.; Waddling, R. E. L. *Tetrahedron Lett.* **1979**, *2*, 193. (k) Kay, P. B.; Trippett, S. *J. Chem. Res. (s)*, **1986**, 62. (l) Debruin, K. E.; Padilla, A. G.; Campbell, M. T. *J. Am. Chem. Soc.* **1973**, *95*, 4681. (m) Emsley, J.; Hall, D. *The Chemistry of Phosphorus*, Happer and Row, London, 1976. (n) McDowell, R. S.; Streitwieser, H.Jr. *J. Am. Chem. Soc.* **1985**, *94*, 3047. (o) Buono, G.; Llinas, J. R. *J. Am. Chem. Soc.* **1981**, *103*, 4532. (p) Cavell, R. G.; Gibson, J. A.; Gibson, K. I. *J. Am. Chem. Soc.* **1977**, *99*, 7841.

(16) (a) Peake, S. C.; Schmutzler, R. *J. Chem. Soc. A.* **1970**, 1049. (b) Landau, M. A.; Sheluchenko, V. V.; Drozd, G. I.; Dubov, S. S.; Ivin, S. Z. *Zh. Strukt. Khim.* **1967**, *8*, 1097. (c) Harris, J. J.; Rudner, B. *J. Org. Chem.* **1968**, *33*, 1392. (d) Harman, J. S.; Sharp, D. W. N. *Inorg. Chem.* **1971**, *10*, 1538. (e) Muetterties, E. L.; Meakin, P.; Hoffmann, R. *J. Am. Chem. Soc.* **1972**, *94*, 5674.

(17) Gregory, R. J.; Thatcher, E. S.; Krol, R.; Dale, R. *J. Chem. Soc., Perkin Trans.* **1994**, *2*, 683.

(18) (a) Ugi, I.; Marquarding, D.; Klusacek, H.; Gillespie, P. *Acc. Chem. Res.* **1971**, *4*, 288. (b) Windus, T. L.; Gordon, M. S.; Burggraf, L. W.; Davis, L. P. *J. Am. Chem. Soc.* **1994**, *116*, 3568.

(19) Mislow, K. *Acc. Chem. Res.* **1970**, *3*, 321.

(20) Holmes, R. R. *J. Am. Chem. Soc.* **1978**, *100*, 433.

(21) (a) Tang, J.; Dopke, J.; Verkade, J. G. *J. Am. Chem. Soc.* **1993**, *115*, 5015. (b) Bosco, A. D'Sa.; Verkade, J. G. *J. Org. Chem.* **1996**, *61*, 2963.

(22) (a) McClure, C. K.; Grote, C. W.; Lockett, B. A. *J. Org. Chem.* **1992**, *57*, 2963. (b) Moriarty, R. M.; Hiratake, J.; Liu, K.; Wendler, A.; Awasthi, A. K.; Gilardi, R. *J. Am. Chem. Soc.* **1991**, *113*, 9374. (c) Acher, F.; Juge, S.; Wakselman, M. *Tetrahedron* **1987**, *43*, 3721. (d) Klaebe, A.; Brazier, J. F.; Carrelhas, C.; Garrigues, B.; Marre, M. R. *Tetrahedron* **1982**, *38*, 2111. (e) Devillers, P. J.; Garrigues, B.; Wolf, R. *Acta Crystallogr.* **1979**, *B35*, 2153. (f) Contreras, R.; Brazier, J. F.; Klaebe, A.; Wolf, R. *Phosphorus*, **1972**, *2*, 67. (g) Newton, M. G.; Collier, J. E.; Wolf, R. *J. Am. Chem. Soc.* **1974**, *96*, 6888 and references cited therein.

(23) Perkins, C. W.; Martin, J. C.; Arduengo, A. J.; Lau, W.; Alegria, A.; Kochi, J. K. *J. Am. Chem. Soc.* **1980**, *102*, 7753.

(24) (a) Kojima, S.; Kajiyama, K.; Akiba, K.-y. *Tetrahedron Lett.* **1994**, *35*, 7037. (b) Kojima, S.; Kajiyama, K.; Akiba, K.-y. *Bull. Chem. Soc. Jpn.* **1995**, *68*, 1785. (c) Kojima, S.; Nakamoto, M.; Kajiyama, K.; Akiba, K.-y. *Tetrahedron Lett.* **1995**, *36*, 22617.

(25) (a) Perozzi, E. F.; Martin, J. C. *J. Am. Chem. Soc.* **1972**, *94*, 5519. (b) Perozzi, E. F.; Michalak, R. S.; Figuly, G. D.; Stevenson, W. H., III; Dess, D. B.; Ross, M. R.; Martin, J. C. *J. Org. Chem.* **1981**, *46*, 1049. (c) Granoth, I.; Martin, J. C. *J. Am. Chem. Soc.* **1979**, *101*, 4618, 4623. (d) Stevenson, W. H., III; Wilson, S.; Martin, J. C.; Farnham, W. B. *J. Am. Chem. Soc.* **1985**, *107*, 6340.

(26) (a) Beesley, R. M.; Ingold, C. K.; Thorpe, J. F. *J. Chem. Soc.* **1915**, *107*, 1080. (b) Ingold, C. K. *J. Chem. Soc.* **1921**, *119*, 305.

(27) (a) Malavaud, C.; Barrans, J. *Tetrahedron Lett.* **1975**, *35*, 3077. (b) Boisdon, M. T.; Maravaud, C.; Mathis, F.; Barrans, J. *Tetrahedron Lett.* **1977**, *39*, 3501. (c) Laurenco, C.; Burgada, R. *Tetrahedron.* **1976**, *32*, 2253. (d) Lopez, L.; Fabas, C.; Barrans, J. *Phosphorus Sulfur* **1979**, *7*, 81. (e) Tangom, B.; Malavaud, C.; Boisdon, M. T.; Barrans, J. *Phosphorus Sulfur* **1988**, *40*, 33.

(28) Ross, M. R.; Martin, J. C. *J. Am. Chem. Soc.* **1981**, *103*, 1234.

(29) (a) Holmes, R. R. *Pentacoordinated Phosphorus-Structure and Spectroscopy*; ACS Monograph 175, 176; American Chemical Society: Washington, DC, 1980; Vols. I, II. (b) Trippett, S. *Phosphorus, Sulfur Silicon Relat. Elem.* **1976**, *1*, 89. (c) McDowell, R. S.; Streitwieser, A. *J. Am. Chem. Soc.* **1985**, *107*, 55. (d) Wang, P.; Zhang, Y.; Glaser, R.; Reed, A. E.; Schleyer, P. v. R.; Streitwieser, A. *J. Am. Chem. Soc.* **1991**, *113*, 55. (e) Thatcher, G. R. J.; Campbell, A. S. *J. Org. Chem.* **1993**, *58*, 2272. (f) Wasada, H.; Hirao, K. *J. Am. Chem. Soc.* **1992**, *114*, 16.

Chapter 2

Syntheses and Characterization of Intra- and Intermolecular Hydrogen Bonding Isomers of P–H (Apical) Phosphoranes Bearing a Hydroxy Group

A. Introduction

Known examples of 10-P-5[1] phosphoranes bearing a P–H bond which are mostly mono- or bicyclic phosphoranes containing some heteroatoms bonded to phosphorus, which stabilize the hypervalent compounds. Although a large number of monocyclic P–H phosphoranes have been reported,[2] most of them could only be observed in solution since they usually exist in the equilibrium with tricoordinate phosphorus species (eq. 1). As for phosphoranes bearing monodentate oxygen or fluorine (Z = OR', F) ligands, the $^1J_{P-H}$ coupling constant in various solutions are 650–800 Hz, which indicates the presence of an equatorial P–H.[2a–d, 3] The equatorial orientation of the hydrogen atom is probably due to its lower apicophilicity compared with oxygen and fluorine. In the case of phosphorus bearing nitrogen monodentates the $^1J_{P-H}$ coupling constant comes in the range of 350–500 Hz implying the existence of equilibrium between phosphoranes with apical H and equatorial H.[2e]

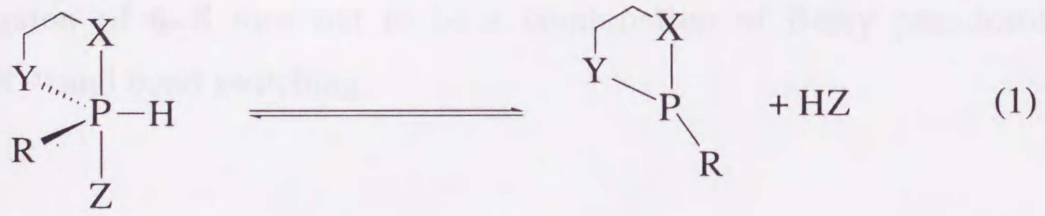

(1)

The only one example of a stable and isolable P–H phosphorane bearing an apical hydrogen has been reported by M. R. Ross and J. C. Martin,[4] where the $^1J_{P-H}$ coupling constant (266 Hz) in $CDCl_3$ of the compound **A** was much smaller than those of P–H (equatorial) phosphoranes.

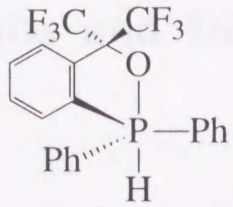

A

We have succeeded in the isolation of monocyclic P–H (apical) phosphoranes **6–8** bearing a hydroxy group by the reaction of 10-P-5 P–H (equatorial) spirophosphorane **1** with 3 equivalents of RLi (R = Me, *n*-Bu, *t*-Bu) in Et_2O followed by careful treatment with 1 M HCl (Scheme 3-1). The reactions involve the nucleophilic attack of RLi to the 10-P-4 phosphoranide **2** generated by incipient deprotonation of **1** to give ring opened dianionic species **3–5**, which are diprotonated upon acidic workup. Although we obtained **6** and **7** as intramolecular hydrogen bonding isomers, in the case of **8**, both the intra- (**8a**) and intermolecular hydrogen bonding isomer (**8b**) could be crystallized out as single compounds by changing the solvent. Furthermore, we found that these P–H (apical) phosphoranes existed in solution as equilibrating mixtures of intra- and intermolecular hydrogen bonding isomers by their ^{31}P NMR chemical shifts in various solvents. The inversion of **6–8** turn out to be a combination of Berry pseudorotation (BPR)[5] and bond switching.

B. Results and Discussion

1. Preparation and the Structure of Monocyclic P–H (Apical) Phosphoranes in Solution.

Scheme 2-1

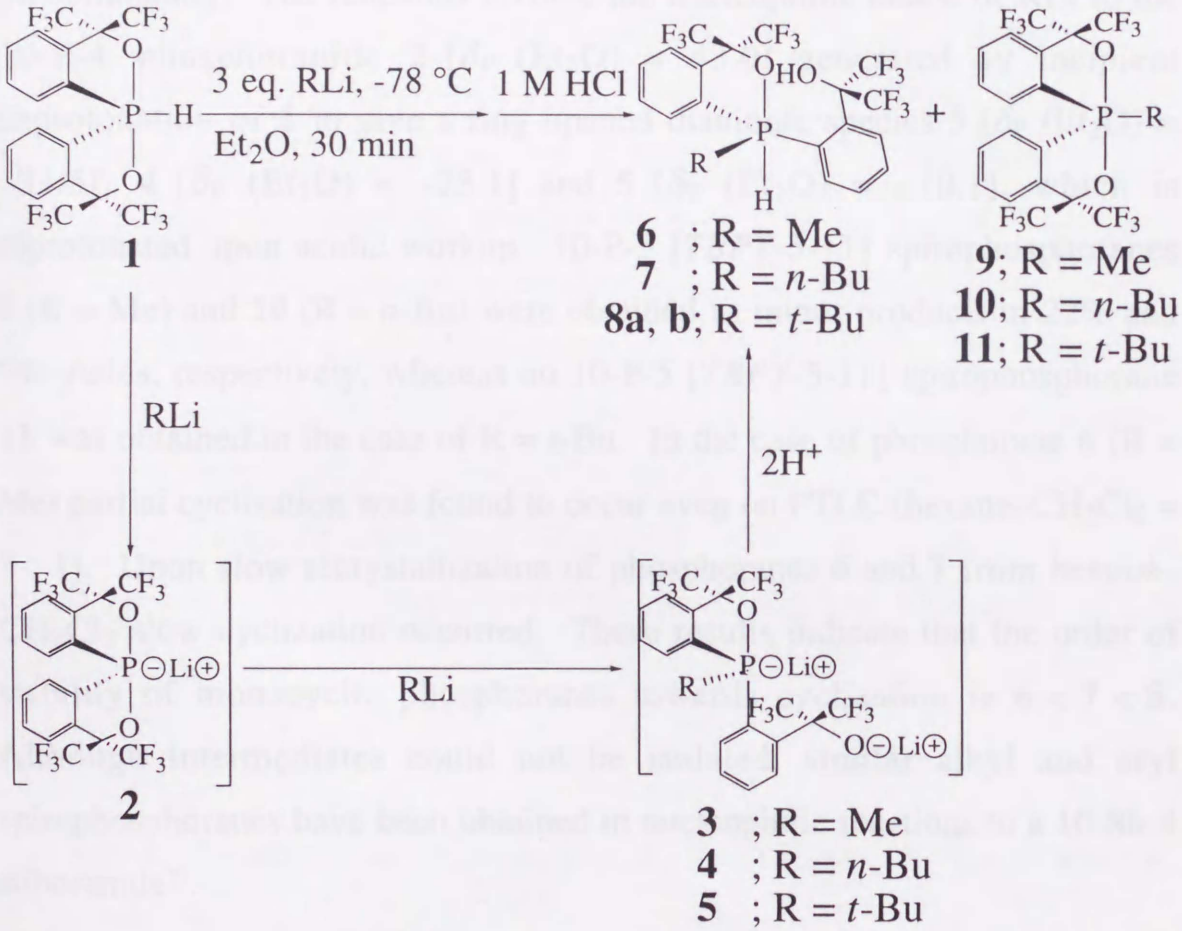

The preparation of monocyclic 10-P-5 P–H (apical) phosphoranes **6–8** was carried out as shown in Scheme 2-1. The reaction of 10-P-5 P–H (equatorial) spirophosphorane **1** [δ_P ($CDCl_3$) = –45.8, $^1J_{P-H}$ = 729 Hz][6] with 3 equivalents of alkyl lithium reagents in Et_2O at –78 °C followed by careful

treatment with 1 M HCl gave stable phosphoranes **6** [y. 68%, δ_P ($CDCl_3$) = –51.9, $^1J_{P-H}$ = 276 Hz], **7** [y. 90%, δ_P ($CDCl_3$) = –34.4, $^1J_{P-H}$ = 273 Hz] and **8a** [δ_P ($CDCl_3$) = –14.7, $^1J_{P-H}$ = 273 Hz], **8b** [δ_P ($CDCl_3$) = –42.7, $^1J_{P-H}$ = 293 Hz] (combined y. 92%). However, in the case of MeLi and *n*-BuLi when the reactions were performed in THF at –78 °C, during the workup the formation of cyclization products **9** and **10** or oxidation of 10-P-4 phosphoranide **2** generating hydroxyphosphorane **12** occurred predominantly. The reactions involve the nucleophilic attack of RLi to the 10-P-4 phosphoranide **2** [δ_P (Et_2O) = 43.0] generated by incipient deprotonation of **1** to give a ring opened dianionic species **3** [δ_P (Et_2O) = –33.5], **4** [δ_P (Et_2O) = –23.1] and **5** [δ_P (Et_2O) = –10.1], which is diprotonated upon acidic workup. 10-P-5 [*TBPY*-5-11] spirophosphoranes **9** (R = Me) and **10** (R = *n*-Bu) were obtained as minor products in 22% and 9% yields, respectively, whereas no 10-P-5 [*TBPY*-5-11] spirophosphorane **11** was obtained in the case of R = *t*-Bu. In the case of phosphorane **6** (R = Me) partial cyclization was found to occur even on PTLC (hexane–CH_2Cl_2 = 5 : 1). Upon slow recrystallization of phosphoranes **6** and **7** from hexane–CH_2Cl_2 slow cyclization occurred. These results indicate that the order of stability of monocyclic phosphoranes towards cyclization is **6** < **7** < **8**. Although intermediates could not be isolated, similar alkyl and aryl spirophosphoranes have been obtained in nucleophilic reactions to a 10-Sb-4 stiboranide[7].

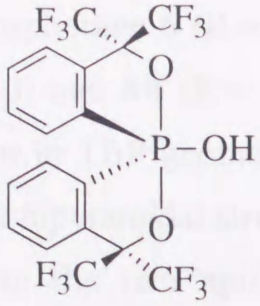

12

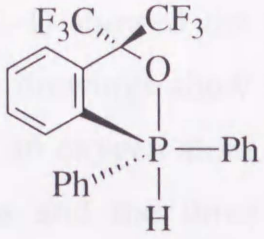

A

The $^1J_{P-H}$ coupling constant (273–293 Hz) of monocyclic phosphoranes **6–8** revealed the presence of an apical hydrogen in solution. As the only known phosphorane bearing an apical hydrogen, J. C. Martin et al. has reported that $^1J_{P-H}$ coupling constant of **A** ($CDCl_3$, δ_P = –49.3) was 266 Hz.[4] In contrast, $^1J_{P-H}$ coupling constant of bicyclic phosphorane **1** ($CDCl_3$, δ_P = –45.8) bearing an equatorial hydrogen was 729 Hz.[6] This difference can be understood as the difference in the bonding scheme about phosphorus. The apical hydrogen is expected to bond with an essentially p-type phosphorus orbital, while the equatorial hydrogen is attached to an essentially sp^2 hybrid phosphorus orbital in trigonal bipyramid (TBP) geometry[8].

2. Crystal Structure of Monocyclic P–H (Apical) Phosphoranes 6, 7, 8a and 8b.

Single crystals of **6** and **7** could be obtained as prisms from hexane–CH_2Cl_2. Although isomers **8a** and **8b** couldn't be separated by chromatography, they could each be crystallized out as single compounds by changing the solvent, nondonor solvents (cyclohexane–CCl_4) for the former and donor solvents (CH_3CN or EtOH) for the latter. X-ray structural

analysis of phosphorane **6** (R = Me, Fig. 2-1), **7**(R = *n*-Bu, Fig. 2-2), **8a** (R = *t*-Bu, Fig. 2-3) and **8b** (R = *t*-Bu, Fig. 2-4) showed the presence of an apical hydrogen in TBP geometry. As the drawings show the compounds assume trigonal bipyramidal structures with an oxygen atom and a hydrogen atom occupying the two apical positions and the three carbon atoms occupying the three equatorial positions. The angles around the phosphorus atom are nearly ideal as TBP with the apical O(1)–P(1)–H(1) angle being 172–176°, and the sum of the angles formed by the equatorial atoms and phosphorus being 359.4–360° implying coplanarity of the phosphorus atom and the three equatorial carbon atoms. The structures of **6** and **7** were essentially the same as **8a**, differing only in the alkyl substituent. Compounds **8a** and **8b** were found to differ only in the hydrogen bonding partner of the hydroxy group, the former intramolecularly with the apical oxygen of the bidentate and the latter intermolecularly with the nitrogen atom of CH_3CN, a solvent molecule. This is the first structural characterization of hydrogen bonding isomers involving hypervalent phosphorus. Although intramolecular hydrogen bond (O1–H2) length of **6** [1.74 (4) Å] and **7** [1.82 (5) Å] was similar, that of **8a** [1.4 (1) Å] was significantly shorter because of the constraint imposed by the steric hindrance of *t*-Bu group. The P1-O1 (apical) bond was longer in **8a** [1.922 (5)] than in **8b** [1.865 (2)]. This could be considered a consequence of weakening of this polarizable bond by the intramolecular hydrogen bonding. Additionally, the P1–O2 (hydroxy) length of **8b** [2.84 (4)] was shorter than that of **8a** [3.131 (5)], thus we could expect the presence of stronger intramolecular interaction of the hydroxy oxygen to phosphorus in donor solvents.

Table 2-1. Selected Bond Lengths and Angles for **6**, **7**, **8a** and **8b**

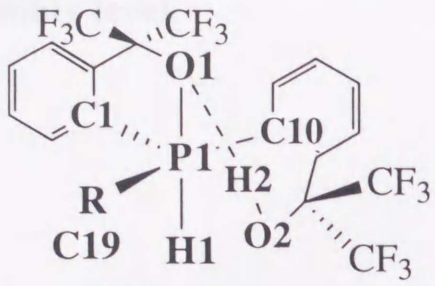

6; R = Me
7; R = *n*-Bu
8a; R = *t*-Bu

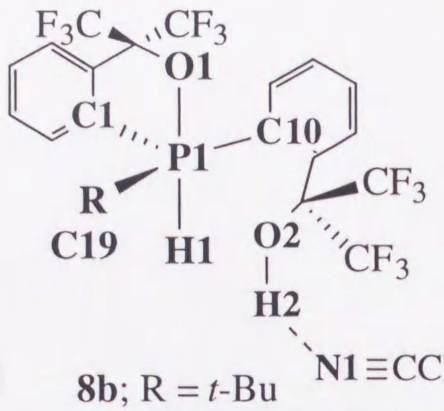

8b; R = *t*-Bu

	6	**7**	**8a**	**8b**
Bond length (Å)				
P1–O1	1.920 (3)	1.952 (2)	1.922 (5)	1.865 (2)
P1–H1	1.38 (4)	1.40 (4)	1.47 (7)	1.33 (3)
P1–C1	1.814 (4)	1.805 (3)	1.790 (7)	1.826 (2)
P1–C10	1.842 (4)	1.845 (3)	1.881 (7)	1.855 (2)
P1–C19	1.796 (6)	1.812 (3)	1.854 (9)	1.878 (3)
P1–O2	3.100 (3)	3.074 (2)	3.131 (5)	2.84 (2)
O1–H2	1.74 (4)	1.82 (5)	1.4 (1)	2.16 (4) (N1–H2)
Bond angle (deg)				
O1–P1–H1	176 (2)	176 (1)	172 (3)	175 (1)
O1–P1–C1	83.5 (2)	83.4 (1)	83.6 (3)	84.1 (1)
C1–P1–H1	92 (1)	93 (2)	89 (3)	93 (1)
O1–P1–C10	88.1 (2)	87.3 (1)	90.9 (3)	87.75 (9)
C10–P1–H1	95 (2)	93 (1)	90 (3)	91 (1)
O1–P1–C19	90.6 (2)	91.0 (1)	95.0 (3)	94.1 (1)
C19–P1–H1	90 (2)	92 (2)	91 (3)	90 (1)
C1–P1–C10	117.0 (2)	116.5 (1)	111.4 (3)	131.2 (1)
C10–P1–C19	125.1 (2)	125.8 (1)	129.1 (4)	111.5 (1)
C19–P1–C1	117.4 (2)	117.1 (1)	119.5 (4)	117.0 (1)

Figure 2-1. ORTEP drawing of **6** showing thermal ellipsoids at the 30% probability level.

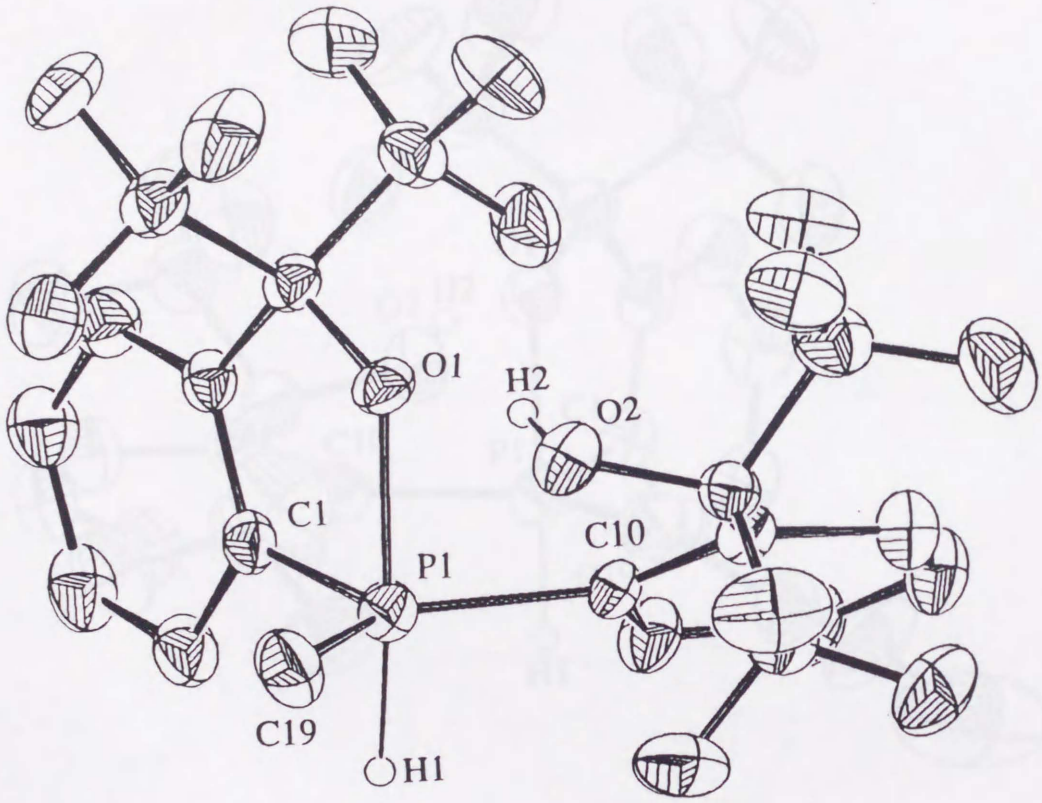

Figure 2-2. ORTEP drawing of **7** showing thermal ellipsoids at the 30% probability level.

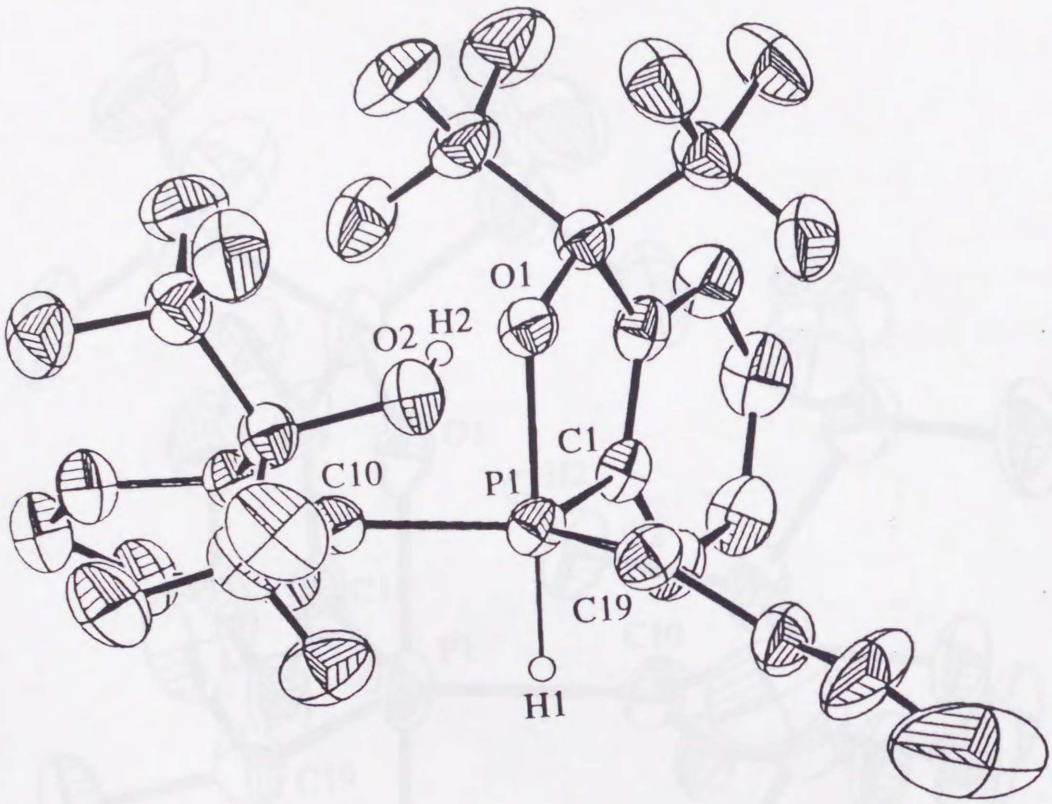

Figure 2-3. ORTEP drawing of **8a** showing thermal ellipsoids at the 30% probability level.

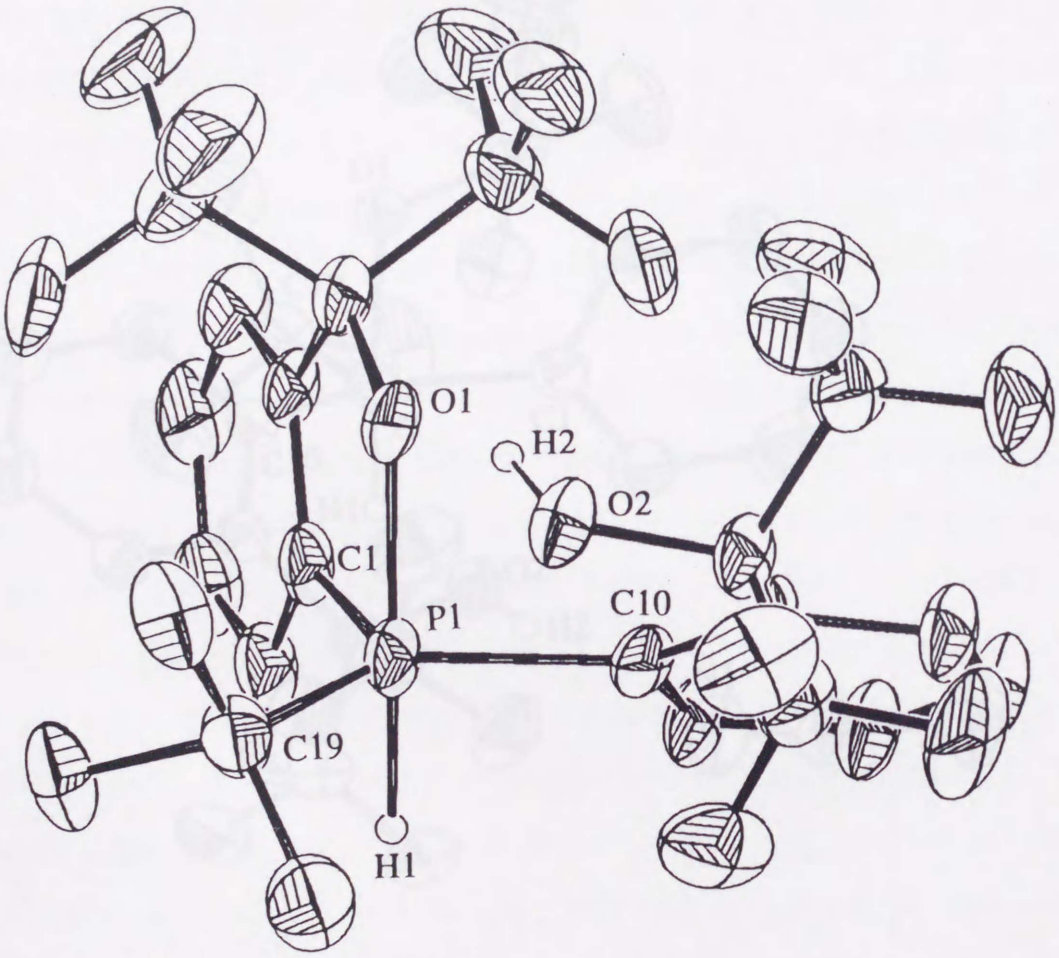

Figure 2-4. ORTEP drawing of **8b** showing thermal ellipsoids at the 30% probability level.

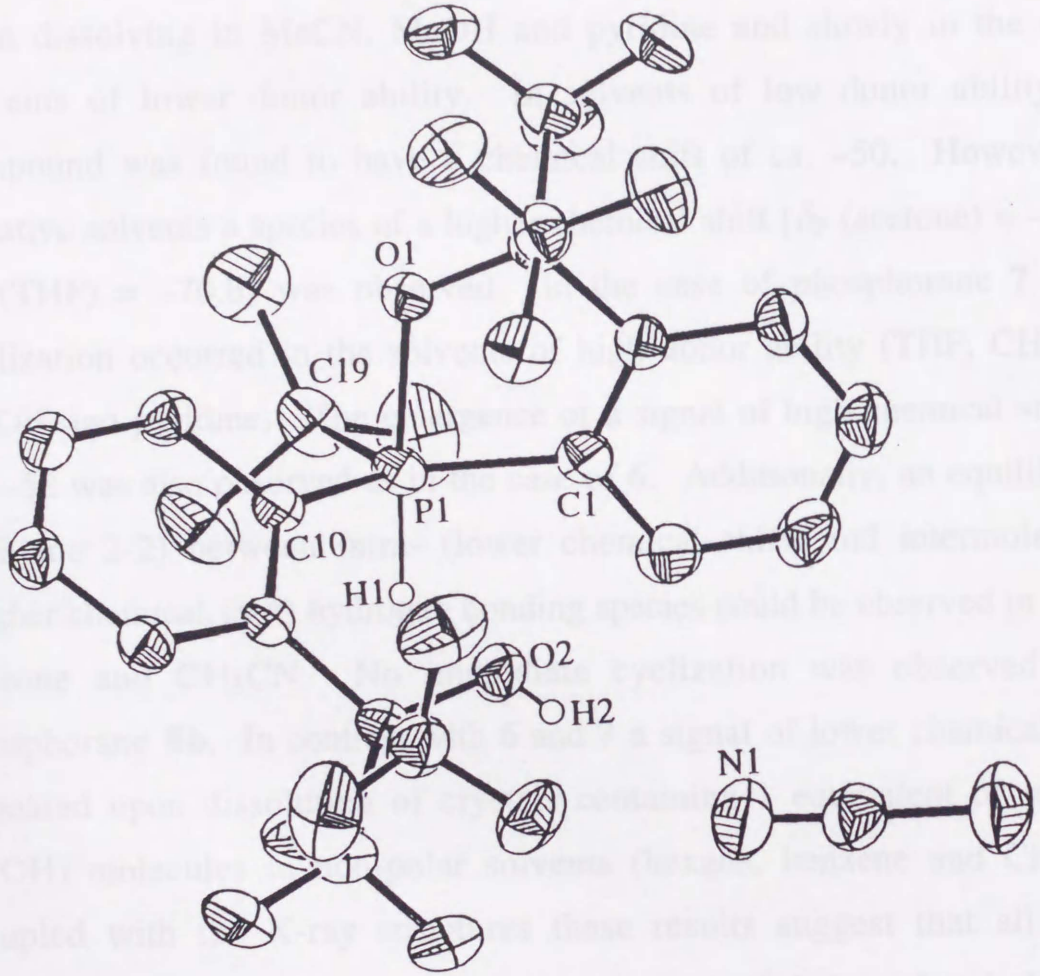

3. Solvent Effect

In order to gain further insight into structures in solution we examined ^{31}P NMR chemical shifts of monocyclic phosphoranes **6–8** in various solvents at rt (Table 2-2). Phosphorane **6** was found to cyclize instantly upon dissolving in MeCN, MeOH and pyridine and slowly in the other solvents of lower donor ability. In solvents of low donor ability the compound was found to have a chemical shift of ca. –50. However in donative solvents a species of a higher chemical shift [δ_P (acetone) = –68.8, δ_P (THF) = –70.6] was observed. In the case of phosphorane **7** slow cyclization occurred in the solvents of high donor ability (THF, CH_3CN, MeOH and pyridine). The emergence of a signal of high chemical shift at ca. –52 was also observed as in the case of **6**. Additionally, an equilibrium (Scheme 2-2) between intra- (lower chemical shift) and intermolecular (higher chemical shift) hydrogen bonding species could be observed in Et_2O, acetone and CH_3CN. No immediate cyclization was observed with phosphorane **8b**. In contrast with **6** and **7** a signal of lower chemical shift appeared upon dissolution of crystals containing 1 equivalent of solvent (EtOH) molecules in non-polar solvents (hexane, benzene and $CHCl_3$). Coupled with the X-ray structures these results suggest that all three compounds exist as an equilibrating mixture of intermolecularly and intramolecularly hydrogen bonding species in solution and the ratio of the two is dependent on the solvent. In the case of **8**, the bulky *t*-Bu group suppresses intramolecular hydrogen bonding by steric repulsion in the conformation required for it. The general trend of the species (**8b**) of intermolecular hydrogen bonding having a higher chemical shift than those of intramolecular interaction (**8a**) can be attributed to the shorter distance between the phosphorus and the hydroxy oxygen in the intermolecular

hydrogen bonding **8b** (2.84 Å) compared with that of **8a** (3.131 Å) as evident from the X-ray structures.

Scheme 2-2.

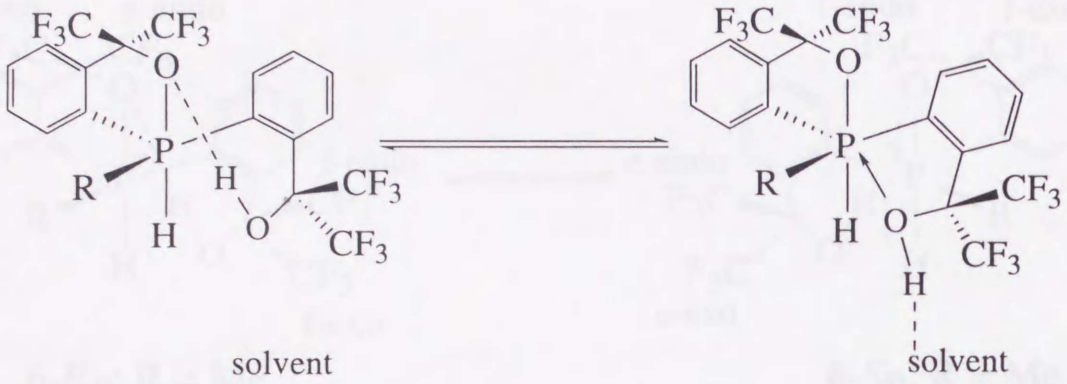

Table 2-2. ^{31}P NMR Chemical Shifts of Phosphoranes **6**–**8** in Various Solvents at RT.

solvent	**6**	**7**	**8b**
hexane	–53.0 [b]	–35.5	–15.5 (**8a**) : –43.9 = 1 :1
benzene	–52.6 [b]	–34.2	–14.5 (**8a**) : –42.8 = 3 :2
$CHCl_3$	–51.9 [b]	–34.4	–14.7 (**8a**) : –43.0 = 2 :1
Et_2O	–53.4 [b]	–35.0 : –52.3 = 3 : 1	–42.2
acetone	–68.8 [b]	–31.3 : –51.4 = 1 : 3	–40.1
THF	–70.6 [b]	–53.0 [b]	–41.2
CH_3CN	a	–31.7 : –51.4 = 1 : 1 [b]	–39.7
MeOH	a	–52.3 [b]	–40.6
pyridine	a	–53.2 [b]	–39.3

[a] Only the signal of the bicyclic compound was observed.
[b] The signal of the bicyclic compound was also observed.

4. Kinetic Studies and Mechanism of Inversion of Configuration at Phosphorus in Monocyclic 10-P-5 P–H (Apical) Phosphoranes.

Scheme 2-3.

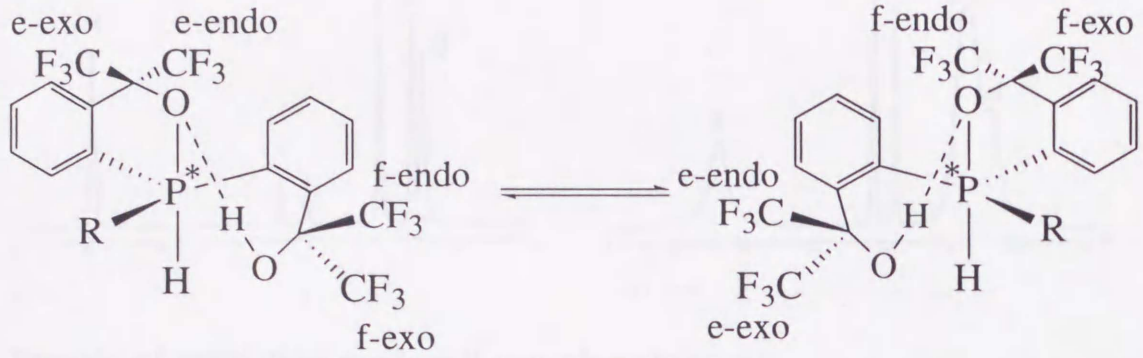

6-R_P; R = Me
7-R_P; R = *n*-Bu
8-R_P; R = *t*-Bu

6-S_P; R = Me
7-S_P; R = *n*-Bu
8-S_P; R = *t*-Bu

Although ^{19}F NMR spectrum of monocyclic 10-P-5 P–H (apical) phosphoranes **6** (R = Me) and **7** (R = *n*-Bu) in toluene-d_8 not only at low temperature but also at rt showed four signals (a–d) for the four CF_3 groups, we could observe coalescence of peak b and c at 327 and 363 K (Fig. 2-5 and 2-6), respectively. In the case of **8** (R = *t*-Bu) we could not observe the coalescence of them. From ^{19}F HOMO decoupling in $CDCl_3$ at rt of **7** (Fig. 2-7), signals a (δ –72.9), b (δ –76.3), c (δ –76.8) and d (δ –77.0) were found to be of CF_3 groups of f-endo, e-exo, f-exo and e-endo in **7-R_P** (Scheme 2-3), respectively. Correlated exchange between e-exo and f-exo, and e-endo and f-endo takes place for the dynamical process. Thus the inversion of phosphoranes **6** and **7** should be explained with a combination of BPR and bond switching.

Figure 2-5. ^{19}F NMR spectra of **6** in toluene-d_8

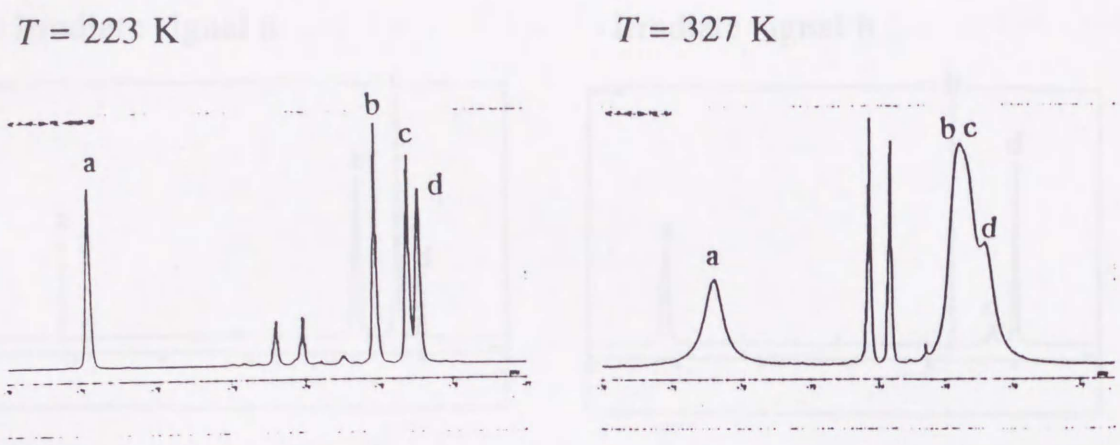

* Signals of cycliztion product **9** was also observed.

Figure 2-6. ^{19}F NMR spectra of **7** in toluene-d_8

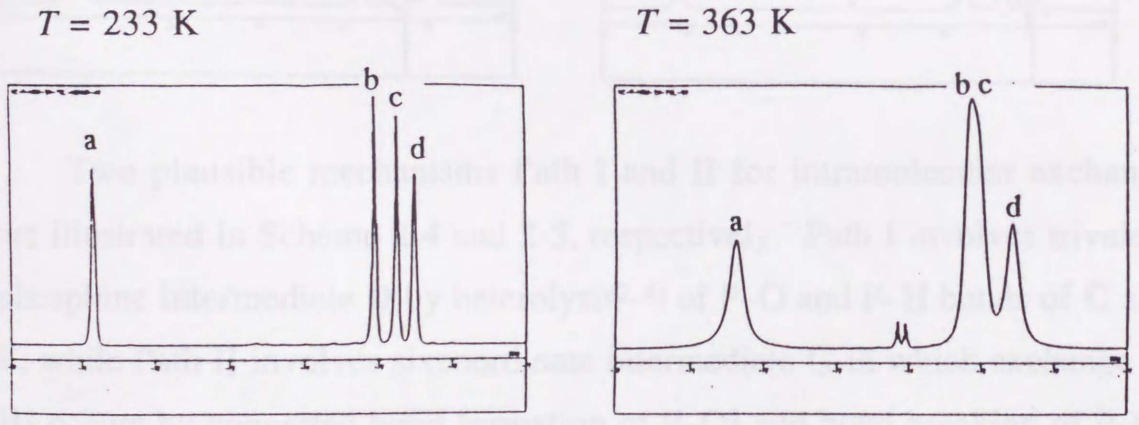

* Signals of cycliztion product **10** was also observed.

Figure 2-7. HOMO decouple of ^{19}F NMR spectra of **7** in $CDCl_3$

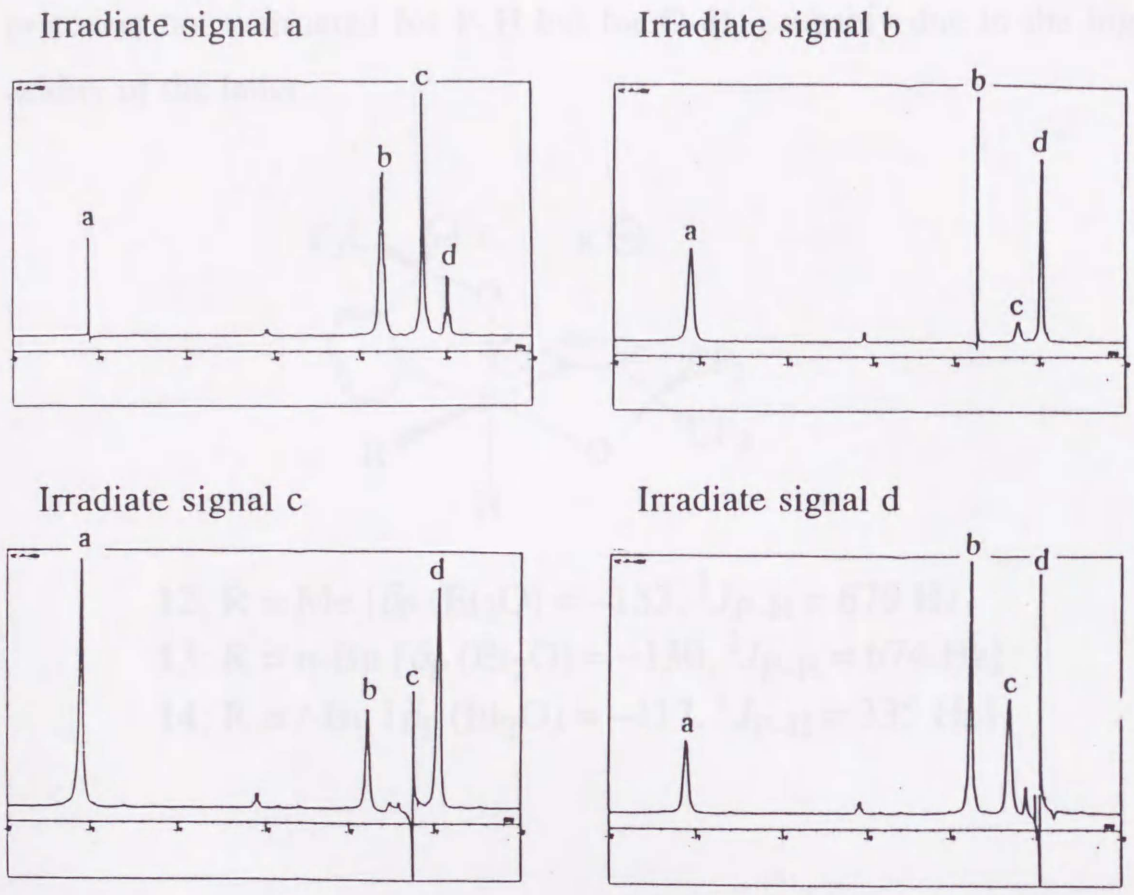

Two plausible mechanisms Path I and II for intramolecular exchange are illustrated in Scheme 2-4 and 2-5, respectively. Path I involves trivalent phosphine intermediate **D** by heterolysis[2, 4] of P–O and P–H bonds of **C** and **E**, while Path II involves sixcoordinate intermediate **G** in which exchange of H^2 occurs by concerted bond formation of P–O^2 and bond breaking of P–O^1 (R_P to S_P), that is, bond switching. When an equivalent of CD_3OD was added to the solution of phosphorane **6** and **7** in toluene-d_8 at rt, the magnitude of integration of O–H proton decreased much more rapidly than that of P–H proton. Furthermore, we could observe monoanionic derivatives **12–14** retaining the P–H bonding in Et_2O by the treatment of the solution of **6–8** in Et_2O with excess amount of aqueous KOH. This implies

that it is facile to attain the hexacoordinate state in P with compounds **6–8**. Therefore, we should believe Path II to be the case in which the exchange of proton is not warranted for P–H but for O–H, probably due to the higher acidity of the latter.

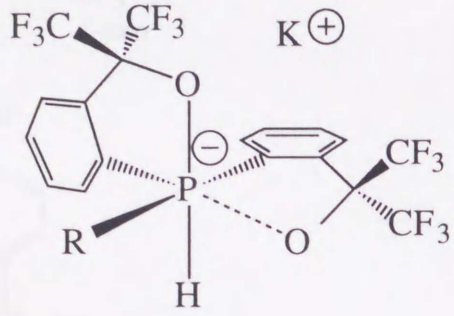

12; R = Me [δ_P (Et_2O) = –153, $^1J_{P-H}$ = 679 Hz]
13; R = *n*-Bu [δ_P (Et_2O) = –130, $^1J_{P-H}$ = 674 Hz]
14; R = *t*-Bu [δ_P (Et_2O) = –117, $^1J_{P-H}$ = 335 Hz]

Scheme 2-4. <Path I>

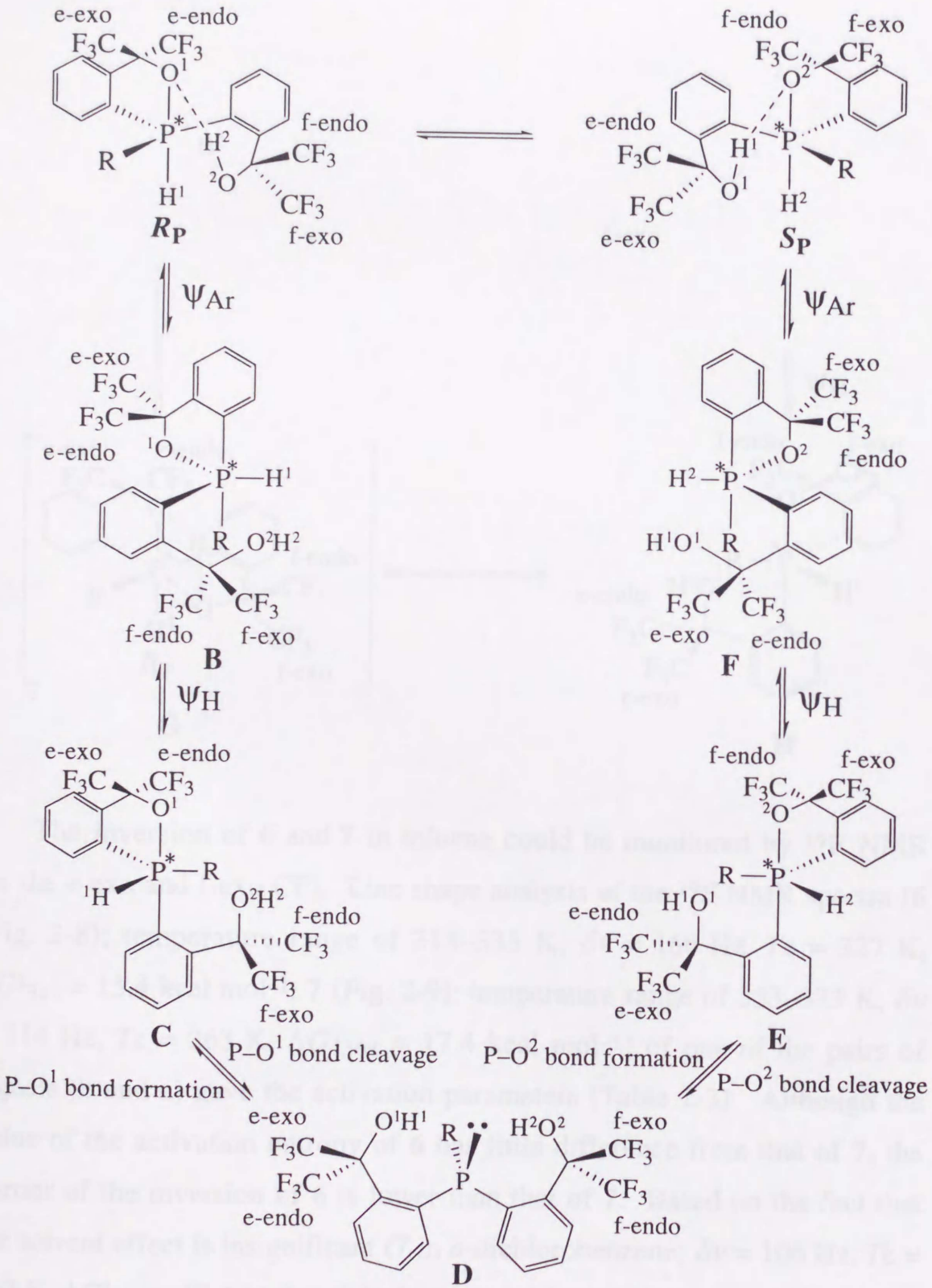

Scheme 2-5. <Path II>

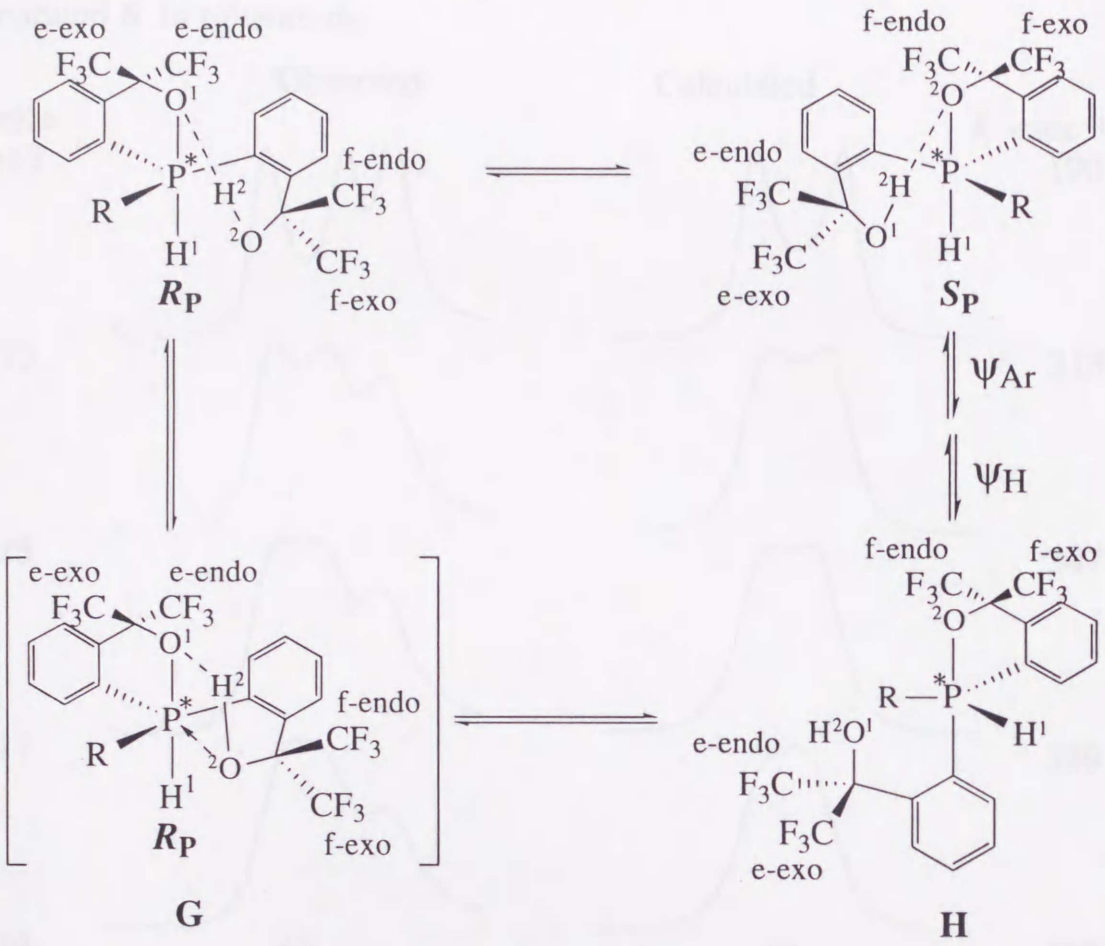

The inversion of **6** and **7** in toluene could be monitored by ^{19}F NMR for the e-exo and f-exo CF_3. Line shape analysis of the ^{19}F NMR spectra [**6** (Fig. 2-8); temperature range of 313–335 K, $\delta\nu$ = 166 Hz, Tc = 327 K, $\Delta G^{\ddagger}_{327}$ = 15.4 kcal mol^{-1}: **7** (Fig. 2-9); temperature range of 353–373 K, $\delta\nu$ = 114 Hz, Tc = 363 K, $\Delta G^{\ddagger}_{363}$ = 17.4 kcal mol^{-1}] of one of the pairs of signals (b and c) gave the activation parameters (Table 2-3). Although the value of the activation entropy of **6** has little difference from that of **7**, the barrier of the inversion of **6** is lower than that of **7**. Based on the fact that the solvent effect is insignificant (**7** in *o*-dichlorobenzene; $\delta\nu$ = 106 Hz, Tc = 363 K, $\Delta G^{\ddagger}_{363}$ = 17.4 kcal mol^{-1}), bond switching takes place rapidly and the rate determining step exists in the BPR process.

Figure 2-8. Observed and Calculated line shape for CF_3 groups in compound **6** in toluene-d_8.

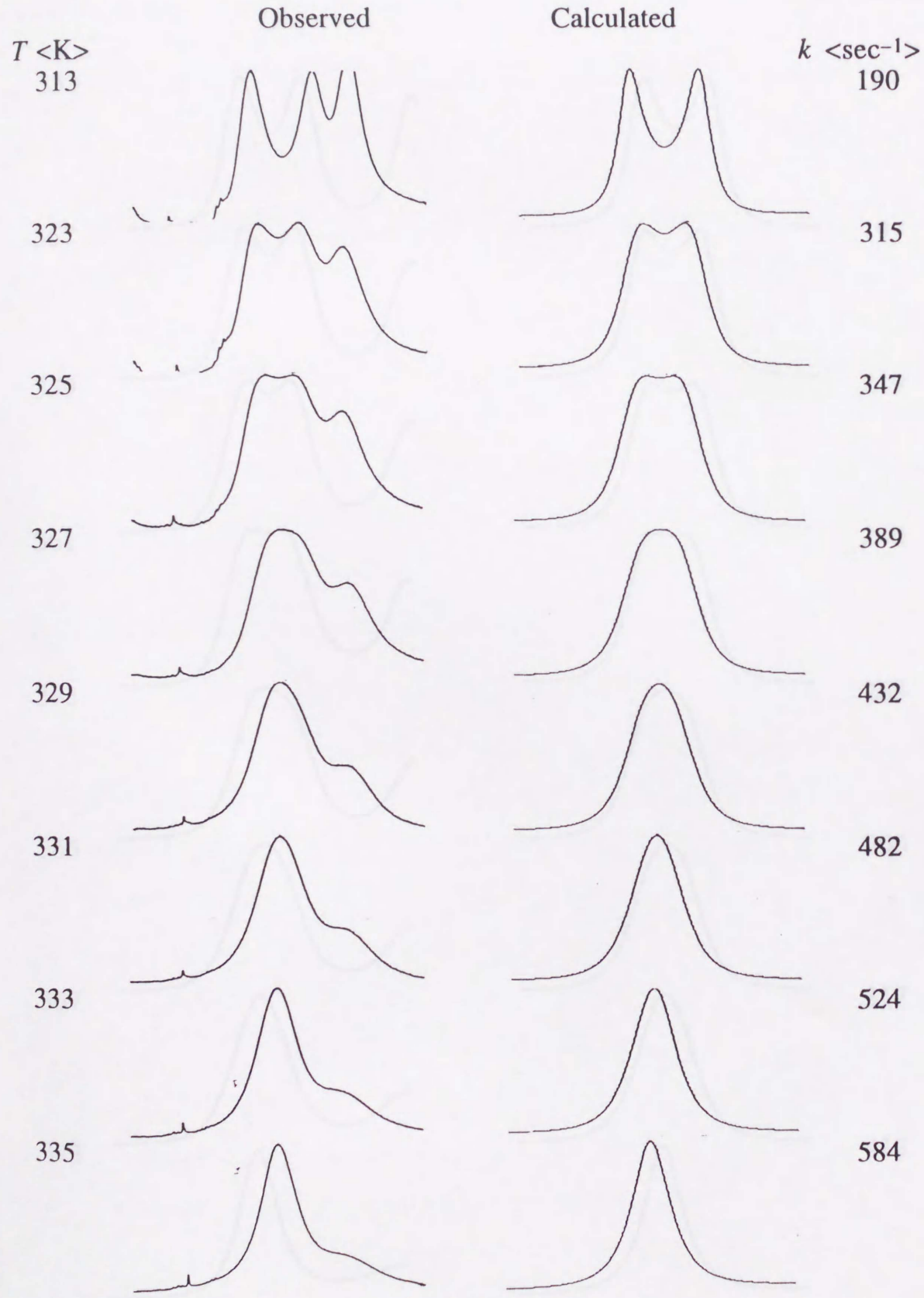

Figure 2-9. Observed and Calculated line shape for CF_3 groups in compound **7** in toluene-d_8.

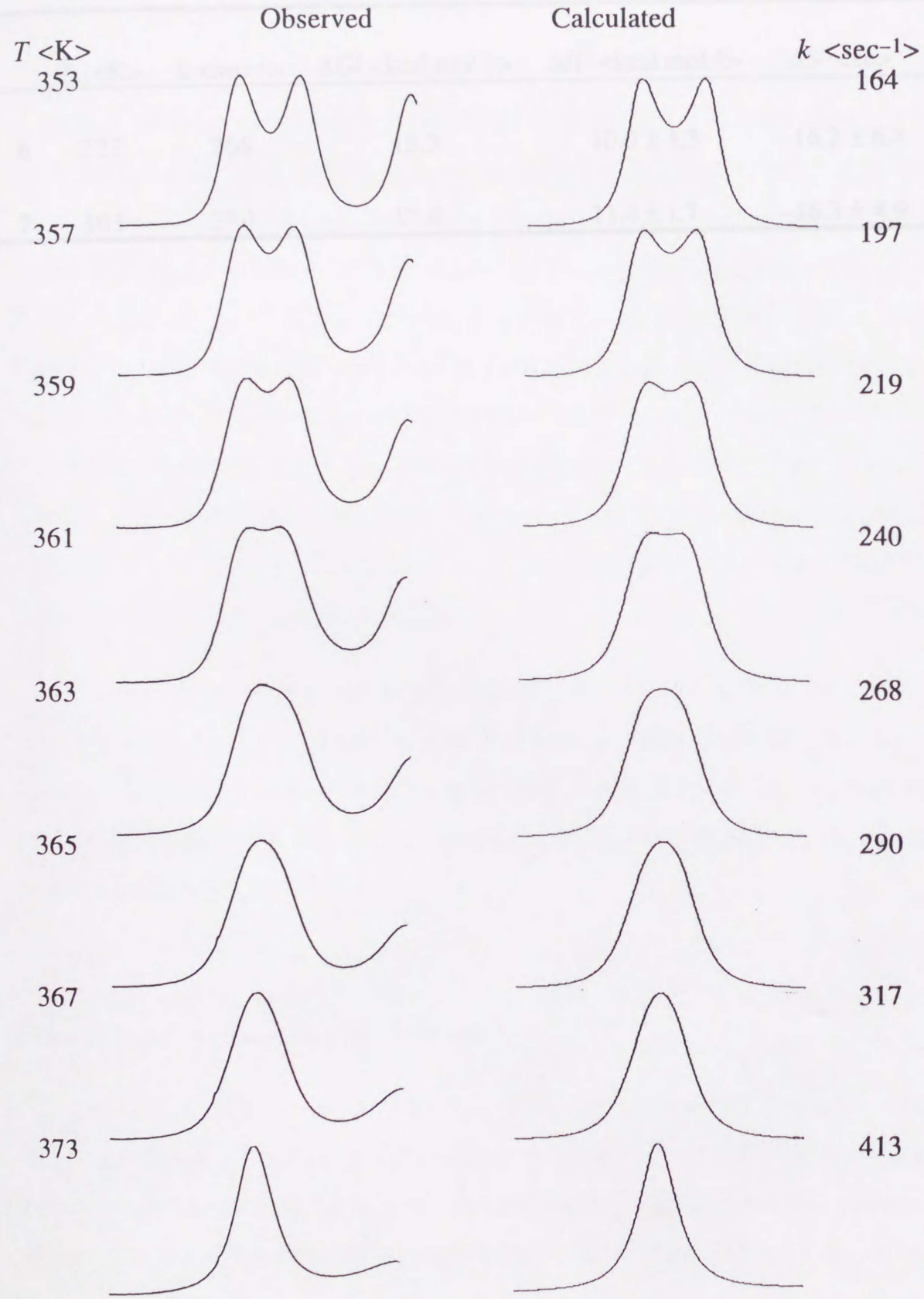

Table 2-3. Kinetic parameters of the inversion of **6** and **7** in toluene-d_8

	T_c <K>	k <sec^{-1}>	$\Delta G^{\ddagger}$ <kcal mol^{-1}>	$\Delta H^{\ddagger}$ <kcal mol^{-1}>	$\Delta S^{\ddagger}$ <eu>
6	327	268	15.3	10.0 ± 1.3	–16.2 ± 6.8
7	363	290	17.4	11.4 ± 1.7	–16.3 ± 4.9

C. Experimental Section

Melting points were measured with a Yanaco micro melting point apparatus and are uncorrected. ^{1}H NMR (400 MHz), ^{13}C (100 MHz), ^{19}F (376 MHz), ^{31}P (162 MHz) spectra were recorded on a JEOL EX-400 spectrometer. ^{1}H NMR chemical shifts (δ) are given in ppm downfield from internal Me_4Si, determined by Me_4Si or by residual chloroform-*d* (δ = 7.26), acetone-d_6 (δ = 2.0) or toluene-d_8 (CD_3 group; of δ = 2.31). ^{13}C NMR chemical shifts (δ) are given in ppm downfield from internal Me_4Si, determined by Me_4Si or by chloroform (δ = 77.0) or acetone (δ = 30.3). ^{19}F NMR chemical shifts (δ) are given in ppm downfield from external $CFCl_3$. ^{31}P NMR chemical shifts (δ) are given in ppm downfield from external 85 % H_3PO_4. Elemental analyses were performed on a Perkin-Elmer 2400 CHN elemental analyzer.

All reactions were carried out under N_2. Et_2O and THF were freshly distilled from Na-benzophenone, and all other solvents were distilled from CaH_2. Methyllithium, *n*-butyllithium and *t*-butyllithium were used as received. Preparative thin layer chromatography was carried out on plates of Merck silica gel 60 GF254.

Reaction of 1 with Methyllithium.

MeLi (*c* 1.14 M in Et_2O, 5.67 mL, 6.46 mmol) was added to a solution of phosphorane **1** (460 mg, 0.891 mmol) in Et_2O (10 mL) at –78 °C. After removal of the cooling bath, the solution was stirred at room temperature (rt) for 50 min. The solution was quenched with 1 M HCl (3 mL), extracted

with Et_2O (3 x 30 mL), dried with $MgSO_4$, and concentrated in vacuo. Separation and purification of the residue was carried out on TLC (hexane–CH_2Cl_2 = 5 : 1) to give **6** (322 mg, 68 %) and **9** (105 mg, 22 %) as white solids. Recrystallization of **6** from hexane–CH_2Cl_2 gave crystals for X-ray analysis:

[*TBPY*-5-15]-1-Hydro-1-methyl-1-{2-[2,2,2-trifluoro-1-hydroxy-1-(trifluoromethyl)ethyl]phenyl}-3,3-bis(trifluoromethyl)-[3*H*,2,1,λ^5-benzoxaphosphole] (6): Mp 101 °C; ^{1}H NMR ($CDCl_3$) δ 8.86 (br s, 1H), 8.10–7.90 (m, 1H), 7.79 (br s, 4H), 7.55–7.20 (m, 3H), 6.37 (dq, $^1J_{H\text{-}P}$ = 276 Hz, $^3J_{H\text{-}H}$ = 3.9 Hz, 1H), 2.44 (dd, $^2J_{H\text{-}P}$ = 14.7 Hz, $^3J_{H\text{-}H}$ = 3.9 Hz, 3H), ^{1}H NMR (toluene-d_8) δ 9.26 (br s, 1H), 8.04 (br s, 1H), 7.71 (br s, 1H), 7.57–6,92 (m, 6H), 6.21 (br d, $^1J_{H\text{-}P}$ = 274 Hz, 1H), 2.44 (dd, $^2J_{H\text{-}P}$ = 14.6 Hz, $^3J_{H\text{-}H}$ = 3.9 Hz, 3H); ^{13}C NMR ($CDCl_3$) δ 136.7 (d, $^2J_{C\text{-}P}$ = 11.0 Hz), 134.8 (br s), 133.7 (d, $^4J_{C\text{-}P}$ = 3.7 Hz), 133.5 (br s), 131.4 (d, $^3J_{C\text{-}P}$ = 14.7 Hz), 131.1 (br d, $^2J_{C\text{-}P}$ = 12.9 Hz), 129.8 (br s), 129.6 (d, $^1J_{C\text{-}P}$ = 123.2 Hz), 129.1 (br d, $^3J_{C\text{-}P}$ = 14.7 Hz), 128.3 (d, $^1J_{C\text{-}P}$ = 141.3 Hz), 128.2 (d, $^2J_{C\text{-}P}$ = 25.7 Hz), 125.4 (q, $^1J_{C\text{-}F}$ = 286.8 Hz), 124.8 (d, $^3J_{C\text{-}P}$ = 14.7 Hz), 122.6 (q, $^1J_{C\text{-}F}$ = 284.8 Hz), 122.4 (q, $^1J_{C\text{-}F}$ = 290.4 Hz), 122.2 (q, $^1J_{C\text{-}F}$ = 290.5 Hz), 79.0 (sept, $^2J_{C\text{-}F}$ = 35.0 Hz), 78.9 (sept, $^2J_{C\text{-}F}$ = 33.1 Hz), 22.4 (d, $^1J_{C\text{-}P}$ = 99.3 Hz); ^{19}F NMR ($CDCl_3$) δ –72.9 (br s, 3F), –76.3 (br s, 3F), –76.9 (br s, 3F), –77.0 (br s, 3F), ^{19}F NMR (toluene-d_8, T = 223 K) δ –71.1 (br s, 3F), –75.0 (q, $^2J_{F\text{-}F}$ = 8.5 Hz, 3F), –75.4 (q, $^2J_{F\text{-}F}$ = 7.9 Hz, 3F), –75.5 (br s, 3F), ^{19}F NMR (toluene-d_8, T = 327 K) δ –71.6 (br s, 3F), –75.2 (br s, 6F), –75.6 (br s, 3F); ^{31}P NMR ($CDCl_3$) δ –51.9; Anal. calcd for $C_{19}H_{13}F_{12}O_2P$: C, 42.88; H, 2.46. Found: C, 42.75; H, 2.37.

[*TBPY*-5-11]-1-Methyl-3,3,3',3'-tetrakis(trifluoromethyl)-1,1'-spirobi[3*H*,2,1,λ^5-benzoxaphosphole] (9): Mp 134 °C; ^{1}H NMR ($CDCl_3$) δ 8.43–8.38 (m, 2H), 7.79–7.69 (m, 6H), 2.11 (d, $^2J_{H\text{-}P}$ = 16.6 Hz, 3H); ^{13}C NMR ($CDCl_3$) δ 136.8 (d, $^3J_{C\text{-}P}$ = 9.1 Hz), 136.1 (d, $^2J_{C\text{-}P}$ = 20.2 Hz), 133.7 (d, $^4J_{C\text{-}P}$ = 3.7 Hz), 131.4 (d, $^2J_{C\text{-}P}$ = 14.7 Hz), 130.6 (d, $^1J_{C\text{-}P}$ = 176.5 Hz), 124.8 (d, $^3J_{C\text{-}P}$ = 14.7 Hz), 122.6 (q, $^1J_{C\text{-}F}$ = 285.0 Hz), 122.4 (q, $^1J_{C\text{-}F}$ = 288.6 Hz), 81.3 (sept, $^2J_{C\text{-}F}$ = 31.2 Hz), 25.2 (d, $^1J_{C\text{-}P}$ = 125.0 Hz); ^{19}F NMR ($CDCl_3$) δ –75.1 (q, $^4J_{F\text{-}F}$ = 9.5 Hz, 6F), –75.4 (q, $^4J_{F\text{-}F}$ = 9.5 Hz, 6F); ^{31}P NMR ($CDCl_3$) δ –22.6; Anal. calcd for $C_{19}H_{11}F_{12}O_2P$: C, 43.04; H, 2.09. Found: C, 42.83; H, 1.86.

Reaction of 1 with Butyllithium.

n-BuLi (*c* 1.62 M in hexane, 2.00 mL, 3.24 mmol) was added to a solution of phosphorane **1** (500 mg, 0.969 mmol) in Et_2O (10 mL) at –78 °C. After removal of the cooling bath, the solution was stirred at rt for 60 min. The solution was quenched with 1 M HCl (10 mL), extracted with Et_2O (3 x 30 mL), dried with $MgSO_4$, and concentrated in vacuo. Purification of the residue was carried out on TLC (hexane–CH_2Cl_2 = 5 : 1) to give **7** (500 mg, 90 %) and **10** (47.2 mg, 9 %) as white solids. Recrystallization of **7** from hexane–CH_2Cl_2 gave crystals for X-ray analysis:

[*TBPY*-5-15]-1-Butyl-1-hydro-1-{2-[2,2,2-trifluoro-1-hydroxy-1-(trifluoromethyl)ethyl]phenyl}-3,3-bis(trifluoromethyl)-[3*H*,2,1λ^5-benzoxaphosphole] (7): Mp 119 °C; ^{1}H NMR ($CDCl_3$) δ 9.13 (br s, 1H), 8.07–8.02 (m, 1H), 7.89–7.85 (m, 1H), 7.80–7.72 (m, 3H), 7.55–

7.48 (m, 1H), 7.45–7.41 (m, 1H), 7.36–7.32 (m, 1H), 6.16 (dd, $^{1}J_{H\text{-}P}$ = 273 Hz, $^{3}J_{H\text{-}H}$ = 5.9 Hz, 1H), 3.21–3.06 (m, 1H), 2.69–2.52 (m, 1H), 1.65–1.46 (m, 1H), 1.45–1.36 (m, 2H), 1.35–1.22 (m, 1H), 0.88 (t, $^{3}J_{H\text{-}H}$ = 7.3 Hz, 3H), ^{1}H NMR (toluene-d_8) δ 9.44 (br s, 1H), 8.06 (br s, 1H), 7.73 (br s, 1H), 7.64–6.93 (m, 6H), 6.14 (dd, $^{1}J_{H\text{-}P}$ = 279 Hz, 1H), 3.41–3.35 (m, 1H), 2.84–2.79 (m, 1H), 1.58–1.50 (m, 1H), 1.39–1.28 (m, 3H), 0.92 (t, $^{3}J_{H\text{-}H}$ = 7.3 Hz, 3H); ^{13}C NMR ($CDCl_3$) δ 136.6 (d, $^{2}J_{C\text{-}P}$ = 12.8 Hz), 136.1 (d, $^{1}J_{C\text{-}P}$ = 139.7 Hz), 134.7, 134.3 (d, $^{3}J_{C\text{-}P}$ = 14.7 Hz), 134.1 (d, $^{3}J_{C\text{-}P}$ = 14.7 Hz), 130.8 (d, $^{2}J_{C\text{-}P}$ = 16.5 Hz), 130.2, 129.8 (d, $^{1}J_{C\text{-}P}$ = 139.7 Hz), 129.7, 129.1 (d, $^{2}J_{C\text{-}P}$ = 16.6 Hz), 127.0 (d, $^{3}J_{C\text{-}P}$ = 12.9 Hz), 123.4 (q, $^{1}J_{C\text{-}F}$ = 290.4 Hz), 122.7 (q, $^{1}J_{C\text{-}F}$ = 286.8 Hz), 122.5 (q, $^{1}J_{C\text{-}F}$ = 286.8 Hz), 122.3 (q, $^{1}J_{C\text{-}F}$ = 288.6 Hz), 78.9 (sept, $^{2}J_{C\text{-}F}$ = 31.2 Hz), 78.6 (sept, $^{2}J_{C\text{-}F}$ = 31.2 Hz), 34.7 (d, $^{1}J_{C\text{-}P}$ = 90.1 Hz), 27.7, 23.5 (d, $^{2}J_{C\text{-}P}$ = 23.9 Hz), 13.6; ^{19}F NMR ($CDCl_3$) δ –72.9 (br s, 3F), –76.3 (q, $^{4}J_{F\text{-}F}$ = 9.2 Hz, 3F), –76.8 (q, $^{4}J_{F\text{-}F}$ = 8.2 Hz, 3F), –77.0 (qq, $^{4}J_{F\text{-}F}$ = 9.2 Hz, $^{9}J_{F\text{-}F}$ = 4.9 Hz, 3F), ^{19}F NMR (toluene-d_8, 233 K) δ –71.2 (br s, 3F), –74.9 (q, $^{4}J_{F\text{-}F}$ = 8.6 Hz, 3F), –75.2 (q, $^{4}J_{F\text{-}F}$ = 8.7 Hz, 3F), –75.5 (br s, 3F), ^{19}F NMR (toluene-d_8, 363 K) δ –71.6 (br s, 3F), –74.9 (br s, 6F), –75.4 (br s, 3F); ^{31}P NMR ($CDCl_3$) δ –34.4; Anal. calcd for $C_{22}H_{19}F_{12}O_2P$: C, 46.01; H, 3.33. Found: C, 46.09; H, 3.24.

[*TBPY*-5-11]-1-Butyl-3,3,3',3'-tetrakis(trifluoromethyl)-1,1'-spirobi[3*H*,2,1λ^5-benzoxaphosphole] (10): Mp 109 °C; ^{1}H NMR ($CDCl_3$) δ 8.43–8.38 (m, 2H), 7.72–7.58 (m, 6H), 2.34 (ddt, $^{2}J_{H\text{-}P}$ = 28.3 Hz, $^{2}J_{H\text{-}H}$ = 12.2 Hz, $^{3}J_{H\text{-}H}$ = 4.9 Hz, 1H), 2.20 (ddt, $^{2}J_{H\text{-}P}$ = 12.2 Hz, $^{2}J_{H\text{-}H}$ = 12.2 Hz, $^{3}J_{H\text{-}H}$ = 4.4 Hz, 1H), 1.86–1.70 (m, 1H), 1.32–1.20 (m, 3H), 0.81 (t, $^{3}J_{H\text{-}H}$ = 7.3 Hz, 3H); ^{13}C NMR ($CDCl_3$) δ 137.1 (d, $^{3}J_{C\text{-}P}$ = 9.2 Hz), 136.2 (d, $^{2}J_{C\text{-}P}$ = 18.4 Hz), 133.6 (d, $^{4}J_{C\text{-}P}$ = 3.6 Hz), 131.3(d, $^{2}J_{C\text{-}P}$ = 14.7 Hz), 130.3 (d,

$^{1}J_{C\text{-}P}$ = 160.0 Hz), 124.8 (d, $^{3}J_{C\text{-}P}$ = 14.7 Hz), 122.7 (q, $^{1}J_{C\text{-}F}$ = 286.8 Hz), 122.5 (q, $^{1}J_{C\text{-}F}$ = 290.5 Hz), 81.3 (sept, $^{2}J_{C\text{-}F}$ = 31.2 Hz), 39.2 (d, $^{1}J_{C\text{-}P}$ = 115.8 Hz), 25.3 (d, $^{3}J_{C\text{-}P}$ = 7.4 Hz), 23.6 (d, $^{2}J_{C\text{-}P}$ = 23.9 Hz), 13.2; ^{19}F NMR ($CDCl_3$) δ –75.1 (q, $^{4}J_{F\text{-}F}$ = 9.3 Hz, 6F), –75.4 (q, $^{4}J_{F\text{-}F}$ = 9.3 Hz, 6F); ^{31}P NMR ($CDCl_3$) δ –18.8; Anal. calcd for $C_{22}H_{17}F_{12}O_2P$: C, 46.17; H, 2.99. Found: C, 46.19; H, 2.84.

Reaction of 1 with *t*-Butyllithium.

t-BuLi (*c* 1.70 M in pentane, 3.60 mL, 6.12 mmol) was added to a solution of phosphorane **1** (1.00 g, 1.94 mmol) in Et_2O (20 mL) at –78 °C. After removal of the cooling bath, the solution was stirred at rt for 30 min. The solution was quenched with 1 M HCl (20 mL), extracted with Et_2O (3 x 50 mL), dried with $MgSO_4$, and concentrated in vacuo. Purification of the residue was carried out on TLC (hexane–CH_2Cl_2 = 5 : 1) to give a mixture (1.01 g, 92 %) of **8a** and **8b** as white powder.

[*TBPY*-5-15]-1-(1,1-Dimethyl)ethyl-1-hydro-1-{2-[2,2,2-trifluoro-1-hydroxy-1-(trifluoromethyl)ethyl]phenyl}-3,3-bis(trifluoromethyl)-[3*H*,2,1λ^5-benzoxaphosphole] (8a): Mp 108 °C; ^{1}H NMR ($CDCl_3$) δ 8.58 (br s, 1H), 8.00–7.89 (m, 1H), 7.80–7.48 (m, 7H), 5.81 (d, $^{1}J_{H\text{-}P}$ = 273Hz, 1H), 1.30 (d, $^{3}J_{H\text{-}P}$ = 23.4 Hz, 9H); ^{13}C NMR ($CDCl_3$) δ 139.3 (d, $^{1}J_{C\text{-}P}$ = 139.7 Hz), 136.7 (d, $^{1}J_{C\text{-}P}$ = 132.4 Hz), 136.2 (d, $J_{C\text{-}P}$ = 16.6 Hz), 134.6 (d, $J_{C\text{-}P}$ = 12.9 Hz), 134.0, 131.3 (d, $J_{C\text{-}P}$ = 14.7 Hz), 130.6 (d, $J_{C\text{-}P}$ = 14.7 Hz), 129.5, 129.2 (d, $J_{C\text{-}P}$ = 16.6 Hz), 129.0, 128.8 (d, $J_{C\text{-}P}$ = 3.6 Hz), 126.5 (d, $J_{C\text{-}P}$ = 16.6 Hz), 123.4 (d, $^{1}J_{C\text{-}F}$ = 286.8 Hz), 123.1

(d, $^{1}J_{C\text{-}F}$ = 290.4 Hz), 122.7 (d, $^{1}J_{C\text{-}F}$ = 288.6 Hz), 122.3 (d, $^{1}J_{C\text{-}F}$ = 288.6 Hz), 79.7 (d, $^{2}J_{C\text{-}F}$ = 31.3 Hz), 78.4 (d, $^{1}J_{C\text{-}F}$ = 31.3 Hz), 43.8 (d, $^{1}J_{C\text{-}P}$ = 90.1 Hz), 15.1; ^{19}F NMR ($CDCl_3$) δ –73.4 (q, $^{4}J_{F\text{-}F}$ = 9.5 Hz, 3F), –73.5 (q, $^{4}J_{F\text{-}F}$ = 9.5 Hz, 3F), –74.6 (q, $^{4}J_{F\text{-}F}$ = 9.1 Hz, 3F), –76.1 (q, $^{4}J_{F\text{-}F}$ = 10.7 Hz, 3F); ^{31}P NMR ($CDCl_3$) δ –14.7; Anal. calcd for $C_{22}H_{19}F_{12}O_2P$: C, 46.01; H, 3.33. Found: C, 45.85; H, 3.23.

[*TBPY*-5-15]-1-(1,1-Dimethyl)ethyl-hydro-1-{2-[2,2,2-trifluoro-1-hydroxy-1-(trifluoromethyl)ethyl]phenyl}-3,3-bis(trifluoromethyl)-[3*H*,2,1λ^5-benzoxaphosphole] (8b): Mp 83–84 °C (containing EtOH); ^{1}H NMR (acetone-d_6) δ 8.77–8.72 (m, 1H), 7.87–7.82 (m, 1H), 7.75–7.63 (m, 4H), 7.63–7.54 (m, 2H), 7.48 (s, 1H), 6.07 (d, $^{1}J_{H\text{-}P}$ = 293 Hz, 1H), 1.17 (d, $^{3}J_{H\text{-}P}$ = 19.5 Hz, 9H); ^{13}C NMR (acetone-d_6) δ 141.3 (d, $^{1}J_{C\text{-}P}$ = 141.3 Hz), 139.0 (d, $^{4}J_{C\text{-}P}$ = 5.5 Hz), 137.1 (d, $^{2}J_{C\text{-}P}$ = 14.7 Hz), 136.1 (d, $^{2}J_{C\text{-}P}$ = 14.7 Hz), 135.1 (d, $^{1}J_{C\text{-}P}$ = 139.7 Hz), 133.9, 132.7 (d, $^{2}J_{C\text{-}P}$ = 3.6 Hz), 131.3 (d, $^{2}J_{C\text{-}P}$ = 16.6 Hz), 130.7, 130.1 (d, $^{3}J_{C\text{-}P}$ = 12.9 Hz), 128.6 (d, $^{3}J_{C\text{-}P}$ = 7.4 Hz), 125.9 (d, $^{3}J_{C\text{-}P}$ = 12.9 Hz), 125.2 (q, $^{1}J_{C\text{-}F}$ = 286.8 Hz), 124.7 (q, $^{1}J_{C\text{-}F}$ = 288.6 Hz), 124.6 (q, $^{1}J_{C\text{-}F}$ = 290.5 Hz), 124.5 (q, $^{1}J_{C\text{-}F}$ = 288.7 Hz), 81.0 (sept, $^{2}J_{C\text{-}F}$ = 29.5 Hz), 80.0 (sept, $^{2}J_{C\text{-}F}$ = 29.4 Hz), 38.6 (d, $^{1}J_{C\text{-}P}$ = 97.5 Hz), 19.4; ^{19}F NMR (acetone-d_6) δ –73.3 (qq, $^{4}J_{F\text{-}F}$ = 8.9 Hz, $^{9}J_{F\text{-}F}$ = 3.1 Hz, 3F), –73.6 (q, $^{4}J_{F\text{-}F}$ = 9.5 Hz, 3F), –74.3 (q, $^{4}J_{F\text{-}F}$ = 8.6 Hz, 3F), –75.5 (qq, $^{4}J_{F\text{-}F}$ = 9.2 Hz, $^{9}J_{F\text{-}F}$ = 2.8 Hz, 3F); ^{31}P NMR (acetone-d_6) δ –40.1; Anal. (containing EtOH) calcd for $C_{24}H_{25}F_{12}O_3P$: C, 46.46; H, 4.06. Found: C, 46.26; H, 3.90.

NMR data was taken after removal of EtOH.

Crystallographic Studies.

Crystal Structure of 6, 7, 8a and 8b

Crystal data and numerical details of the structure determinations are given in Table 2-4 and 2-5. Crystals suitable for X-ray structure determination were mounted on a Mac Science MXC3 diffractometer and irradiated with graphite-monochromated Mo $K\alpha$ radiation (λ = 0.71073) (for **6**) or graphite-monochromated Cu $K\alpha$ radiation (λ = 1.54178) (for **7**, **8a** and **8b**) for collection. Lattice parameters were determined by least-squares fitting of 31 reflections for all compounds with $20° < 2\theta < 35°$, $55° < 2\theta < 60°$, $41° < 2\theta < 45°$ and $31° < 2\theta < 35°$ for **6**, **7**, **8a** and **8b**, respectively. Data were collected with the ω scan mode. All data were corrected for absorption[9] and extinction[10]. The structures were solved by a direct method with the Shelx 86 program[11]. Refinement on F was carried out by full-matrix least squares. All non-hydrogen atoms were refined with anisotropic thermal parameters. All hydrogen atoms in **6** and **8b**, and the hydroxyl hydrogen atoms and apical hydrogen in **7** and **8a** were located from a difference Fourier map calculated at the final stage of structural analysis. The other hydrogen atoms in **7** and **8a** were included in the refinement on calculated positions (C–H = 1.0 Å) riding on their carrier atoms with isotropic thermal parameters. All the computations were carried out on a Titan-750 computer.

Table 2-4. Details of the crystallographic data collection for **6** and **7**

Compound	**6**	**7**
Formula	$C_{19}H_{13}F_{12}O_2P_1$	$C_{22}H_{19}F_{12}O_2P_1$
Mol wt	532.27	574.40
Cryst syst	Triclinic	Monoclinic
Space group	*P*-1	$P2_1/n$
Cryst dimens, mm	0.40 x 0.40 x 0.10	0.60 x 0.50 x 0.40
Color	colorless	colorless
Habit	prism	prism
a, Å	9.214 (3)	16.653 (4)
b, Å	10.777 (4)	12.570 (3)
c, Å	11.518 (3)	11.523 (3)
α, deg	93.63 (2)	90
β, deg	92.26 (2)	92.72 (2)
γ, deg	113.05 (2)	90
V, Å^3	1047.7 (6)	2409 (1)
Z	2	4
D_{obs}, D_{calc}, g cm^{-3}	-, 1.69	-, 1.58
Abs coeff, cm^{-1}	1.96	19.25
F (000)	532	1160
Radiation; λ, Å	Mo $K\alpha$, 0.71073	Cu $K\alpha$, 1.54178
Temp, °C	23±1	23±1
$2\theta_{max}$, deg	55.0	130
Scan rate, deg/min	3	6
Linear decay, %	—	—
Data collected	$\pm h$, $\pm k$, $-l$	$\pm h$, $-k$, $\pm l$
Total data collcd, unique, obsd	3925, 3686, 2330 ($\|F\| > 1.56\ \sigma(\|F\|)$)	4518, 4029, 3594 ($\|F\| > 3.00\ \sigma(\|F\|)$)
R int	0.05	0.01
No of params refined	352	350
R, R_w, *S*	0.056, 0.051, 1.65	0.057, 0.091, 3.40
Max shift in final cycle	0.17	0.43
Final diff map, max, e/Å^3	0.44	0.91

Function minimized was sum $[w(|F_o|^2 - |F_c|^2)^2]$ which $w = 1.0/[(\text{sigma}|F_o|^2 + 0.0007|F_o|^2]$. $R = \text{sum}[||F_o| - |F_c||)/\text{sum}|F_o|$. $R_w = [\text{sum}w(|F_o| - |F_c|)^2/\text{sum}|F_o|^2]^{1/2}$.

Table 2-5. Details of the crystallographic data collection for **8a** and **8b**

Compound	**8a**	**8b**
Formula	$C_{22}H_{19}F_{12}O_2P_1$	$C_{24}H_{22}F_{12}O_2P_1N_1$
Mol wt	574.40	615.40
Cryst syst	Orthorhombic	Monoclinic
Space group	*P*212121	$P2_1/n$
Cryst dimens, mm	0.55 x 0.40 x 0.30	0.50 x 0.50 x 0.30
Color	colorless	colorless
Habit	prism	prism
a, Å	14.027 (4)	15.748 (1)
b, Å	16.421 (4)	16.986 (2)
c, Å	10.704 (3)	11.016 (2)
α, deg	90	90.00 (1)
β, deg	90	110.257 (9)
γ, deg	90	90.03 (1)
V, Å^3	2465 (1)	2764.4 (5)
Z	4	4
D_{obs}, D_{calc}, g cm^{-3}	-, 1.55	-, 1.48
Abs coeff, cm^{-1}	18.82	17.23
F (000)	1160	1248
Radiation; λ, Å	Cu $K\alpha$, 0.71073	Cu $K\alpha$, 1.54178
Temp, °C	23±1	23±1
$2\theta_{max}$, deg	130	130
Scan rate, deg/min	3	5
Linear decay, %	10	—
Data collected	$-h, -k, \pm l$	$+h, +k, +l$
Total data collcd, unique, obsd	2413, 2350, 1977 ($\|F\| > 3.00\ \sigma\ (\|F\|)$)	4492, 4103, 3632 ($\|F\| > 3.00\ \sigma\ (\|F\|)$)
R int	0.00	0.02
No of params refined	350	437
R, R_W, *S*	0.068, 0.082, 2.72	0.042, 0.068, 3.16
Max shift in final cycle	1.00	0.19
Final diff map, max, e/Å^3	0.44	0.28

Function minimized was sum $[w(|F_o|^2 - |F_c|^2)^2]$ which w = $1.0/[(\text{sigma}|F_o|^2 + 0.0007|F_o|^2]$. $R = \text{sum}[||F_o| - |F_c||)/\text{sum}|F_o|$. $R_w = [\text{sumw}(|F_o| - |F_c|)^2/\text{sum}|F_o|^2]^{1/2}$.

Table 2-6. Positional parameters and equivalent isotropic temperature factors (B*eq*) for non-H atoms and H bonded to P1 and O2

$Beq = 4/3\Sigma_i\Sigma_j\beta_{ij}a_ia_j$

6

atom	x	y	z	B(*eq*)
P 1	–0.3696 (1)	–0.2475 (1)	0.1201 (1)	3.88 (4)
F 1	–0.3895 (3)	–0.0577 (3)	0.4739 (2)	7.8 (1)
F 2	–0.1382 (3)	0.0491 (3)	0.4853 (2)	6.6 (1)
F 3	–0.2414 (3)	–0.1639 (3)	0.4387 (2)	6.7 (1)
F 4	–0.4181 (3)	0.1077 (3)	0.3101 (3)	7.4 (1)
F 5	–0.2814 (4)	0.1261 (3)	0.1618 (2)	7.2 (1)
F 6	–0.1668 (3)	0.2146 (2)	0.3299 (2)	6.4 (1)
F 7	–0.9135 (3)	–0.3224 (3)	0.3503 (2)	7.8 (1)
F 8	–0.7078 (4)	–0.3129 (4)	0.4470 (2)	8.3 (1)
F 9	–0.9011 (4)	–0.5036 (4)	0.4017 (3)	9.2 (1)
F 10	–0.7908 (3)	–0.4884 (3)	0.0560 (2)	6.8 (1)
F 11	–0.9790 (3)	–0.4579 (3)	0.1380 (3)	8.3 (1)
F 12	–0.9122 (3)	–0.6184 (3)	0.1833 (3)	7.7 (1)
O 1	–0.3999 (3)	–0.1301 (2)	0.2404 (2)	3.68 (9)
O 2	–0.6923 (3)	–0.2672 (3)	0.2054 (3)	4.5 (1)
C 1	–0.1623 (4)	–0.1389 (4)	0.1511 (4)	3.7 (1)
C 2	–0.0440 (6)	–0.1594 (5)	0.0907 (4)	5.1 (2)
C 3	0.1122 (6)	–0.0740 (6)	0.1209 (5)	5.9 (2)
C 4	0.1505 (6)	0.0302 (6)	0.2064 (5)	5.6 (2)
C 5	0.0330 (5)	0.0519 (5)	0.2656 (4)	4.6 (2)
C 6	–0.1224 (4)	–0.0334 (4)	0.2371 (3)	3.5 (1)
C 7	–0.2673 (4)	–0.0282 (4)	0.2946 (3)	3.4 (1)
C 8	–0.2606 (5)	–0.0484 (5)	0.4235 (4)	4.8 (2)
C 9	–0.2824 (6)	0.1083 (4)	0.2754 (4)	4.8 (2)
C 10	–0.4552 (4)	–0.3878 (4)	0.2130 (3)	3.4 (1)
C 11	–0.3454 (5)	–0.4466 (4)	0.2311 (4)	4.7 (2)
C 12	–0.3712 (6)	–0.5506 (5)	0.3017 (5)	6.0 (2)
C 13	–0.5109 (6)	–0.6015 (5)	0.3549 (5)	5.8 (2)
C 14	–0.6235 (6)	–0.5493 (5)	0.3366 (4)	5.0 (2)
C 15	–0.5981 (4)	–0.4398 (4)	0.2677 (3)	3.5 (1)
C 16	–0.7343 (4)	–0.3936 (4)	0.2497 (3)	3.6 (1)
C 17	–0.8145 (6)	–0.3832 (6)	0.3641 (5)	5.7 (2)
C 18	–0.8553 (5)	–0.4901 (5)	0.1577 (4)	5.0 (2)
C 19	–0.4804 (6)	–0.1966 (6)	0.0152 (4)	5.5 (2)
H 1	–0.337 (4)	–0.324 (4)	0.033 (3)	3.38 (0)
H 2	–0.604 (6)	–0.221 (5)	0.234 (4)	4.68 (0)

Table 2-6. Continued (1)

7

atom	x	y	z	B(*eq*)
P 1	0.21788 (4)	–0.38258 (6)	–0.17388 (6)	4.23 (9)
F 1	0.1442 (2)	–0.2832 (2)	0.1092 (2)	8.0 (1)
F 2	0.0512 (2)	–0.1681 (3)	0.0866 (2)	9.5 (1)
F 3	0.1742 (2)	–0.1207 (2)	0.0812 (2)	8.2 (1)
F 4	0.1376 (2)	–0.0383 (2)	–0.1321 (2)	8.1 (1)
F 5	0.0917 (2)	–0.1437 (2)	–0.2638 (2)	7.7 (1)
F 6	0.0164 (1)	–0.0938 (2)	–0.1316 (3)	8.7 (1)
F 7	0.3578 (2)	–0.1451 (2)	0.1008 (3)	8.7 (1)
F 8	0.4389 (2)	–0.0824 (2)	–0.0183 (3)	9.0 (1)
F 9	0.4802 (2)	–0.1951 (2)	0.1074 (2)	8.0 (1)
F 10	0.4415 (2)	–0.3723 (2)	–0.1938 (2)	8.4 (1)
F 11	0.5184 (1)	–0.3469 (2)	–0.0425 (3)	8.6 (1)
F 12	0.5021 (2)	–0.2241 (2)	–0.1690 (3)	9.6 (1)
O 1	0.1980 (1)	–0.2417 (2)	–0.1101 (2)	4.3 (1)
O 2	0.3449 (1)	–0.2067 (2)	–0.1383 (2)	5.2 (1)
C 1	0.1115 (2)	–0.4002 (2)	–0.1568 (2)	4.3 (1)
C 2	0.0722 (2)	–0.4942 (3)	–0.1900 (3)	5.3 (1)
C 3	–0.0096 (2)	–0.5026 (3)	–0.1763 (3)	6.2 (1)
C 4	–0.0506 (2)	–0.4197 (4)	–0.1283 (3)	6.6 (1)
C 5	–0.0122 (2)	–0.3276 (3)	–0.0958 (3)	5.8 (1)
C 6	0.0688 (2)	–0.3172 (2)	–0.1105 (2)	4.5 (1)
C 7	0.1209 (2)	–0.2199 (2)	–0.0807 (3)	4.4 (1)
C 8	0.1220 (2)	–0.1969 (3)	0.0496 (3)	5.9 (1)
C 9	0.0916 (2)	–0.1228 (3)	–0.1521 (4)	5.7 (1)
C 10	0.2844 (2)	–0.4071 (2)	–0.0440 (2)	4.2 (1)
C 11	0.2578 (2)	–0.4981 (2)	0.0125 (3)	5.2 (1)
C 12	0.2921 (2)	–0.5325 (3)	0.1168 (3)	6.0 (1)
C 13	0.3566 (2)	–0.4784 (3)	0.1658 (3)	6.4 (1)
C 14	0.3861 (2)	–0.3906 (3)	0.1101 (3)	5.7 (1)
C 15	0.3500 (2)	–0.3522 (2)	0.0064 (3)	4.4 (1)
C 16	0.3917 (2)	–0.2579 (2)	–0.0519 (3)	4.7 (1)
C 17	0.4183 (2)	–0.1700 (3)	0.0359 (4)	6.1 (1)
C 18	0.4639 (2)	–0.3010 (3)	–0.1153 (4)	6.4 (1)
C 19	0.2480 (2)	–0.3246 (3)	–0.3091 (3)	5.3 (1)
C 20	0.2032 (2)	–0.3737 (4)	–0.4136 (3)	6.4 (1)
C 21	0.2369 (6)	–0.3293 (4)	–0.5262 (4)	13.5 (3)
C 22	0.219 (1)	–0.3616 (9)	–0.6218 (8)	25.8 (8)
H 1	0.227 (2)	–0.486 (3)	–0.216 (3)	4.30 (0)
H 2	0.302 (3)	–0.201 (4)	–0.119 (4)	5.31 (0)

Table 2-6. Continued (2)

8a

atom	x	y	z	B (*eq*)
P 1	–0.0865 (1)	0.0384 (1)	0.3271 (2)	4.26 (6)
F 1	0.1694 (4)	0.0158 (4)	0.4005 (5)	7.9 (2)
F 2	0.2139 (4)	0.1393 (4)	0.3777 (6)	9.4 (2)
F 3	0.2574 (4)	0.0494 (5)	0.2479 (6)	10.2 (2)
F 4	0.0346 (5)	0.1696 (4)	0.0747 (5)	8.5 (2)
F 5	0.1851 (6)	0.1534 (5)	0.0790 (6)	10.5 (2)
F 6	0.1174 (6)	0.2324 (4)	0.2117 (6)	9.7 (2)
F 7	0.1435 (4)	0.1295 (4)	0.6164 (7)	9.5 (2)
F 8	0.0897 (5)	0.1273 (4)	0.7990 (5)	9.4 (2)
F 9	0.0760 (4)	0.2329 (3)	0.6924 (6)	8.1 (2)
F 10	–0.1875 (4)	0.1187 (4)	0.6720 (6)	8.4 (2)
F 11	–0.1153 (4)	0.2227 (3)	0.7349 (6)	8.8 (2)
F 12	–0.0953 (5)	0.1120 (4)	0.8279 (5)	10.2 (2)
O 1	0.0213 (4)	0.1105 (3)	0.3226 (4)	4.4 (1)
O 2	–0.0405 (4)	0.1742 (3)	0.5234 (5)	5.2 (2)
C 1	–0.0249 (6)	–0.0123 (4)	0.2030 (6)	4.3 (2)
C 2	–0.0626 (6)	–0.0826 (5)	0.1448 (7)	5.0 (2)
C 3	–0.0091 (8)	–0.1212 (6)	0.0538 (7)	6.2 (3)
C 4	0.0784 (8)	–0.0945 (6)	0.0228 (8)	6.6 (3)
C 5	0.1160 (6)	–0.0261 (6)	0.0780 (6)	6.0 (2)
C 6	0.0639 (5)	0.0147 (4)	0.1686 (6)	4.4 (2)
C 7	0.0945 (6)	0.0891 (5)	0.2398 (7)	4.8 (2)
C 8	0.1850 (6)	0.0730 (8)	0.3184 (9)	6.9 (3)
C 9	0.1083 (9)	0.1634 (6)	0.150 (1)	7.2 (3)
C 10	–0.0488 (5)	–0.0016 (4)	0.4842 (6)	4.1 (2)
C 11	–0.0472 (6)	–0.0861 (4)	0.4745 (6)	4.9 (2)
C 12	–0.0170 (7)	–0.1360 (5)	0.5691 (6)	5.6 (2)
C 13	0.0090 (6)	–0.1020 (5)	0.6823 (8)	6.2 (2)
C 14	0.0048 (6)	–0.0181 (5)	0.6940 (7)	5.7 (2)
C 15	–0.0225 (5)	0.0336 (4)	0.5976 (5)	4.2 (2)
C 16	–0.0229 (6)	0.1235 (4)	0.6278 (6)	4.6 (2)
C 17	0.0724 (7)	0.1532 (6)	0.6859 (8)	5.6 (2)
C 18	–0.1059 (6)	0.1452 (6)	0.7168 (8)	5.9 (3)
C 19	–0.1753 (6)	0.1184 (5)	0.2895 (8)	5.2 (2)
C 20	–0.1453 (7)	0.2080 (6)	0.280 (1)	7.1 (3)
C 21	–0.2588 (7)	0.1103 (7)	0.379 (1)	7.8 (3)
C 22	–0.2077 (7)	0.0950 (6)	0.1545 (9)	7.0 (3)
H 1	–0.161 (5)	–0.025 (5)	0.321 (8)	4.30 (0)
H 2	0.003 (6)	0.141 (5)	0.44 (1)	5.03 (0)

Table 2-6. Continued (3)

8b

atom	x	y	z	B (*eq*)
P 1	–0.25727 (4)	0.11027 (4)	–0.49748 (6)	4.0 (1)
F 1	–0.2085 (1)	0.3049 (1)	–0.3854 (2)	6.3 (1)
F 2	–0.2461 (1)	0.3657 (1)	–0.5662 (2)	7.2 (1)
F 3	–0.1075 (1)	0.3618 (1)	–0.4413 (2)	8.1 (1)
F 4	–0.1247 (1)	0.1928 (1)	–0.7173 (2)	7.7 (1)
F 5	–0.0778 (1)	0.3079 (1)	–0.6494 (2)	8.6 (1)
F 6	–0.2159 (1)	0.2897 (1)	–0.7674 (2)	7.3 (1)
F 7	–0.2866 (2)	0.2617 (1)	–0.1587 (2)	8.7 (1)
F 8	–0.2307 (1)	0.1799 (1)	–0.0078 (2)	7.4 (1)
F 9	–0.3716 (1)	0.1983 (2)	–0.0795 (2)	10.1 (1)
F 10	–0.3342 (2)	–0.0069 (1)	–0.2586 (2)	10.3 (1)
F 11	–0.4060 (1)	0.0470 (2)	–0.1495 (2)	9.9 (1)
F 12	–0.2664 (1)	0.0243 (1)	–0.0627 (2)	8.4 (1)
O 1	–0.2522 (1)	0.2020 (1)	–0.5878 (2)	4.1 (1)
O 2	–0.2205 (1)	0.1238 (1)	–0.2271 (2)	5.1 (1)
N 1	–0.0671 (2)	0.0869 (2)	–0.0104 (3)	7.6 (2)
C 1	–0.1355 (2)	0.1255 (2)	–0.4209 (2)	4.3 (1)
C 2	–0.0792 (2)	0.0720 (2)	–0.3350 (3)	6.0 (1)
C 3	0.0136 (2)	0.0866 (3)	–0.2860 (4)	7.0 (2)
C 4	0.0490 (2)	0.1526 (2)	–0.3198 (3)	6.6 (2)
C 5	–0.0066 (2)	0.2064 (2)	–0.4036 (3)	5.5 (1)
C 6	–0.0992 (2)	0.1916 (2)	–0.4545 (2)	4.1 (1)
C 7	–0.1712 (2)	0.2421 (1)	–0.5502 (2)	4.0 (1)
C 8	–0.1828 (2)	0.3194 (2)	–0.4862 (3)	5.0 (1)
C 9	–0.1472 (2)	0.2583 (2)	–0.6719 (3)	5.5 (1)
C 10	–0.3546 (1)	0.1542 (1)	–0.4638 (2)	3.7 (1)
C 11	–0.4221 (2)	0.1844 (2)	–0.5738 (2)	4.6 (1)
C 12	–0.5074 (2)	0.2037 (2)	–0.5753 (3)	5.2 (1)
C 13	–0.5279 (2)	0.1948 (2)	–0.4653 (3)	5.4 (1)
C 14	–0.4617 (2)	0.1693 (2)	–0.3534 (3)	5.2 (1)
C 15	–0.3749 (2)	0.1495 (1)	–0.3497 (2)	4.0 (1)
C 16	–0.3061 (2)	0.1278 (2)	–0.2170 (2)	4.4 (1)
C 17	–0.3004 (2)	0.1919 (2)	–0.1158 (3)	5.8 (1)
C 18	–0.3292 (2)	0.0479 (2)	–0.1722 (3)	6.3 (2)
C 19	–0.2958 (2)	0.0470 (2)	–0.6465 (3)	5.9 (1)
C 20	–0.3302 (4)	0.0891 (3)	–0.7781 (4)	8.6 (2)
C 21	–0.3704 (3)	–0.0068 (3)	–0.6357 (5)	8.7 (2)
C 22	–0.2133 (3)	–0.0033 (3)	–0.6376 (5)	9.7 (2)
C 23	0.1008 (3)	0.1149 (3)	0.1096 (6)	9.7 (2)
C 24	0.0061 (2)	0.0990 (2)	0.0450 (3)	6.1 (2)
H 1	–0.258 (2)	0.048 (2)	–0.424 (3)	4.02 (0)
H 2	–0.188 (3)	0.115 (2)	–0.173 (4)	5.61 (0)

^{31}P NMR chemical shifts of 6–8 in various solvents at r.t.

^{31}P NMR spectra were measured on a JEOL EX-400 (162 MHz) spectrometer at 22 ± 1 °C. Samples of **6**, **7**, and **8** including EtOH (**8b**) were dissolved in distilled solvents. The concentration of the solution was ca 0.016–0.018 M.

Dynamic NMR Measurement and Line Shape Analysis

Samples of **6**, **7** and **8** (ca. 15 mg) dissolved in freshly distilled solvents (0.5–0.6 mL) were sealed in NMR tubes under N_2. ^{19}F NMR spectra were measured on a JEOL EX-400 (376 MHz) in a variable temperature mode, and the specified temperatures were maintained throughout each set of measurements (error within ± 1 °C). The observed temperatures were calibrated with the ^{1}H NMR chemical shift difference of signals of neat 1,3-propanediol (high temperature region) and MeOH (low temperature region). The rates and activation free energies at the coalessence point were calculated using the following equations derived from the Gutowsky-Holm appoximation of $k = \pi \Delta\nu/2^{-1/2}$.[11]

$$\Delta G^{\ddagger} = 19.14\, T_c \{9.97 + \log (T_c/\delta_\nu)\}/4.184 \quad \text{<kcal mol}^{-1}\text{>}$$

$$\Delta G^{\ddagger} = \{23.76 - \ln (k/T)\}\, RT$$

The line shape analysis was performed in a narrow temperature range around the coalescence point according to the classical Gutowsky-Holm method neglecting $^{4}J_{F-F}$ coupling since the condition $J/\Delta\nu << 1$ is met. The activation enthalpies and entropies were calculated according to the transition state theory of Eyring[12] using the following equations by linear regression.

$$\ln (k/T) = \Delta H^{\ddagger}/RT + \Delta S^{\ddagger} + \ln (k_B/h)$$

The systematic error associated with the simulated rates was estimated to be 10% and calculated with the following equation since the proportional error for $\Delta H^{\ddagger}$ and $\Delta S^{\ddagger}$ are the same as for Ea[11].

$$(\delta_{Ea}/E)^2 \approx [2T^2/(\Delta T)^2]\ (\delta_T/T)^2 + 2[\Delta(\ln k)]^{-2}\ (\delta_k/k)^2$$

Table 2-7. Rate Constants of Inversion at the Phosphorus Atom in **6** and **7**.

6 in toluene-d_8

T <K>	k <sec^{-1}>	$\Delta G^{\ddagger}$ <kcal mol^{-1}>	$\Delta H^{\ddagger}$ <kcal mol^{-1}>	$\Delta S^{\ddagger}$ <eu>
313	190	15.1		
323	315	15.3		
325	347	15.3		
327	389	15.3	10.0 ± 1.3	−16.2 ± 6.8
329	432	15.4	(± 0.1)*	(± 0.3)*
331	482	15.4		
333	524	15.4		
335	584	15.4		

* Statistical error in parenthesis

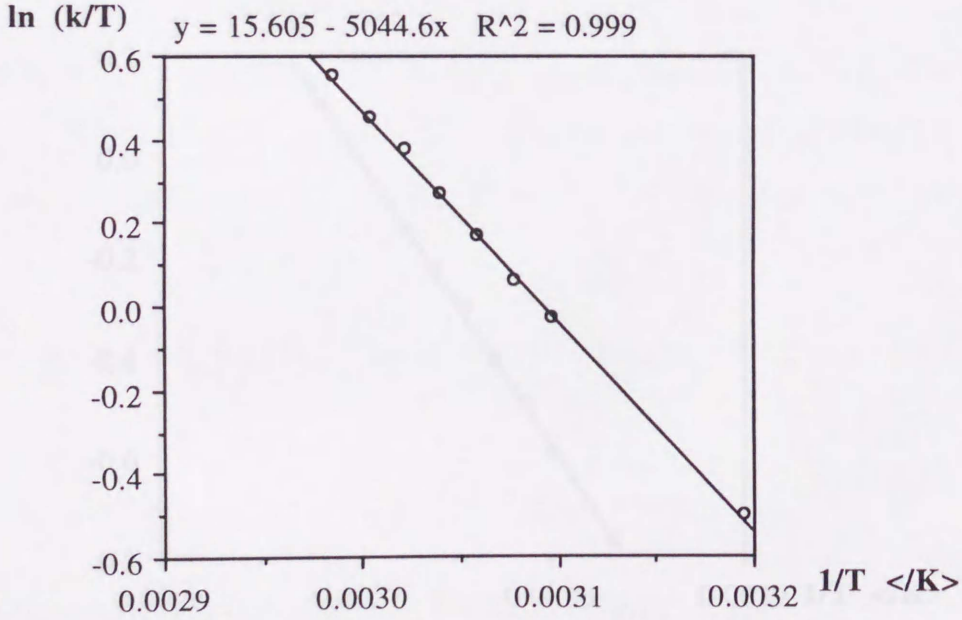

Table 2-7. Continued (1)

7 in toluene-d_8

T <K>	k <sec^{-1}>	$\Delta G^{\ddagger}$ <kcal mol^{-1}>	$\Delta H^{\ddagger}$ <kcal mol^{-1}>	$\Delta S^{\ddagger}$ <eu>
353	164	17.2		
357	197	17.3		
359	219	17.3		
361	240	17.3	11.4 ± 1.7	–16.3 ± 4.9
363	268	17.4	(± 0.1)*	(± 0.3)*
365	290	17.4		
367	317	17.4		
373	413	17.5		

* Statistical error in parenthesis

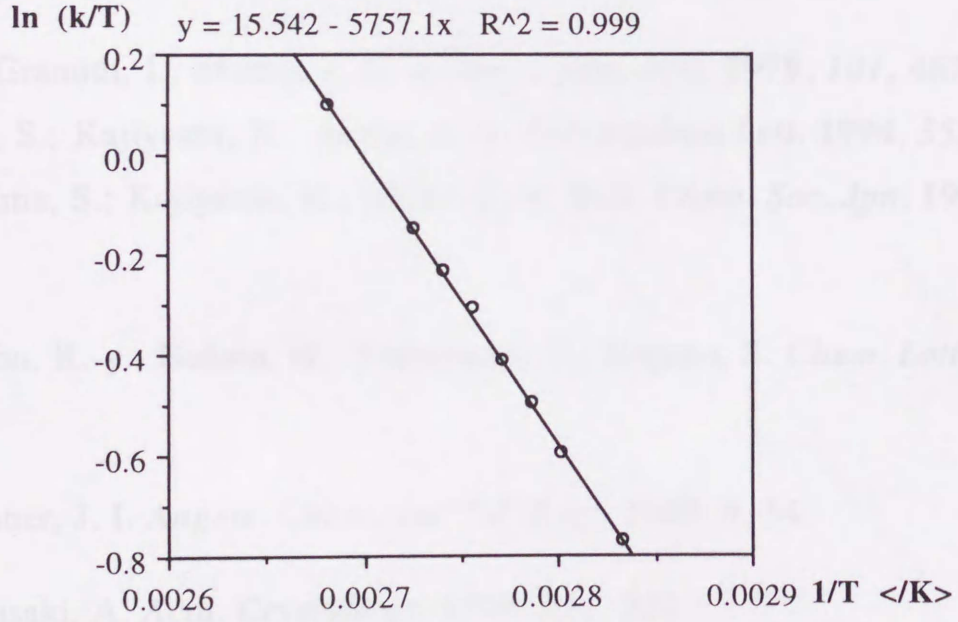

D. References

(1) For designation: Perkins, C. W.; Martin, J. C.; Arduengo, A. J.; Lau, W.; Alegria, A.; Kochi, J. K. *J. Am. Chem. Soc.* **1980**, *102*, 7753.

(2) (a) Malavaud, C.; Barrans, J. *Tetrahedron Lett.* **1975**, *35*, 3077. (b) Boisdon, M. T.; Maravaud, C.; Mathis, F.; Barrans, J. *Tetrahedron Lett.* **1977**, *39*, 3501. (c) Laurenco, C.; Burgada, R. *Tetrahedron*. **1976**, *32*, 2253. (d) Lopez, L.; Fabas, C.; Barrans, J. *Phosphorus Sulfur* **1979**, *7*, 81. (e) Tangom, B.; Malavaud, C.; Boisdon, M. T.; Barrans, J. *Phosphorus Sulfur* **1988**, *40*, 33.

(3) Brazier, J. F.; Houalla, D.; Loenig, M.; Wolf, R. *Top. Phosphorus. Chem*. **1976**, *8*, 99.

(4) Ross, M. R.; Martin, J. C. *J. Am. Chem. Soc.* **1981**, *103*, 1234.

(5) Berry, R. S. *J. Chem. Phys.* **1960**, *32*, 933.

(6) (a) Granoth, I.; Martin, J. C. *J. Am. Chem. Soc.* **1979**, *101*, 4623. (b) Kojima, S.; Kajiyama, K.; Akiba, K.-y. *Tetrahedron Lett.* **1994**, *35*, 7037. (c) Kojima, S.; Kajiyama, K.; Akiba, K.-y. *Bull. Chem. Soc. Jpn.* **1995**, *68*, 1785.

(7) Akiba, K.-y.; Nakata, H.; Yamamoto, Y.; Kojima, S. *Chem. Lett.* **1992**, 1559.

(8) Musher, J. I. *Angew. Chem., Int. Ed. Engl.* **1969**, *8*, 54.

(9) Furusaki, A. *Acta. Crystallogr.* **1979**, *A35*, 220.

(10) Katayama, C. *Acta. Crystallogr.* **1986**, *A42*, 19.

(11) Jackman, L. M.; Cotton, F. A. "*Dynamic Nuclear Magnetic Resonance Spectroscopy*", Academic Press, New York 1975.

(12) Wynne-Jones, W. F. K.; Eyring, H. *J. Chem. Phys.* **1935**, *3*, 492.

Chapter 3

First Characterization

of 10-P-5 Spirophosphoranes

with an Apical Carbon–Equatorial Oxygen ring.

Kinetic Studies on Pseudorotation

of Stereoisomers

A. Introduction

Most pentacoordinate phosphorus compounds usually assume trigonal bipyramidal (TBP) structures in the ground state, in which there are two distinctive sites, the apical and the equatorial positions. As described in Chapter 1 the apical bond consisting of three atoms (two apical and the phosphorus atoms) could be regarded as a three-center four-electron (3c-4e) bond[1] similar to the delocalized π electron conjugation as seen in the allylic anion. The stable phosphoranes would naturally prefer to have electron negative substituents in these apical positions, leading to the concept of apicophilicity. It is well-known that phosphoranes bearing oxygen and carbon substituents preferentially have oxygen atoms in the apical positions as the most stable stereoisomer according to the apicophilicity of the elements.[2] However, no example of the isolation and characterization of the relatively less stable stereoisomers has been reported[3] because of the low activation energy of the permutation of pentacoordinate compounds assuming TBP structures, normally accounted for by the Berry pseudorotation (BPR) mechanism.[4]

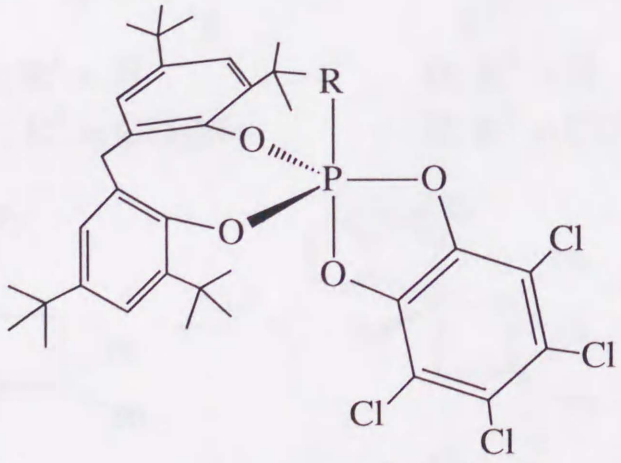

A; R = Ph, Et

As for phosphoranes that violate the element electronegativity rule, recently, phosphorane **A** bearing an apical carbon and three equatorial oxygen substituents has been reported by Holmes, R. R. et al. However, a stereoisomer having an apical oxygen in the eight-membered ring could not be observed because of the steric effect of aryl groups bearing *t*-Bu groups.[5] The kawashima-Okazaki group has reported that pentacoordinate 1,2-oxaphosphetanes **B** and **C** had an apical oxygen-equatorial carbon four-membered ring, and the equatorial oxygen-apical carbon stereoisomers **D** and **E** could not be observed.[6] However, recently, on dissolution of 1,2-azaphosphetidine **F** (δ_P –29.9), in which the oxygen has been exchanged with a nitrogen substituent, in toluene-d_8 at rt they observed another signal which was assigned to the pseudorotamer **G** (δ_P –50.9) with the nitrogen being equatorial (eq 1).[7] However, the isomer **G** could not be isolated. In both of these examples the unusual phosphoranes obtained or observed are due to thermodynamic stabilization of these configuration relative to the ordinarily expected phosphoranes.

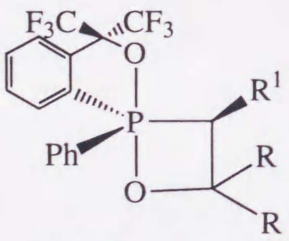

B; $R^1 = H$
C; $R^1 = CO_2Me$

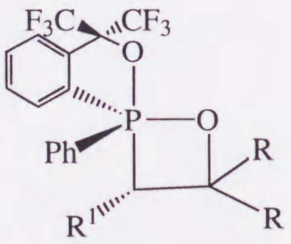

D; $R^1 = H$
E; $R^1 = CO_2Me$

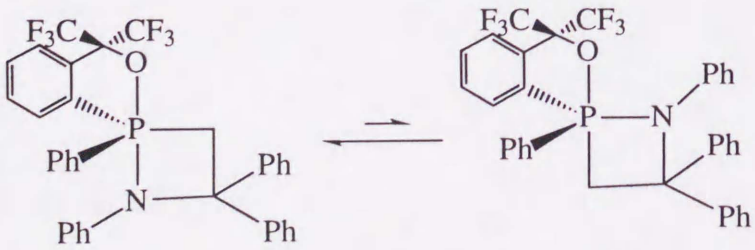

F **G**

(1)

We have succeeded in the first isolation and characterization of both [*TBPY*-5-12] spirophosphoranes **7–9** having an apical carbon-equatorial oxygen five-membered ring along with their thermodynamically more stable apical oxygen-equatorial carbon isomers **4–6** {[TBPY-5-11] spirophosphoranes}. Here, we report on their characterization and discuss the relative thermal stability of **5** and **8** on the basis of kinetic studies.

B. Results and Discussion

1. Preparation and the Structure of [*TBPY*-5-12] P–R Spirophosphoranes.

When the recrystallization of monocyclic 10-P-5 P–H (apical) phosphorane[8] **2** (R = n-Bu) was being carried out from CH_3CN standing at room temperature for a week, the author could obtain as the first crystals what were later found by X-ray crystal analysis (vide infra) to be unexpected [*TBPY*-5-12] P–*n*-Bu spirophosphorane **8**, having C(apical)–O(equatorial) configuration. Subsequent crystallizations of the remaining substance in solution yielded the [*TBPY*-5-11] P–*n*-Bu spirophosphorane **5**, bearing C(equatorial)–O(apical) configuration. In order to examine the chemistry of this novel type of phosphoranes, reaction conditions for obtaining them were optimized.

Scheme 3-1

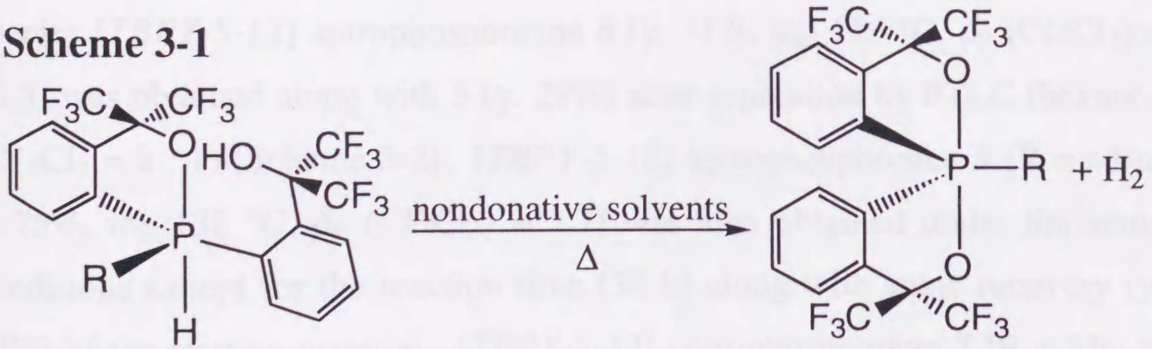

1; R = Me
2; R = *n*-Bu
3; R = *t*-Bu

4; R = Me
5; R = *n*-Bu
6; R = *t*-Bu

Scheme 3-2

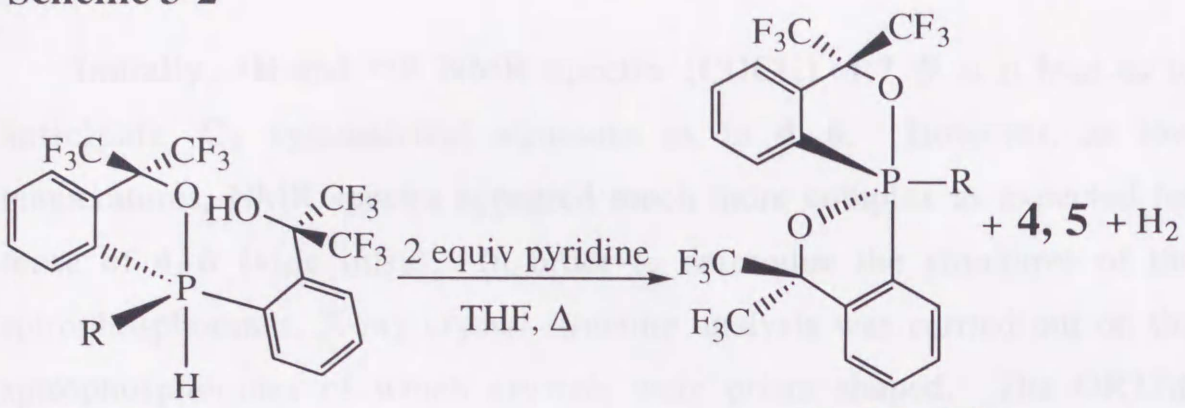

1; R = Me
2; R = *n*-Bu
3; R = *t*-Bu

7; R = Me
8; R = *n*-Bu
9; R = *t*-Bu

Thermal reactions of monocyclic 10-P-5 P–H (apical) phosphoranes **1** (R = Me), **2** (R = *n*-Bu) and **3** (R = *t*-Bu) in nondonative solvents led to the exclusive formation of [*TBPY*-5-11] spirophosphoranes **4** [mp 134 °C, δ_P ($CDCl_3$) = –22.6], **5** [mp 109 °C, δ_P ($CDCl_3$) = –18.8] and **6** [mp 128 °C, δ_P ($CDCl_3$) = –9.8], respectively (Scheme 3-1). However, when phosphorane **2** was treated with 2 equiv of pyridine in THF at 60 °C for 20 min, the new species [*TBPY*-5-12] spirophosphorane **8** [y. 71%, mp 115 °C, δ_P ($CDCl_3$) = –3.5] was obtained along with **5** (y. 29%) after separation by PTLC (hexane–CH_2Cl_2 = 2 : 1) (Scheme 3-2). [*TBPY*-5-12] spirophosphorane **9** [R = *t*-Bu, y. 75%, mp 138 °C, δ_P ($CDCl_3$) = 7.7] was also obtained under the same conditions except for the reaction time (36 h) along with some recovery (y. 18%) of the starting material. [*TBPY*-5-12] spirophosphorane **7** [R = Me, y. 46%, mp , δ_P ($CDCl_3$) = –6.3] could be obtained along with **4** (y. 52%) by heating a solution of **1** in THF at 40 °C for 1h. In this case pyridine was not used because of the rapid cyclization of **1** to [*TBPY*-5-11] spirophosphorane

4, probably due to the fast permutation of spirophosphorane **7** to **4** in its presence.

Initially, ^{1}H and ^{19}F NMR spectra ($CDCl_3$) of **7–9** at rt lead us to anticipate C_2 symmetrical structure as in **4–6**. However, at low temperatures, NMR spectra appeared much more complex as expected for those of **4–6** (vide infra). In order to determine the structures of the spirophosphoranes, X-ray crystal structure analysis was carried out on the spirophosphoranes of which crystals were prism shaped. The ORTEP structures of **5**, **8** and **9** are shown in Fig. 3-1, 3-2 and 3-3, respectively, along with selected structural parameters in Table 3-1.

X- ray structural analysis of **5** (Fig. 3-1) and **8** (Fig. 3-2) revealed that these compounds were stereoisomers with TBP structures. As the drawing shows the compound **5** assumes a trigonal bipyramidal (TBP) structure with the two oxygen atoms occupying the two apical positions and the three carbon atoms occupying the three equatorial positions. In TBP structures of **8** and **9** (Fig. 3-3) a carbon and an oxygen atoms occupy the two apical positions, and two carbon and an oxygen atoms occupy the three equatorial positions. It is clearly shown that the apical bonds of **8** and **9** are longer than the corresponding equatorial bonds [i.e., **8**; P1–O1 (ap) 1.768> P1–O2 (eq) 1.659 Å and P1–C10 (ap) 1.863 > P1–C1 (eq) 1.813 Å: **9**; P1–O1 (ap) 1.770> P1–O2 (eq) 1.651 Å and P1–C10 (ap) 1.889 > P1–C1 (eq) 1.831 Å]. On the other hand, the pairs of bonds of **5** are almost equal [i.e., P–O (ap) 1.753, 1.765 Å and P–C (aryl; eq) 1.818, 1.820 Å].

Figure 3-1. ORTEP drawing of **5** showing thermal ellipsoids at the 30% probability level.

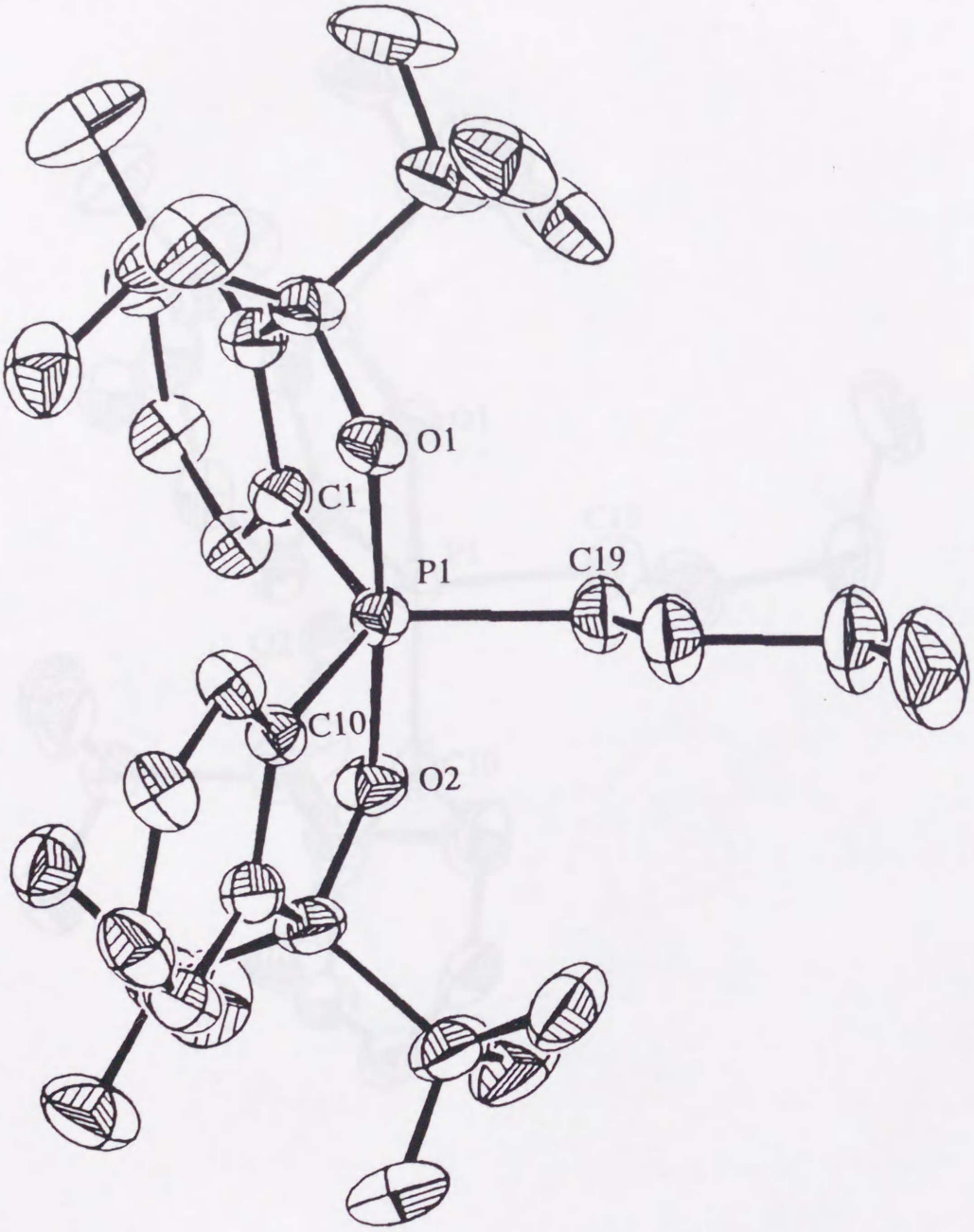

Figure 3-2. ORTEP drawing of **8** showing thermal ellipsoids at the 30% probability level.

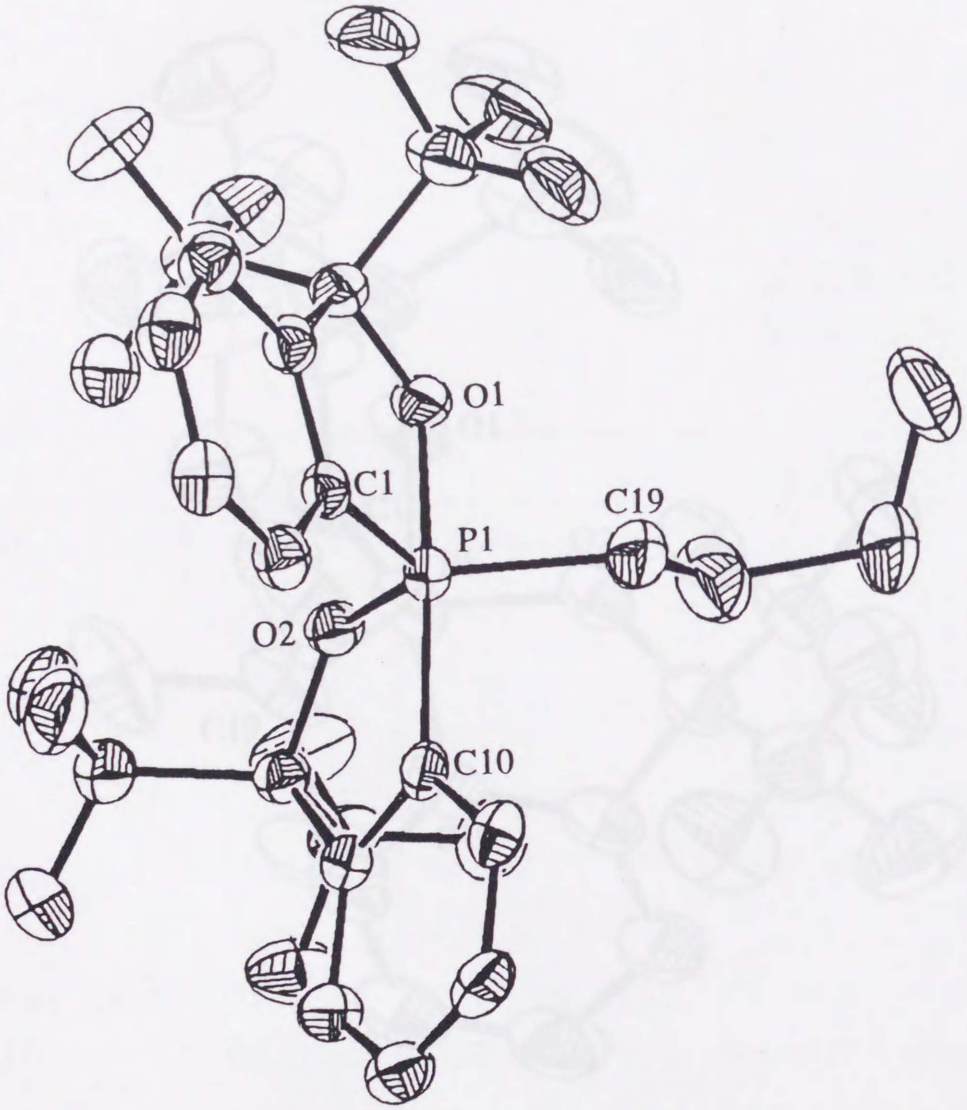

Figure 3-3. ORTEP drawing of **9** showing thermal ellipsoids at the 30% probability level.

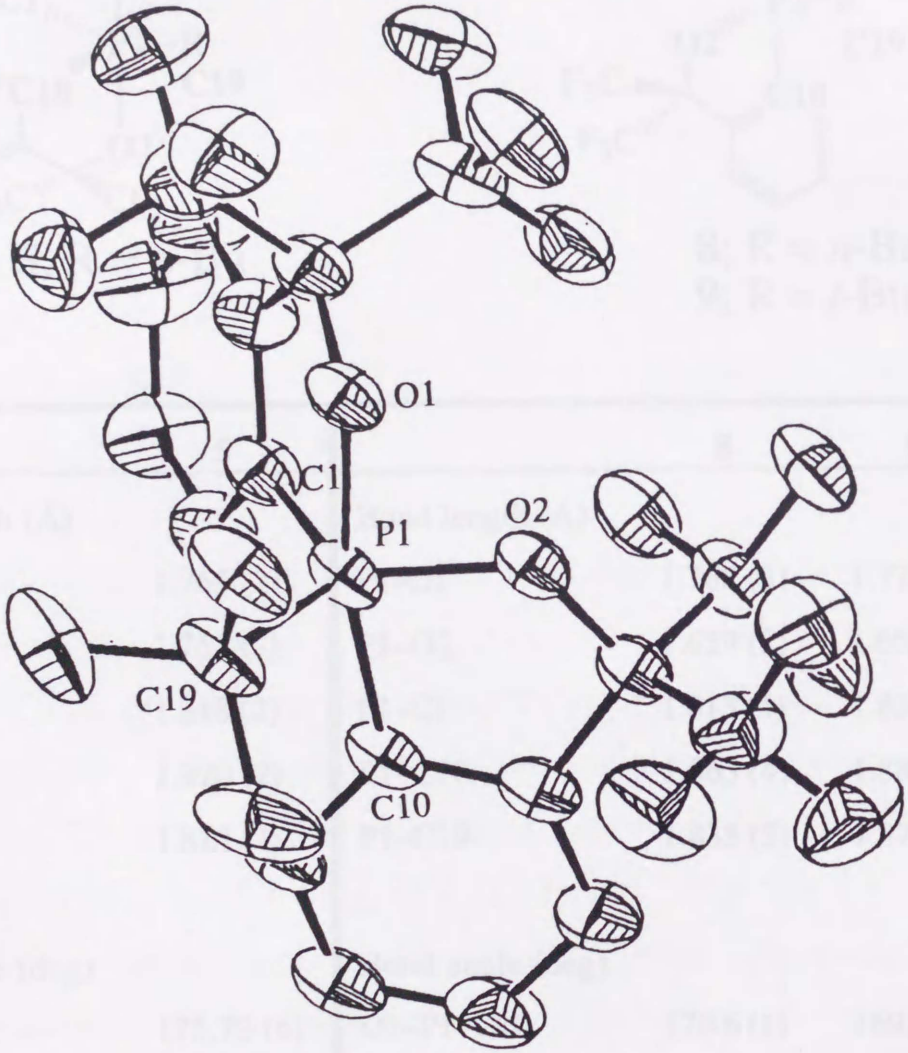

Table 3-1. Selected Bond Lengths and Angles for **5**, **8** and **9**

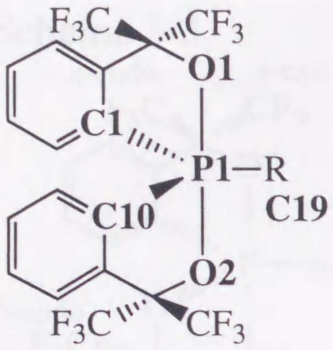

5; R = *n*-Bu

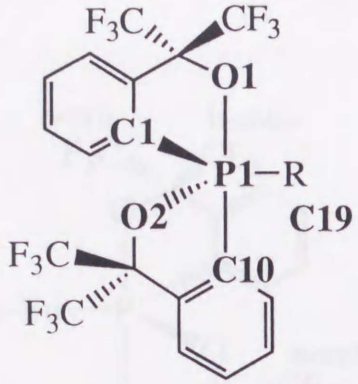

8; R = *n*-Bu
9; R = *t*-Bu

	5		**8**	**9**
Bond length (Å)		Bond length (Å)		
P1–O1	1.765 (2)	P1–O1	1.768 (3)	1.770 (2)
P1–O2	1.753 (2)	P1–O2	1.659 (2)	1.651 (2)
P1–C1	1.818 (2)	P1–C1	1.813 (4)	1.831 (3)
P1–C10	1.820 (2)	P1–C10	1.863 (4)	1.889 (3)
P1–C19	1.818 (2)	P1–C19	1.835 (5)	1.878 (3)
Bond angle (deg)		Bond angle (deg)		
O1–P1–O2	175.79 (6)	O1–P1–C10	170.6 (1)	169.3 (1)
O1–P1–C1	87.32 (8)	O1–P1–C1	87.1 (2)	85.5 (1)
O2–P1–C10	87.30 (8)	O2–P1–C10	87.8 (1)	87.4 (1)
C1–P1–C10	126.84 (8)	O2–P1–C1	119.9 (2)	120.4 (1)
C10–P1–C19	116.6 (1)	C1–P1–C19	114.8 (2)	121.7 (2)
C19–P1–C1	116.6 (1)	C19–P1–O2	124.0 (2)	116.4 (2)

2. Kinetic Study of Inversion of [*TBPY*-5-12] P–*n*-Bu Spirophosphorane 8.

Scheme 3-3

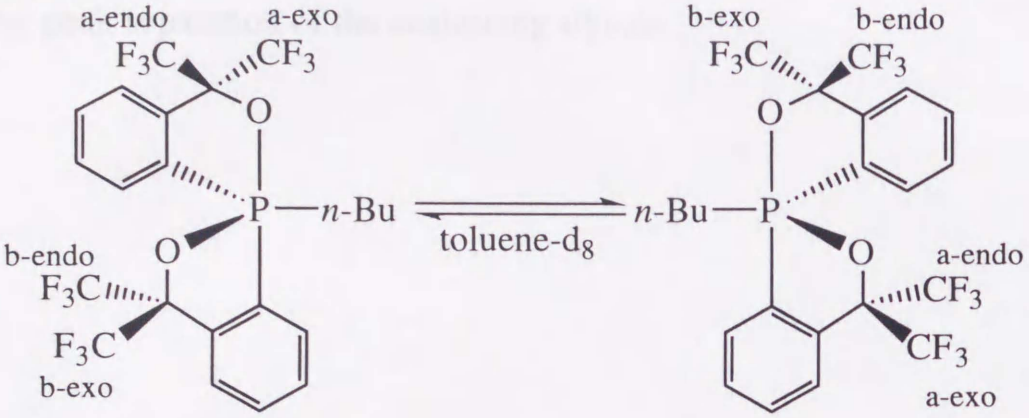

8-R_P **8-S_P**

^{19}F NMR spectra of compound **8** at rt showed only a pair of quartets [^{19}F NMR (toluene-d_8, 293 K) δ –74.7 (q, $^4J_{F-F}$ = 8.5 Hz, 6F), –75.9 (q, $^4J_{F-F}$ = 8.5 Hz, 6F)] for the four anisochronous CF_3 groups. This initially lead us to anticipate C_2 symmetrical structure for this compound. However, at low temperatures, the CF_3 groups decoalesced into four signals [^{19}F NMR (toluene-d_8, 193 K) δ –74.3 (br s, 3F), –74.5 (br s, 3F), –75.5 (br s, 3F),–76.0 (br s, 3F)], whereas only a sole ^{31}P signal [^{31}P NMR (toluene-d_8, 219 K) δ –3.6] could be observed for the compound throughout the temperature range. This dynamic behavior could only be rationalized as due to interconversion between enantiomers **8**-R_P and **8**-S_P (Scheme 3-3), in which exchange between fluorines, *a-endo* and *b-endo*, and *a-exo* and *b-exo*, occurs, respectively, by a single-step pseudorotation with the *n*-Bu group as the pivot. Line shape analysis (Fig. 3-4) of the ^{19}F NMR spectra (temperature range of 223–243 K; $\delta\nu$ = 209 Hz; *Tc* = 235 K; $\Delta G^{\ddagger}$ = 10.8 kcal mol^{-1}) of one of the

pairs of signals (higher field chemical shift) gave the activation parameters $\Delta H^{\ddagger} = 10.0 \pm 0.7$ kcal mol^{-1} and $\Delta S^{\ddagger} = -3.4 \pm 3.0$ eu. ^{19}F NMR spectra of [*TBPY*-5-12] P-*t*-Bu spirophosphorane **9** showed only a pair of quartets even at 193 K in toluene-d_8 probably due either to the faster pseudorotation or smaller peak separation of the coalescing signals.

Figure 3-4. Observed and calculated line shape for CF_3 groups in compound in toluene-d_8.

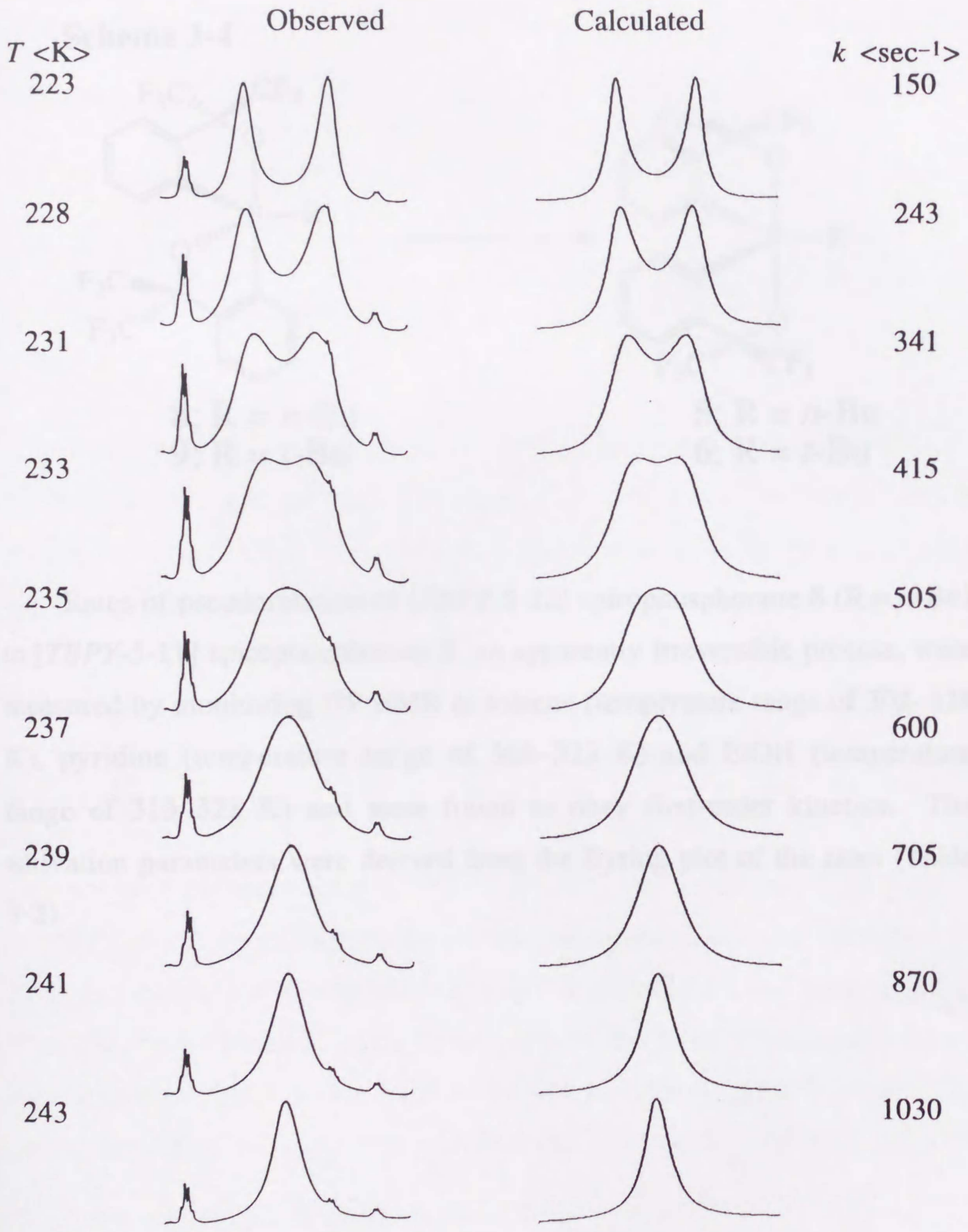

3. Kinetic Study of Pseudorotation of [*TBPY*-5-12] Spirophosphoranes to [*TBPY*-5-11] Spirophosphoranes.

Scheme 3-4

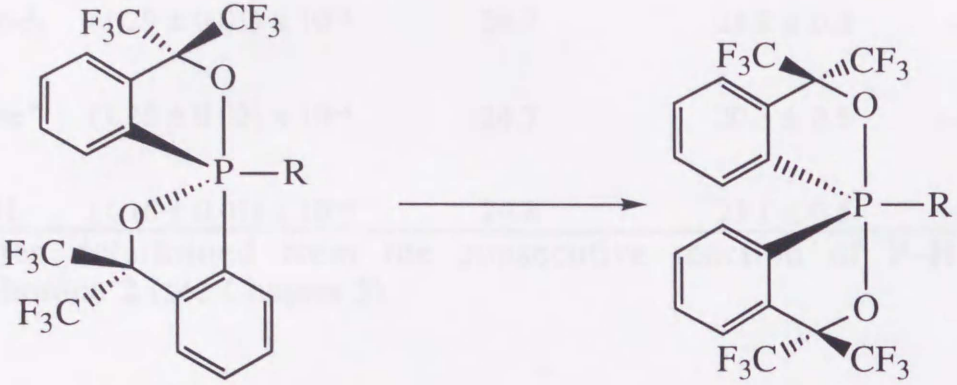

8; R = *n*-Bu
9; R = *t*-Bu

5; R = *n*-Bu
6; R = *t*-Bu

Rates of pseudorotation of [*TBPY*-5-12] spirophosphorane **8** (R = *n*-Bu) to [*TBPY*-5-11] spirophosphorane **5**, an apparently irreversible process, were measured by monitoring ^{19}F NMR in toluene (temperature range of 302–328 K), pyridine (temperature range of 308–323 K) and EtOH (temperature range of 313–328 K) and were found to obey first-order kinetics. The activation parameters were derived from the Eyring plot of the rates (Table 3-2).

Table 3-2. Kinetic Parameters of Pseudorotation of **8** to **5**

Solvent	k <sec^{-1}> (323 K)	$\Delta G^{\ddagger}$ <kcal mol^{-1}> (323 K)	$\Delta H^{\ddagger}$ <kcal mol^{-1}>	$\Delta S^{\ddagger}$ <eu>
toluene-d_8	$(1.29 \pm 0.01) \times 10^{-4}$	24.7	21.8 ± 0.4	-9.0 ± 1.2
pyridine*	$(1.26 \pm 0.02) \times 10^{-4}$	24.7	20.3 ± 0.5	-13.8 ± 1.7
EtOH	$(1.16 \pm 0.01) \times 10^{-4}$	24.8	23.1 ± 0.5	-5.3 ± 1.5

* Rates determined from the consecutive reaction of P–H (apical) phosphorane **2** (see Chapter 5).

The rates [ca. 1.16–1.29 x 10^{-4} s^{-1} (323 K)] were almost identical in all solvents, thus it can be concluded that a P–O (ap) bond cleavage, which should proceed through a very polar transition state or an intermediate, does not take place at all. For pyridine, since the rate measured with isolated **8** to **5** [$(4.24 \pm 0.09) \times 10^{-5}$ sec^{-1} at 313 K] was within experimental error of rate determined from the consecutive reaction of P–H (apical) phosphorane **2** [$(4.36 \pm 0.11) \times 10^{-5}$ sec^{-1} at 313 K], the parameters derived from the latter measurements are shown.

Rates of pseudorotation of [*TBPY*-5-12] spirophosphorane **9** (R = *t*-Bu) to [*TBPY*-5-11] spirophosphorane **6** were also measured by monitoring ^{19}F NMR in *t*-butyltoluene (temperature range of 403–463 K) and were found to obey first-order kinetics. The Eyring plot of the rates gave the activation parameters, i.e., $\Delta H^{\ddagger} = 27.2 \pm 0.8$ kcal mol^{-1} and $\Delta S^{\ddagger} = -13.1 \pm 1.8$ eu. The higher activation enthalpy is presumably due to steric hindrance of the *t*-Bu group.

3. Kinetic Study of Inversion of Diastereomer [*TBPY*-5-11] Spirophosphoranes 10.

Scheme 3-5

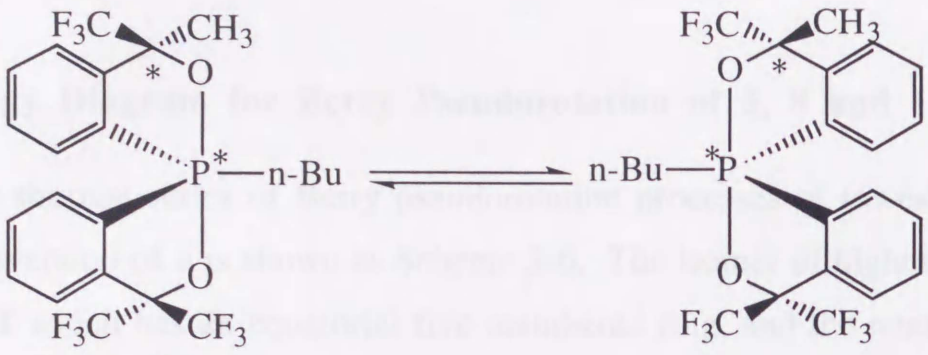

10-*exo* **10-*endo***

The pseudorotation between enantiomers **5**-R_P and **5**-S_P was found to be too slow to measure by NMR techniques such as saturation transfer. Therefore, diastereomers **10-*exo*** [^{31}P NMR ($CDCl_3$) δ –22.2; ^{19}F NMR ($CDCl_3$) δ –75.4 (m, 6F), –79.7 (s, 3F)] and **10-*endo*** [^{31}P NMR ($CDCl_3$) δ –22.7; ^{19}F NMR ($CDCl_3$) δ –74.9 (q, $^4J_{F-F}$ = 9.3 Hz, 3F), –75.4 (q, $^4J_{F-F}$ = 9.3 Hz, 3F), –80.1 (s, 3F)], differing from **5** only by having a CH_3 group in the place of one of the CF_3 groups (Scheme 3-5) were examined.

The pseudorotation between the diastereomers was examined by monitoring the singlet signals of ^{19}F NMR in 4-*t*-butyltoluene (temperature range of 442–463 K). The averaged activation parameters obtained for the **10-*exo*** to **10-*endo*** and **10-*endo*** to **10-*exo*** processes were $\Delta H^{\ddagger}$ = 33.7 ± 0.9 kcal mol^{-1} and $\Delta S^{\ddagger}$ = –8.8 ± 1.9 eu.

Phosphorane **10** should be only slightly less stable than **5**, and therefore the activation enthalpy obtained for pseudorotation between **10-*exo*** and **10-**

endo should differ from that between **5**-R_P and **5**-S_P by only a very small amount. Hence, it is reasonable to use the values to evaluate the activation energy of the permutation process of **5**. Thus, **8** is concluded to be less stable than **5** by at least ca. 12 (34 – 22) kcal mol^{-1}.

4. Energy Diagram for Berry Pseudorotation of 5, 8 and 10.

The shortest series of Berry pseudorotation processes of lowest energy for the inversion of **5** is shown as Scheme 3-6. The isomer of highest energy must be **I** which has an equatorial five membered ring, and the next highest must be **H** which has two equatorial oxgens.

In order to determine the validity of the assumption that **5** and **8** undergo stereomutation via the same transition state and that the value (ca. 12 kcal mol^{-1}) given above is the difference between **5** and **8**, the relative stability of analogous [*TBPY*-5-12] spirophosphorane **J** and [*TBPY*-5-11] spirophosphorane **K** was calculated at the HF/3-21G level using the Gaussian 94 program. **J** was found to be less stable than **K** by 14.7 kcal mol^{-1}, a value very close to the experimental value of 12 kcal mol^{-1}.

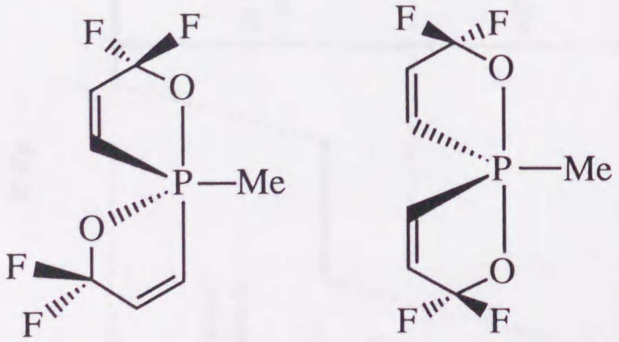

J **K**

Scheme 3-6

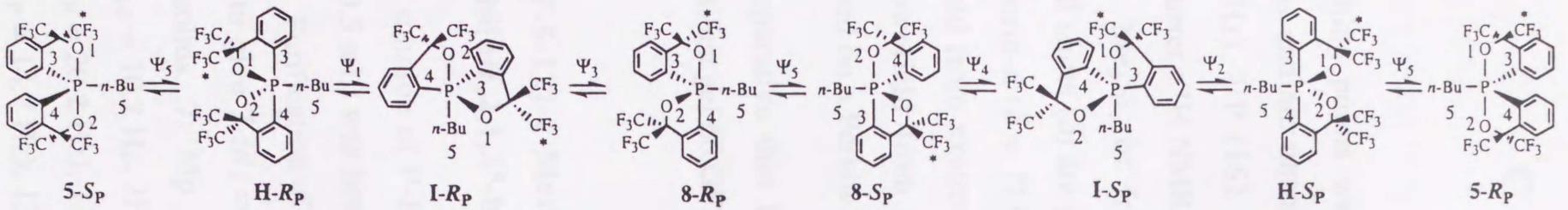
5-S_P
H-R_P
I-R_P
8-R_P
8-S_P
I-S_P
H-S_P
5-R_P

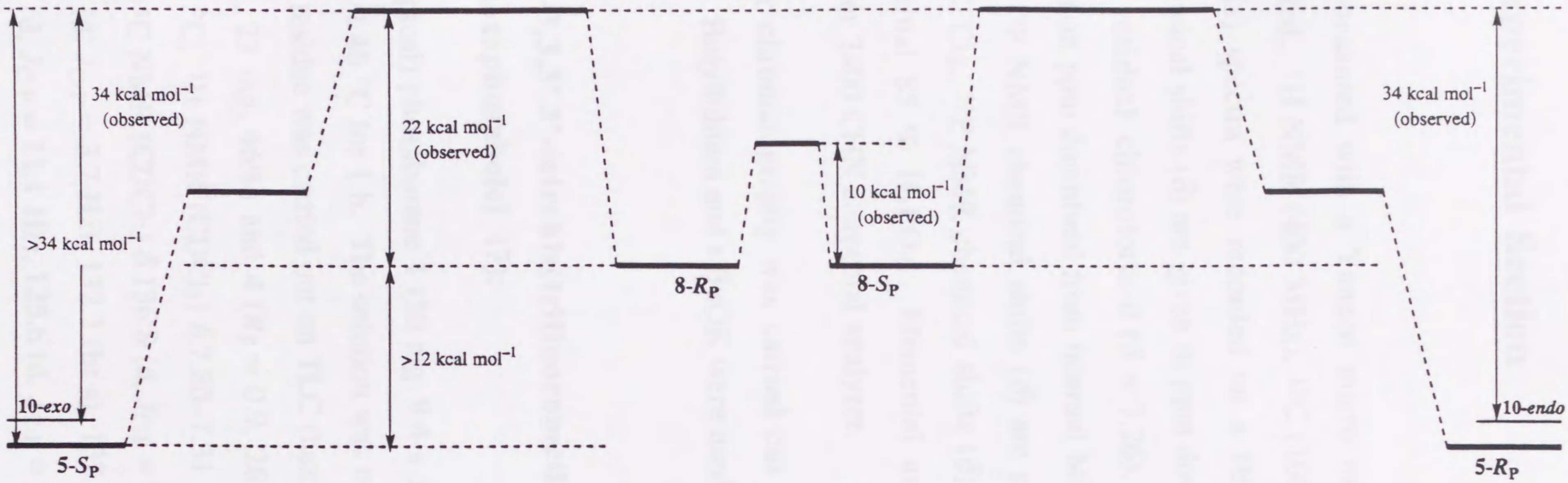
34 kcal mol^{-1} (observed)
>34 kcal mol^{-1}
22 kcal mol^{-1} (observed)
>12 kcal mol^{-1}
10 kcal mol^{-1} (observed)
34 kcal mol^{-1} (observed)
10-*exo*
10-*endo*
8-R_P
8-S_P
5-S_P
5-R_P

C. Experimental Section

Melting points were measured with a Yanaco micro melting point apparatus and are uncorrected. ^{1}H NMR (400 MHz), ^{13}C (100 MHz), ^{19}F (376 MHz), ^{31}P (162 MHz) spectra were recorded on a JEOL EX-400 spectrometer. ^{1}H NMR chemical shifts (δ) are given in ppm downfield from internal Me_4Si, or from residual chloroform-*d* (δ = 7.26). ^{13}C NMR chemical shifts (δ) are given in ppm downfield from internal Me_4Si, or from chloroform-*d* (δ = 77.0). ^{19}F NMR chemical shifts (δ) are given in ppm downfield from external $CFCl_3$. ^{31}P NMR chemical shifts (δ) are given in ppm downfield from external 85 % H_3PO_4. Elemental analyses were performed on a Perkin-Elmer 2400 CHN elemental analyzer.

Preparative thin layer chromatography was carried out on plates of Merck silica gel 60 GF254. Butyllithium and *t*-BuOK were used as received.

[*TBPY*-5-12]-1-Methyl-3,3,3',3'-tetrakis(trifluoromethyl)-1,1'-spirobi[3*H*,2,1,λ^5-benzoxaphosphole] (**7**):

A solution of P–H (apical) phosphorane **1** (50 mg, 9.4 x 10^{-2} mmol) in THF (0.5 mL) was heated at 40 °C for 1 h. The solution was concentrated in vacuo. Purification of the residue was carried out on TLC (hexane–CH_2Cl_2 = 2 : 1) to give **7** (R_f = 0.8, 23 mg, 46%) and **4** (R_f = 0.9, 26 mg, 52%) as white solids. **7**: Mp 127 °C; ^{1}H NMR ($CDCl_3$) δ 7.80–7.31 (m, 8H), 2.28 (d, $^{2}J_{H\text{-}P}$ = 10.2 Hz, 3H); ^{13}C NMR ($CDCl_3$) δ 136.8 (d, $J_{C\text{-}P}$ = 9.1 Hz), 136.1 (d, $J_{C\text{-}P}$ = 20.2 Hz), 133.8 (d, $J_{C\text{-}P}$ = 3.7 Hz), 132.3 (br s), 132.0 (br s), 131.4 (d, $J_{C\text{-}P}$ = 14.7 Hz), 130.3 (d, $J_{C\text{-}P}$ = 11.1 Hz), 125.6 (d, $J_{C\text{-}P}$ = 9.1 Hz), 124.8

(d, $J_{C\text{-}P}$ = 14.7 Hz), 122.6 (q, $^1J_{C\text{-}F}$ = 285.0 Hz), 122.4 (q, $^1J_{C\text{-}F}$ = 288.6 Hz), 122.3 (q, $^1J_{C\text{-}F}$ = 285.9 Hz), 121.9 (q, $^1J_{C\text{-}F}$ = 285.8 Hz), 79.8 (sept, $^2J_{C\text{-}F}$ = 31.3 Hz), 26.2 (d, $^1J_{C\text{-}P}$ = 129.5 Hz); ^{19}F NMR ($CDCl_3$) δ –75.6 (q, $^4J_{F\text{-}F}$ = 9.2 Hz, 6F), –76.4 (q, $^4J_{F\text{-}F}$ = 8.6 Hz, 6F); ^{31}P NMR ($CDCl_3$) δ –6.3; Anal. calcd for $C_{19}H_{11}F_{12}O_2P$: C, 43.04; H, 2.09. Found: C, 43.34; H, 1.99.

[*TBPY*-5-12]-1-Butyl-3,3,3',3'-tetrakis(trifluoromethyl)-1,1'-spirobi[3*H*,2,1,λ^5-benzoxaphosphole] (8):

P–H (apical) phosphorane **2** (200 mg, 0.348 mmol) was treated with pyridine (0.07 mL, 0.8 mmol) in THF (5 ml) at 60 °C for 20 min. The solution was then poured into a separatory funnel containing Et_2O (50 mL) and washed with 1 M HCl (50 mL), aqueus $CuSO_4$ (50 mL), water (50 mL) and brine (50 mL), dried with $MgSO_4$, and concentrated in vacuo. Purification of the residue was carried out on TLC (hexane–CH_2Cl_2 = 2 : 1) to give **8** (R_f = 0.7, 141 mg, 71%) and **5** (R_f = 0.7, 58.2 mg, 29%) as white solids. **8**: Mp 115 °C; ^{1}H NMR ($CDCl_3$) δ 7.75–7.69 (m, 2H), 7.65–7.61 (m, 2H), 7.59–7.56 (m, 4H), 2.48 (dt, $^2J_{H\text{-}P}$ = 17.1 Hz, $^3J_{H\text{-}H}$ = 6.8 Hz, 2H), 1.67–1.54 (m, 2H), 1.39–1.29 (m, 2H), 0.83 (t, $^3J_{H\text{-}H}$ = 7.3 Hz, 3H); ^{13}C NMR ($CDCl_3$) δ 135.9 (br d, $^1J_{C\text{-}P}$ = 88.3 Hz), 134.2 (d, $^2J_{C\text{-}P}$ = 16.5 Hz), 132.2, 132.0 (d, $^3J_{C\text{-}P}$ = 11.1 Hz), 130.3 (d, $^2J_{C\text{-}P}$ = 11.1 Hz), 125.5 (d, $^3J_{C\text{-}P}$ = 11.0 Hz), 122.5 (d, $^3J_{C\text{-}P}$ = 7.4 Hz), 122.5(q, $^1J_{C\text{-}F}$ = 286.8 Hz), 122.0 (q, $^1J_{C\text{-}F}$ = 288.8 Hz), 79.9 (sept, $^2J_{C\text{-}F}$ = 31.3 Hz), 40.2 (d, $^1J_{C\text{-}P}$ = 114.0 Hz), 24.7 (d, $^3J_{C\text{-}P}$ = 7.4 Hz), 24.0 (d, $^2J_{C\text{-}P}$ = 20.2 Hz), 13.3; ^{19}F NMR ($CDCl_3$) δ –74.9 (q, $^4J_{F\text{-}F}$ = 8.5 Hz, 6F), –76.2 (q, $^4J_{F\text{-}F}$ = 8.5 Hz, 6F); ^{31}P NMR ($CDCl_3$) δ –3.5; Anal. calcd for $C_{22}H_{17}F_{12}O_2P$: C, 46.17; H, 2.99. Found: C, 46.17; H, 2.72.

[*TBPY*-5-11]-1-(1,1-Dimethyl)ethyl-3,3,3',3'-tetrakis(trifluoromethyl)-1,1'-spirobi[3*H*,2,1,λ^5-benzoxaphosphole] (6).

A solution of P–H (apical) phosphorane **3** (150 mg, 0.261 mmol) in *o*-dichlorobenzene (10 mL) and CH_3CN (2 mL) was heated at 150 °C for 4 d. The solution was concentrated in vacuo. Purification of the residue was carried out on TLC (hexane) to give **6** (R_f = 0.8, 224 mg, 80%) as a white solids. Recrystallization of **6** from hexane gave an X-ray sample. Mp 128 °C; ^{1}H NMR ($CDCl_3$) δ 8.42–8.38 (m, 2H), 7.66–7.64 (m, 6H), 1.13 (d, $^3J_{H\text{-}P}$ = 20.0 Hz, 9H); ^{13}C NMR ($CDCl_3$) δ 137.2 (d, $^3J_{C\text{-}P}$ = 9.2 Hz), 136.4 (d, $^2J_{C\text{-}P}$ = 16.6 Hz), 132.9 (d, $^4J_{C\text{-}P}$ = 3.7 Hz), 132.5 (d, $^1J_{C\text{-}P}$ = 160.0 Hz), 130.9 (d, $^2J_{C\text{-}P}$ = 12.8 Hz), 124.1 (q, $^3J_{C\text{-}P}$ = 14.7 Hz), 122.7 (q, $^1J_{C\text{-}F}$ = 286.7 Hz), 122.4 (q, $^1J_{C\text{-}F}$ = 288.6 Hz), 81.5 (sept, $^2J_{C\text{-}F}$ = 31.3 Hz), 40.5 (d, $^1J_{C\text{-}P}$ = 103.0 Hz), 28.2; ^{19}F NMR ($CDCl_3$) δ –72.4 (q, $^4J_{F\text{-}F}$ = 10.1 Hz, 6F), –74.5 (q, $^4J_{F\text{-}F}$ = 10.1 Hz, 6F); ^{31}P NMR ($CDCl_3$) δ –9.8; Anal. calcd for $C_{22}H_{17}F_{12}O_2P$: C, 46.17; H, 2.99. Found: C, 46.04; H, 2.73.

[*TBPY*-5-12]-1-(1,1-Dimethyl)ethyl-3,3,3',3'-tetrakis(trifluoromethyl)-1,1'-spirobi[3*H*,2,1,λ^5-benzoxaphosphole] (9).

P–H (apical) phosphorane **3** (300 mg, 0.523 mmol) was treated with pyridine (4.0 mL, 0.8 mmol) in THF (20 ml) at 60 °C for 36 h. The solution was then poured into a separatory funnel containing Et_2O (50 mL) and washed with 1 M HCl (50 mL), aqueus $CuSO_4$ (50 mL), water (50 mL) and brine (50 mL), dried with $MgSO_4$, and concentrated in vacuo. Purification of the residue was carried out on TLC (hexane–CH_2Cl_2 = 3 : 1) to give **9** (R_f = 0.6, 224 mg, 75%) and **3** (R_f = 0.4, 53.7 mg, 18% recovered) as white solids. Recrystallization of **9** from EtOH gave an X-ray sample. **9**: Mp 138

°C; ^{1}H NMR ($CDCl_3$) δ 7.91–7.88 (m, 2H), 7.73–7.71 (m, 2H), 7.62–7.52 (m, 4H), 1.21 (d, $^{3}J_{H\text{-}P}$ = 21.0 Hz, 9H); ^{13}C NMR ($CDCl_3$) δ 136.3 (d, $^{1}J_{C\text{-}P}$ = 77.2 Hz), 134.1 (d, $^{2}J_{C\text{-}P}$ = 14.7 Hz), 133.8 (d, $^{2}J_{C\text{-}P}$ = 12.9 Hz), 131.7, 129.4 (d, $^{3}J_{C\text{-}P}$ = 9.2 Hz), 125.4 (d, $^{3}J_{C\text{-}P}$ = 9.2 Hz), 122.64 (q, $^{1}J_{C\text{-}F}$ = 286.8 Hz), 122.57 (q, $^{1}J_{C\text{-}F}$ = 286.8 Hz), 122.0 (q, $^{1}J_{C\text{-}F}$ = 288.6 Hz), 79.6 (sept, $^{2}J_{C\text{-}F}$ = 31.2 Hz), 44.4 (d, $^{1}J_{C\text{-}P}$ = 112.1 Hz), 29.6; ^{19}F NMR ($CDCl_3$) δ –73.7 (q, $^{4}J_{F\text{-}F}$ = 9.2 Hz, 6F), –75.9 (q, $^{4}J_{F\text{-}F}$ = 9.5 Hz, 6F); ^{31}P NMR ($CDCl_3$) δ 7.7; Anal. calcd for $C_{22}H_{17}F_{12}O_2P$: C, 46.17; H, 2.99. Found: C, 46.32; H, 3.27.

Crystallographic Studies.

Crystal Structure of 5, 6, 8 and 9

Crystal data and numerical details of the structure determinations are given in Tables 3-3. Crystals suitable for X-ray structure determination were mounted on a Mac Science MXC3 diffractometer and irradiated with graphite-monochromated Cu $K\alpha$ radiation (λ = 1.54178 Å) for collection. Lattice parameters were determined by least-squares fitting of 31 reflections for all compounds with $53° < 2\theta < 60°$, $55° < 2\theta < 60°$, $52° < 2\theta < 60°$ and $31° < 2\theta < 35°$ for **5**, **6**, **8** and **9**, respectively. Data were collected with the ω scan mode. All data were corrected for absorption[9] and extinction[10]. The structures were solved by a direct method with the Shelx 86 program. Refinement on F was carried out by full-matrix least squares. All non-hydrogen atoms were refined with anisotropic thermal parameters. All hydrogen atoms in **8** were located from a difference Fourier map calculated at the final stage of structural analysis. All hydrogen atoms in **5** and **6** were included in the refinement on calculated positions (C–H = 1.0 Å) riding on their carrier atoms with isotropic thermal parameters. All the computations were carried out on a Titan-750 computer.

Table 3-3. Details of the crystallographic data collection for **5** and **6**

Compound	**5**	**8**	**9**
Formula	$C_{22}H_{17}F_{12}O_2P_1$	$C_{22}H_{17}F_{12}O_2P_1$	$C_{22}H_{17}F_{12}O_2P_1$
Mol wt	572.3	572.3	574.30
Cryst syst	Monoclinic	Monoclinic	Monoclinic
Space group	$P2_1/a$	$P2_1/n$	$P2_1/c$
Cryst dimens, mm	0.70 x 0.60 x 0.50	0.50 x 0.50 x 0.25	0.60 x 0.50 x 0.15
Color	colorless	colorless	colorless
Habit	prism	prism	prism
a, Å	19.522 (4)	12.041 (2)	14.463 (2)
b, Å	11.819 (2)	16.936 (3)	36.842 (6)
c, Å	10.596 (2)	11.401 (2)	8.973 (1)
α, deg	90	90	90
β, deg	103.50 (2)	96.05 (1)	96.67 (1)
γ, deg	90	90	90
V, Å^3	2377.4 (8)	2311.9 (6)	4749 (1)
Z	4	4	8
D_{obs}, D_{calc}, g cm^{-3}	-, 1.60	-, 1.66	-, 1.61
Abs coeff, cm^{-1}	19.51	20.26	19.54
F (000)	1152	1152	2304
Radiation; λ, Å	Cu $K\alpha$, 0.71073	Cu $K\alpha$, 1.54178	Cu $K\alpha$, 1.54178
Temp, °C	23±1	23±1	23±1
$2\theta_{max}$, deg	130	130	130
Scan rate, deg/min	4	3	5
Linear decay, %	—	—	10
Data collected	$\pm h$, $+k$, $\pm l$	$\pm h$, $+k$, $\pm l$	$+h$, $-k$, $\pm l$
Total data collcd, unique, obsd	4508, 3993, 3767 ($\|F\| > 3.00\ \sigma(\|F\|)$)	4264, 3861, 3016 ($\|F\| > 5.00\ \sigma(\|F\|)$)	8526, 7942, 6890 ($\|F\| > 3.00\ \sigma(\|F\|)$)
R int	0.02	0.03	0.04
No of params refined	395	344	677
R, R_w, *S*	0.045, 0.081, 2.70	0.066, 0.093, 2.67	0.073, 0.112, 2.06
Max shift in final cycle	0.37	0.47	0.14
Final diff map, max, e/Å^3	0.41	0.92	0.75

Function minimized was sum $[w(|F_o|^2 - |F_c|^2)^2]$ which w = $1.0/[(\text{sigma}|F_o|^2 + 0.0007|F_o|^2]$. $R = \text{sum}[||F_o| - |F_c||)/\text{sum}|F_o|$. $R_w = [\text{sumw}(|F_o| - |F_c|)^2/\text{sum}|F_o|^2]^{1/2}$.

Table 3-4. Positional parameters and equivalent isotropic temperature factors (B*eq*) for non-H atoms.

$Beq = 4/3\Sigma_i\Sigma_j\beta_{ij}a_ia_j$

5

atom	x	y	z	B (eq)
P 1	–0.11399 (2)	–0.14888 (4)	0.27026 (4)	3.48 (4)
F 1	–0.30577 (8)	–0.1364 (2)	0.2167 (2)	6.85 (6)
F 2	–0.3370 (1)	–0.0214 (2)	0.3472 (3)	9.84 (9)
F 3	–0.3065 (1)	–0.1900 (2)	0.4072 (2)	8.33 (7)
F 4	–0.1304 (1)	0.0070 (2)	0.5610 (2)	9.31 (8)
F 5	–0.2022 (2)	–0.1128 (2)	0.6060 (2)	9.45 (9)
F 6	–0.2363 (2)	0.0543 (2)	0.5500 (2)	10.8 (1)
F 7	–0.14673 (8)	–0.1294 (1)	–0.0850 (2)	6.15 (6)
F 8	–0.0878 (1)	–0.2532 (2)	–0.1596 (2)	7.98 (7)
F 9	–0.0406 (1)	–0.0955 (2)	–0.0869 (2)	7.76 (6)
F 10	0.02815 (9)	–0.3259 (2)	0.2125 (2)	7.88 (7)
F 11	0.06110 (8)	–0.1992 (2)	0.0976 (2)	8.23 (7)
F 12	0.0192 (1)	–0.3545 (2)	0.0112 (2)	9.10 (8)
O 1	–0.17287 (8)	–0.1590 (1)	0.3734 (1)	4.05 (5)
O 2	–0.06090 (7)	–0.1384 (1)	0.1582 (2)	4.40 (5)
C 1	–0.1484 (1)	–0.0074 (2)	0.2290 (2)	3.67 (6)
C 2	–0.1281 (1)	0.0680 (2)	0.1433 (2)	4.39 (6)
C 3	–0.1580 (1)	0.1745 (2)	0.1272 (3)	5.30 (7)
C 4	–0.2066 (1)	0.2070 (2)	0.1956 (3)	5.70 (8)
C 5	–0.2270 (2)	0.1336 (2)	0.2808 (3)	5.31 (8)
C 6	–0.1979 (1)	0.0264 (2)	0.2961 (2)	4.11 (6)
C 7	–0.2142 (1)	–0.0661 (2)	0.3836 (2)	4.50 (6)
C 8	–0.2921 (1)	–0.1035 (2)	0.3394 (3)	5.94 (8)
C 9	–0.1957 (2)	–0.0293 (3)	0.5271 (3)	6.8 (1)
C 10	–0.1479 (1)	–0.2804 (2)	0.1902 (2)	3.58 (6)
C 11	–0.1983 (1)	–0.3501 (2)	0.2222 (2)	4.41 (6)
C 12	–0.2162 (2)	–0.4503 (2)	0.1556 (2)	5.24 (7)
C 13	–0.1846 (2)	–0.4809 (2)	0.0574 (2)	5.50 (8)
C 14	–0.1337 (2)	–0.4131 (2)	0.0254 (2)	5.13 (7)
C 15	–0.1160 (1)	–0.3122 (2)	0.0921 (2)	4.05 (6)
C 16	–0.0622 (1)	–0.2259 (2)	0.0712 (2)	4.35 (6)
C 17	–0.0837 (1)	–0.1760 (2)	–0.0675 (2)	5.21 (7)
C 18	0.0125 (1)	–0.2765 (2)	0.0972 (3)	5.94 (8)
C 19	–0.0386 (1)	–0.1605 (2)	0.4078 (2)	4.84 (7)
C 20	–0.0351 (2)	–0.2717 (2)	0.4804 (3)	5.98 (8)
C 21	0.0281 (2)	–0.2796 (4)	0.5925 (4)	8.3 (1)
C 22	0.0335 (4)	–0.3908 (5)	0.6635 (5)	10.8 (2)

Table 3-4. Continued (1)

8

atom	x	y	z	B (*eq*)
P 1	0.22201 (8)	0.19316 (6)	–0.10183 (8)	3.5 (3)
F 1	0.1929 (2)	–0.0076 (2)	–0.0198 (2)	6.0 (3)
F 2	0.0776 (2)	0.0148 (2)	0.1070 (3)	7.1 (3)
F 3	0.2406 (2)	–0.0293 (2)	0.1625 (3)	6.8 (3)
F 4	0.2601 (3)	0.2109 (2)	0.2307 (3)	7.7 (3)
F 5	0.2732 (3)	0.0952 (2)	0.3059 (2)	8.0 (3)
F 6	0.1155 (2)	0.1434 (2)	0.2488 (2)	8.0 (3)
F 7	0.2696 (3)	0.0327 (2)	–0.2778 (3)	7.0 (3)
F 8	0.1701 (3)	0.0339 (2)	–0.4443 (2)	7.7 (3)
F 9	0.1015 (3)	–0.0086 (2)	–0.2919 (3)	7.5 (3)
F 10	–0.0175 (2)	0.2196 (2)	–0.3313 (3)	6.4 (3)
F 11	–0.0627 (2)	0.1000 (2)	–0.3135 (3)	7.6 (3)
F 12	–0.0017 (2)	0.1403 (2)	–0.4717 (2)	7.0 (3)
O 1	0.1613 (2)	0.1520 (2)	0.0189 (2)	3.9 (3)
O 2	0.1302 (2)	0.1355 (2)	–0.1795 (2)	3.6 (3)
C 1	0.3538 (3)	0.1526 (2)	–0.0372 (3)	3.4 (3)
C 2	0.4563 (3)	0.1593 (3)	–0.0814 (4)	4.3 (3)
C 3	0.5505 (3)	0.1252 (3)	–0.0207 (4)	4.8 (3)
C 4	0.5417 (4)	0.0846 (3)	0.0829 (4)	5.1 (3)
C 5	0.4398 (4)	0.0760 (3)	0.1261 (4)	4.4 (3)
C 6	0.3460 (3)	0.1101 (2)	0.0656 (3)	3.6 (3)
C 7	0.2277 (3)	0.1052 (2)	0.0972 (3)	3.8 (3)
C 8	0.1843 (4)	0.0200 (3)	0.0877 (4)	4.8 (3)
C 9	0.2190 (4)	0.1394 (4)	0.2214 (4)	5.4 (3)
C 10	0.2667 (3)	0.2286 (2)	–0.2443 (3)	3.6 (3)
C 11	0.3416 (4)	0.2895 (2)	–0.2646 (4)	4.5 (3)
C 12	0.3609 (4)	0.3084 (3)	–0.3790 (4)	5.0 (3)
C 13	0.3068 (4)	0.2688 (3)	–0.4729 (4)	4.9 (3)
C 14	0.2307 (4)	0.2090 (3)	–0.4557 (4)	4.5 (3)
C 15	0.2122 (3)	0.1907 (2)	–0.3408 (3)	3.5 (3)
C 16	0.1322 (3)	0.1299 (2)	–0.3025 (3)	3.6 (3)
C 17	0.1664 (4)	0.0464 (3)	–0.3298 (4)	5.1 (3)
C 18	0.0098 (4)	0.1473 (3)	–0.3547 (4)	4.7 (3)
C 19	0.1892 (5)	0.2917 (3)	–0.0482 (5)	6.5 (3)
C 20	0.0734 (6)	0.3131 (4)	–0.0703 (6)	7.8 (3)
C 21	0.0516 (7)	0.3951 (4)	–0.0123 (7)	10.2 (4)
C 22	0.0549 (7)	0.3916 (4)	0.1145 (6)	9.5 (4)

Table 3-4. Continued (2)

9

atom	x	y	z	B (eq)
P 1	–0.26485 (5)	0.12665 (2)	–0.21990 (8)	4.90 (4)
P 2	0.22229 (5)	0.12121 (2)	0.41435 (9)	4.77 (4)
F 1	–0.3716 (2)	0.13744 (8)	0.1139 (3)	8.97 (9)
F 2	–0.5032 (2)	0.1537 (1)	0.0056 (4)	10.0 (1)
F 3	–0.4207 (2)	0.19056 (8)	0.1470 (4)	10.3 (1)
F 4	–0.3790 (2)	0.22024 (9)	–0.2831 (4)	11.2 (1)
F 5	–0.4288 (2)	0.23683 (7)	–0.0791 (5)	10.8 (1)
F 6	–0.5070 (2)	0.20013 (8)	–0.2252 (4)	9.4 (1)
F 7	–0.2032 (2)	0.09318 (7)	0.1291 (2)	7.40 (8)
F 8	–0.1924 (2)	0.03530 (8)	0.1385 (4)	10.0 (1)
F 9	–0.3250 (2)	0.06066 (7)	0.1413 (3)	8.47 (8)
F 10	–0.3245 (3)	0.0276 (1)	–0.2944 (4)	11.9 (1)
F 11	–0.4015 (2)	0.02871 (7)	–0.1092 (4)	9.4 (1)
F 12	–0.2771 (2)	–0.00195 (7)	–0.0985 (6)	12.0 (2)
F 13	0.2381 (2)	0.1606 (1)	0.7790 (3)	9.8 (1)
F 14	0.0921 (2)	0.1645 (1)	0.7803 (3)	10.7 (1)
F 15	0.1735 (3)	0.21200 (9)	0.7851 (4)	11.0 (1)
F 16	0.0600 (2)	0.20492 (8)	0.3475 (4)	9.8 (1)
F 17	0.0735 (2)	0.23639 (7)	0.5441 (4)	10.3 (1)
F 18	–0.0114 (2)	0.18930 (8)	0.5300 (5)	10.3 (1)
F 19	0.3954 (2)	0.1215 (1)	0.7041 (4)	9.8 (1)
F 20	0.4385 (3)	0.0681 (1)	0.7821 (4)	14.1 (2)
F 21	0.3179 (3)	0.0929 (1)	0.8567 (3)	12.1 (2)
F 22	0.2109 (3)	0.02304 (9)	0.5187 (7)	13.2 (2)
F 23	0.2066 (2)	0.03862 (9)	0.7453 (5)	12.6 (1)
F 24	0.3263 (3)	0.0115 (1)	0.6812 (6)	15.8 (2)
O 1	–0.3703 (1)	0.14861 (6)	–0.1914 (2)	5.19 (7)
O 2	–0.3124 (1)	0.09253 (5)	–0.1368 (2)	5.14 (7)
O 3	0.1346 (1)	0.14432 (6)	0.5017 (3)	5.25 (7)
O 4	0.2292 (2)	0.09641 (6)	0.5689 (2)	5.42 (7)
C 1	–0.2078 (2)	0.16373 (8)	–0.1086 (4)	5.22 (8)
C 2	–0.1119 (2)	0.1698 (1)	–0.0741 (5)	6.5 (1)
C 3	–0.0810 (3)	0.1986 (1)	0.0156 (7)	8.3 (2)
C 4	–0.1412 (4)	0.2207 (1)	0.0785 (8)	9.8 (2)
C 5	–0.2360 (3)	0.2150 (1)	0.0490 (6)	8.6 (2)
C 6	–0.2681 (2)	0.18676 (9)	–0.0449 (5)	6.0 (1)
C 7	–0.3682 (2)	0.17693 (8)	–0.0901 (4)	5.40 (9)
C 8	–0.4166 (3)	0.1645 (1)	0.0451 (4)	6.8 (1)
C 9	–0.4216 (3)	0.2089 (1)	–0.1677 (6)	7.4 (1)
C 10	–0.1573 (2)	0.09758 (9)	–0.2205 (4)	5.46 (9)
C 11	–0.0749 (3)	0.1040 (1)	–0.2834 (5)	6.6 (1)
C 12	–0.0042 (3)	0.0784 (1)	–0.2713 (6)	7.7 (1)
C 13	–0.0166 (3)	0.0458 (1)	–0.2031 (6)	8.4 (2)
C 14	–0.0976 (3)	0.0383 (1)	–0.1409 (6)	7.3 (1)

Table 3-4. Continued (3)

9

atom	x	y	z	B (eq)
C 15	–0.1667 (2)	0.06468 (9)	–0.1520 (4)	5.74 (9)
C 16	–0.2593 (2)	0.06175 (9)	–0.0909 (4)	5.54 (9)
C 17	–0.2446 (3)	0.0626 (1)	0.0825 (4)	6.5 (1)
C 18	–0.3158 (3)	0.0288 (1)	–0.1473 (6)	7.6 (1)
C 19	–0.2956 (3)	0.1305 (1)	–0.4284 (4)	6.7 (1)
C 20	–0.2505 (4)	0.1648 (2)	–0.4800 (6)	9.8 (2)
C 21	–0.4016 (3)	0.1327 (2)	–0.4749 (5)	8.4 (2)
C 22	–0.2617 (5)	0.0980 (2)	–0.5128 (6)	11.0 (2)
C 23	0.2802 (2)	0.16546 (8)	0.4135 (4)	5.18 (8)
C 24	0.3615 (3)	0.1742 (1)	0.3520 (5)	6.5 (1)
C 25	0.3980 (3)	0.2087 (1)	0.3683 (6)	8.1 (1)
C 26	0.3562 (3)	0.2350 (1)	0.4460 (6)	8.2 (2)
C 27	0.2764 (3)	0.2269 (1)	0.5104 (5)	7.1 (1)
C 28	0.2389 (2)	0.19238 (8)	0.4925 (4)	5.66 (9)
C 29	0.1521 (2)	0.17909 (9)	0.5534 (4)	5.45 (9)
C 30	0.1640 (3)	0.1793 (1)	0.7253 (5)	7.1 (1)
C 31	0.0679 (3)	0.2026 (1)	0.4949 (6)	7.3 (1)
C 32	0.3230 (2)	0.09414 (9)	0.3583 (4)	5.15 (8)
C 33	0.3669 (3)	0.0949 (1)	0.2266 (4)	6.1 (1)
C 34	0.4413 (3)	0.0726 (1)	0.2107 (4)	6.5 (1)
C 35	0.4759 (3)	0.0498 (1)	0.3255 (5)	6.6 (1)
C 36	0.4346 (2)	0.0482 (1)	0.4551 (5)	6.5 (1)
C 37	0.3582 (2)	0.07044 (9)	0.4687 (4)	5.40 (9)
C 38	0.3043 (2)	0.0725 (1)	0.6035 (4)	6.2 (1)
C 39	0.3653 (4)	0.0893 (2)	0.7382 (5)	9.0 (2)
C 40	0.2619 (4)	0.0360 (2)	0.6366 (9)	10.5 (2)
C 41	0.1320 (3)	0.1068 (1)	0.2578 (4)	6.4 (1)
C 42	0.1334 (4)	0.1352 (2)	0.1333 (6)	9.3 (2)
C 43	0.0335 (3)	0.1057 (2)	0.3041 (7)	9.8 (2)
C 44	0.1521 (4)	0.0696 (2)	0.1944 (8)	9.7 (2)

Dynamic NMR Measurement and Line Shape Analysis

Samples of **8** (ca. 15 mg in 0.5–0.6 mL of solvent unless noted otherwise) dissolved in freshly distilled toluene-d_8 were sealed in NMR tubes under N_2. ^{19}F NMR spectra were measured on a JEOL EX-400 (376 MHz) in a variable temperature mode, and the specified temperatures were maintained throughout each set of measurements (error within ± 1 °C). The observed temperatures were calibrated with the ^1H NMR chemical shift difference of signals of neat 1,3-propanediol (high temperature region) and MeOH (low temperature region). The rates and activation free energies at the coalescence point were calculated using the following equations derived from the Gutowsky-Holm appoximation of $k = \pi \Delta\nu/2^{-1/2}$.[11]

$$\Delta G^{\ddagger} = 19.14\, T_c\, \{9.97 + \log (T_c/\delta_\nu)\}/4.184 \quad <\text{kcal mol}^{-1}>$$

$$\Delta G^{\ddagger} = \{23.76 - \ln (k/T)\}\, RT$$

The line shape analysis was performed in a narrow temperature range around the coalescence point according to the classical Gutowsky-Holm method neglecting $^4J_{F-F}$ coupling since the condition $J/\Delta\nu << 1$ is met. The activation enthalpies and entropies were calculated according to the transition state theory of Eyring[12] using the following equations by linear regression.

$$\ln (k/T) = \Delta H^{\ddagger}/RT + \Delta S^{\ddagger} + \ln (k_B/h)$$

The systematic error associated with the simulated rates was estimated to be 10% and calculated with the following equation since the proportional error for $\Delta H^{\ddagger}$ and $\Delta S^{\ddagger}$ are the same as for Ea.[11]

$$(\delta_{Ea}/E)^2 \approx [2T^2/(\Delta T)^2]\, (\delta_T/T)^2 + 2[\Delta(\ln k)]^{-2}\, (\delta_k/k)^2$$

Table 3-5. Kinetic Parameters of Inversion at Phosphorus Atom in **8** in toluene-d_8

T <K>	k <sec^{-1}>	$\Delta G^{\ddagger}$ <kcal mol^{-1}>	$\Delta H^{\ddagger}$ <kcal mol^{-1}>	$\Delta S^{\ddagger}$ <eu>
223	150	10.7		
228	243	10.7		
231	341	10.7		
233	415	10.7		
235	505	10.7	10.0 ± 0.7	–3.4 ± 3.0
237	600	10.8	(± 0.1)*	(± 0.4)*
239	705	10.8		
241	870	10.8		
243	1030	10.8		

* Statistical error in parenthesis

Eyring Plot

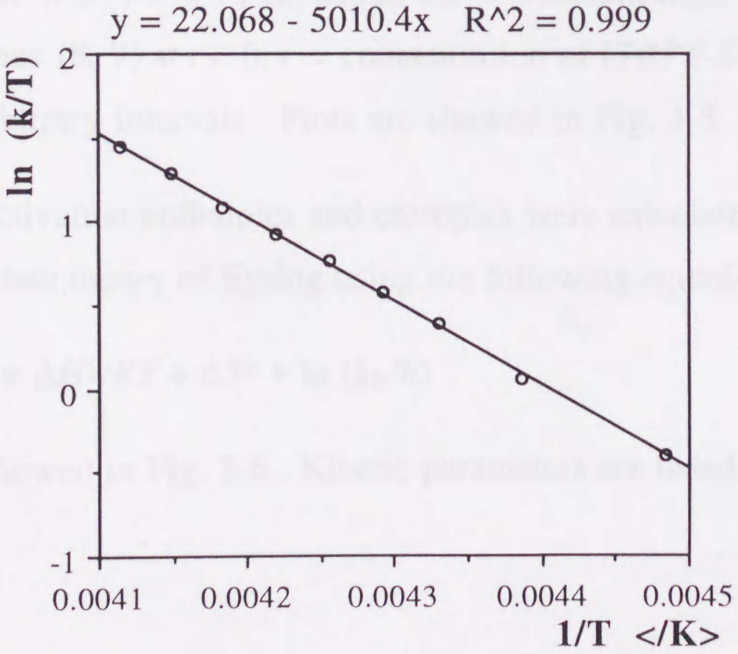

Kinetic Measurements of the Pseudorotation of 8 and 9.

Samples of **8** and **9** (ca. 15 mg in 0.5–0.6 mL of solvent) dissolved in freshly distilled solvents were sealed in NMR tubes under N_2. For the observation of the permutation of **8** ^{19}F NMR spectra were measured on a JEOL EX-400 in a variable temperature mode, and the specified temperatures were maintained throughout each set of measurements (error within ± 1 °C). The observed temperatures were calibrated with the ^{1}H NMR chemical shift difference of signals of neat 1,3-propanediol (high temperature region) and MeOH (low temperature region). For the observation of the pseudorotation of **9**, ^{19}F NMR spectra were measured on a JEOL EX-400 at rt after heating samples at maintained temperatures for arbitrary periods of time, and the specified temperatures were maintained with a silicon oil bath (error within ± 2 °C).

The ratio of [*TBPY*-5-12] phosphoranes (**8**, **9**) and [*TBPY*-5-11] phosphoranes (**5**, **6**) was monitored by integration of ^{19}F NMR signals. The data were analysed by assuming irreversible first-order kinetics using the equation $\ln (c_0/c) = k\,T$, in which c_0 = concentration of [*TBPY*-5-12] phosphoranes (**8**, **9**) at $t = 0$, c = concentration of [*TBPY*-5-12] phosphoranes (**8**, **9**) at arbitrary intervals. Plots are showed in Fig. 3-5.

The activation enthalpies and entropies were calculated according to the transition state theory of Eyring using the following equation.

$$\ln (k/T) = \Delta H^{\ddagger}/RT + \Delta S^{\ddagger} + \ln (k_B/h)$$

Plots are showed in Fig. 3-6. Kinetic parameters are listed in Table 3-6.

Figure 3-5. Plot of ln (c_0/c) vs. time. [c_0 = concentration of [*TBPY*-5-12] phosphoranes (**8**, **9**) at $t = 0$, c = concentration of [*TBPY*-5-12] phosphoranes (**8**, **9**) at arbitrary intervals].

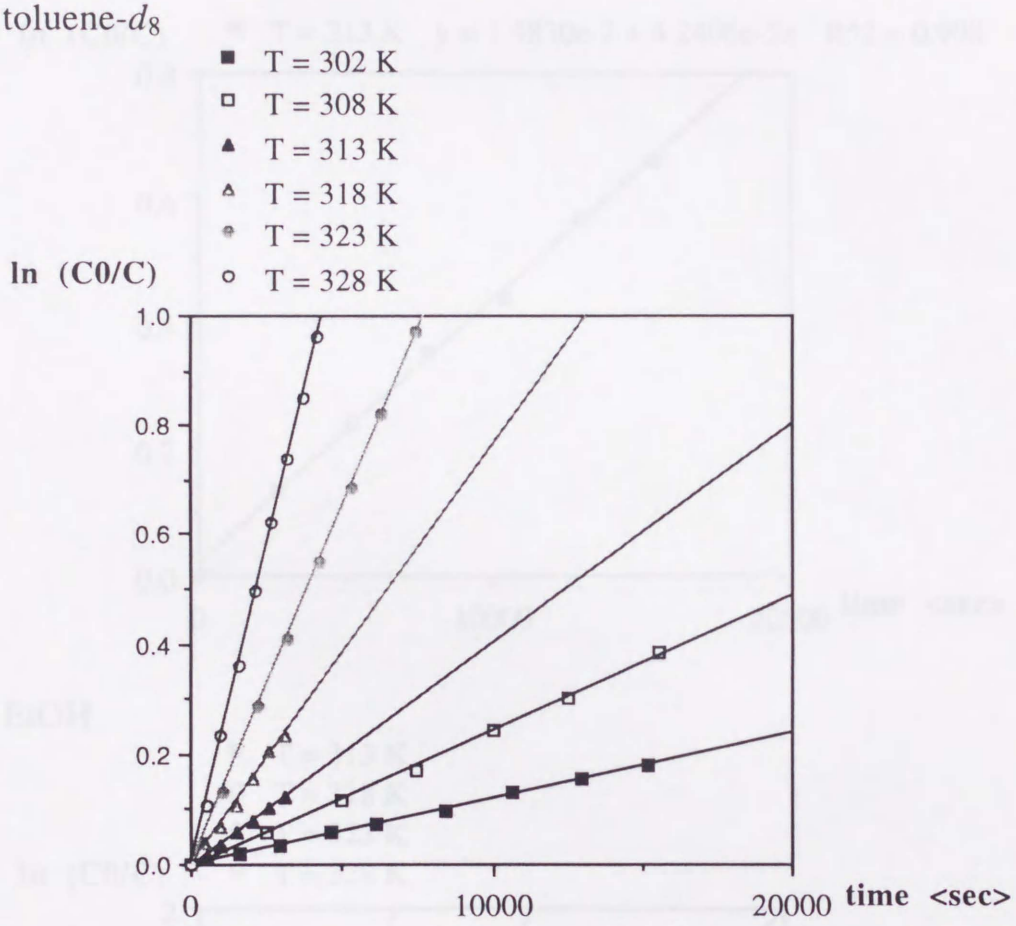

Figure 3-5. Continued (1)

8 in pyridine

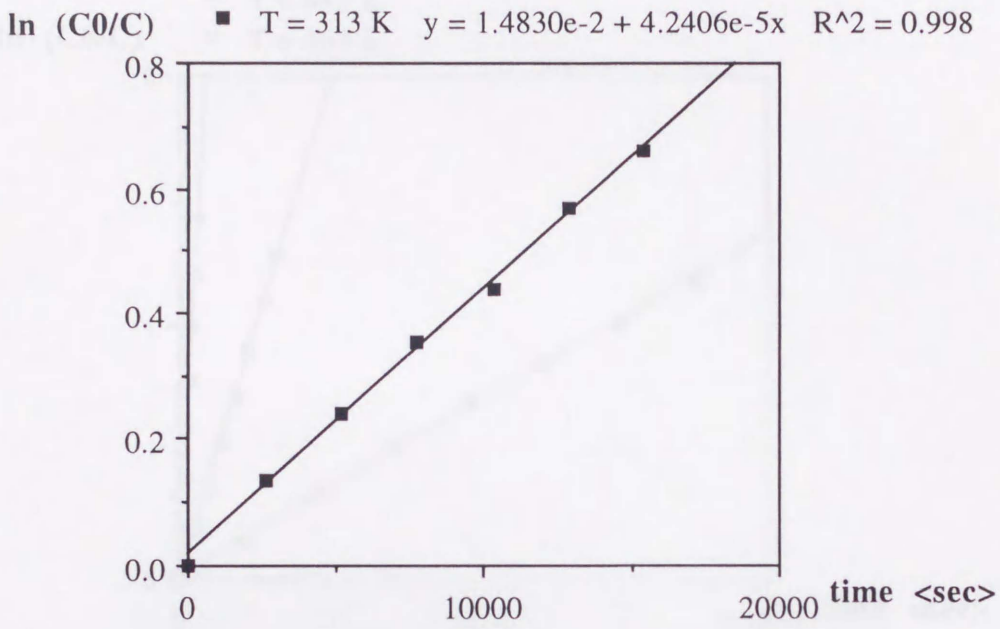

8 in EtOH

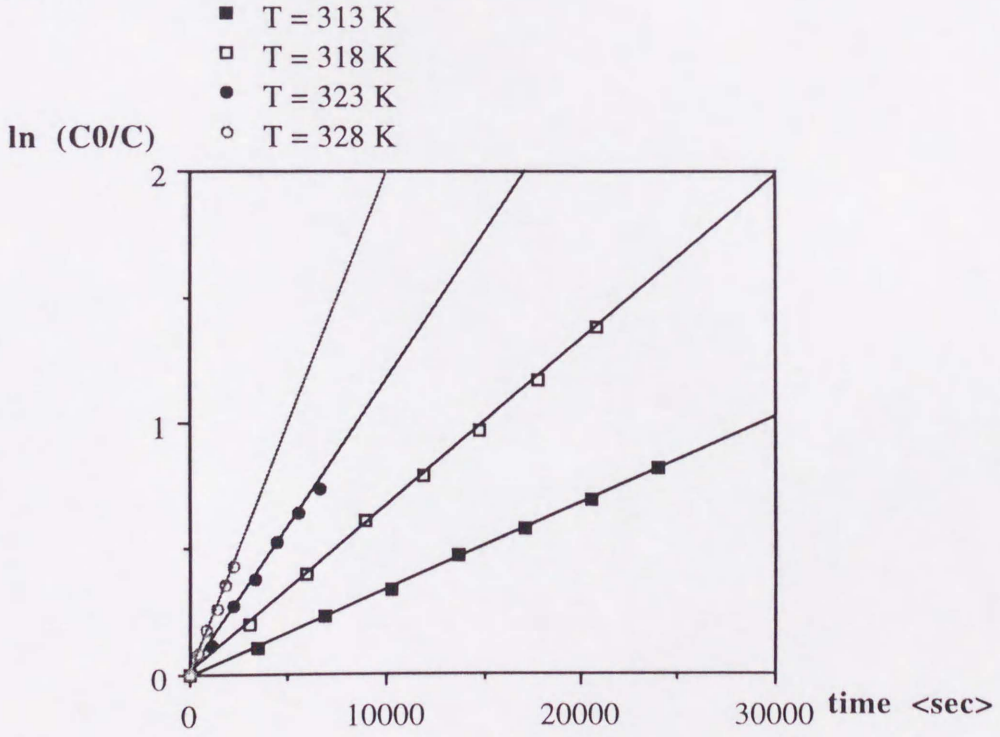

Figure 3-5. Continued (2)

9 in 4-*t*-butyltoluene

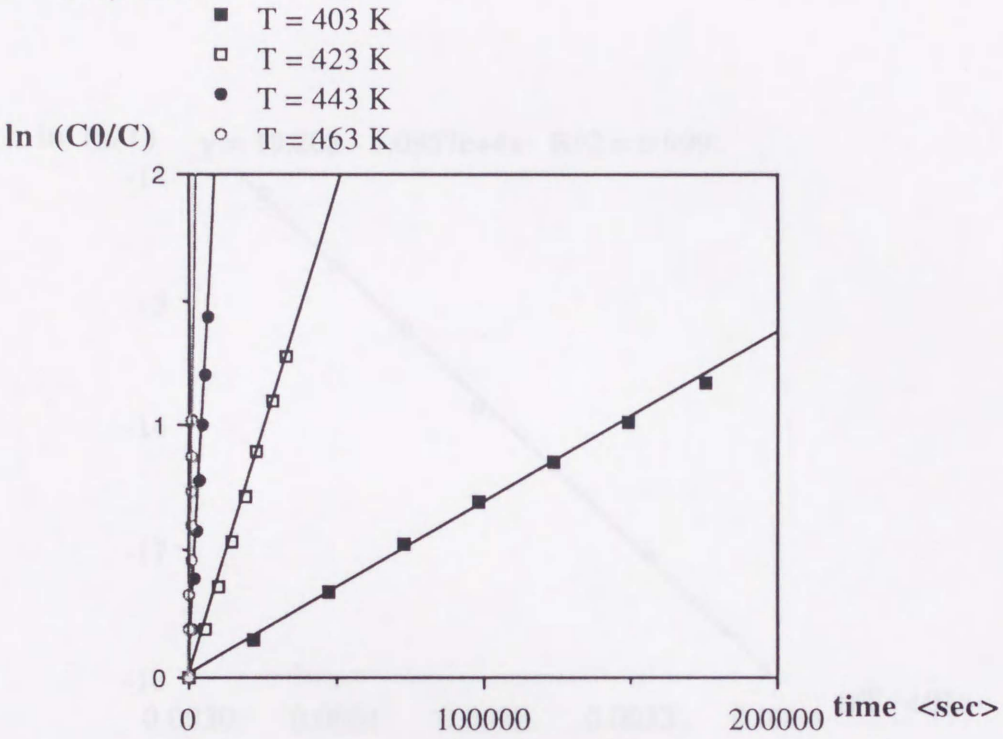

Figure 3-6. Eyring plot.

8 in toluene-d_8

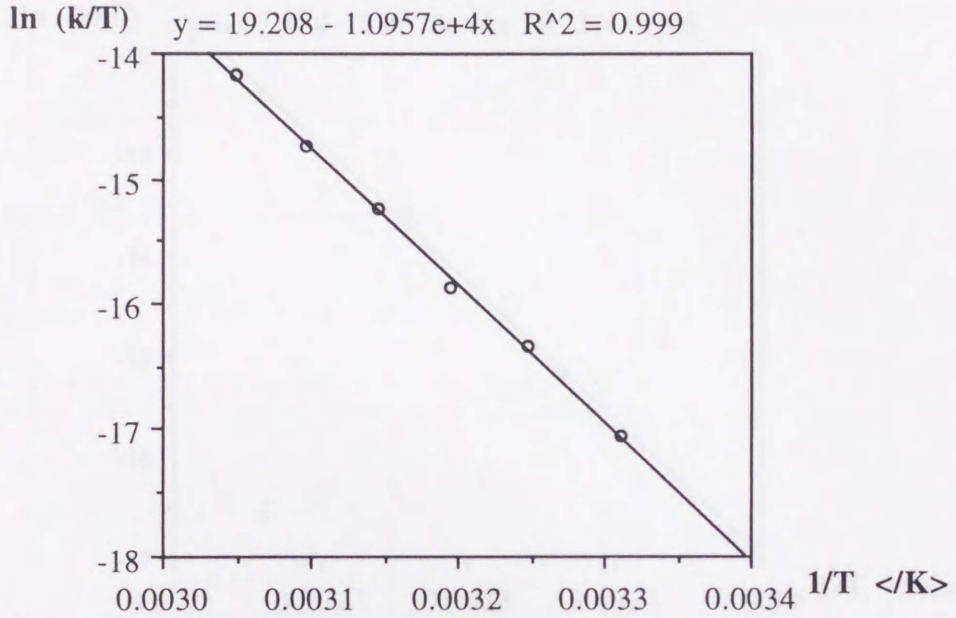

8 in EtOH.

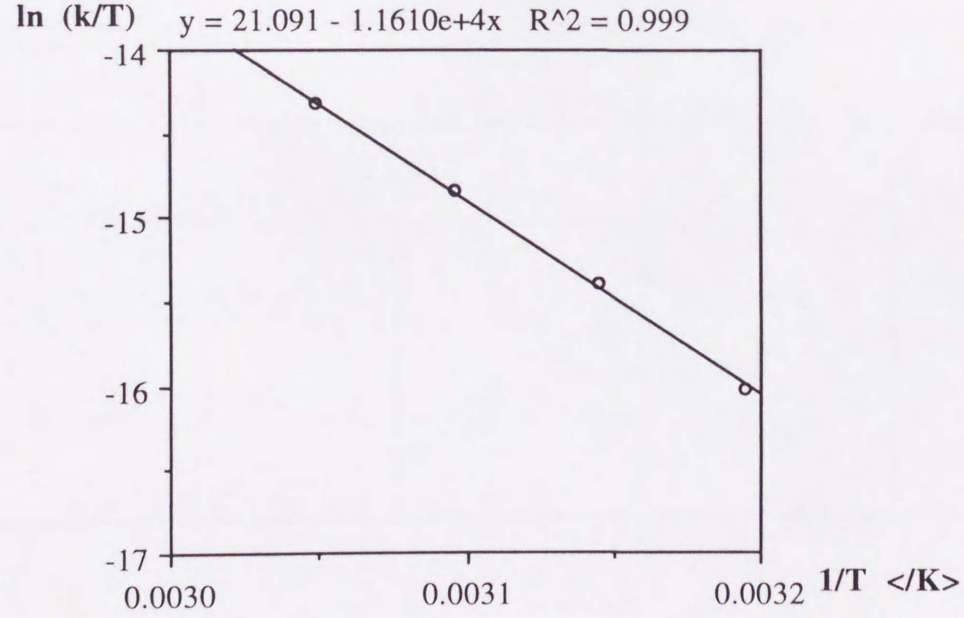

Figure 3-6. Continued (1)

9 in 4-*t*-butyltoluene

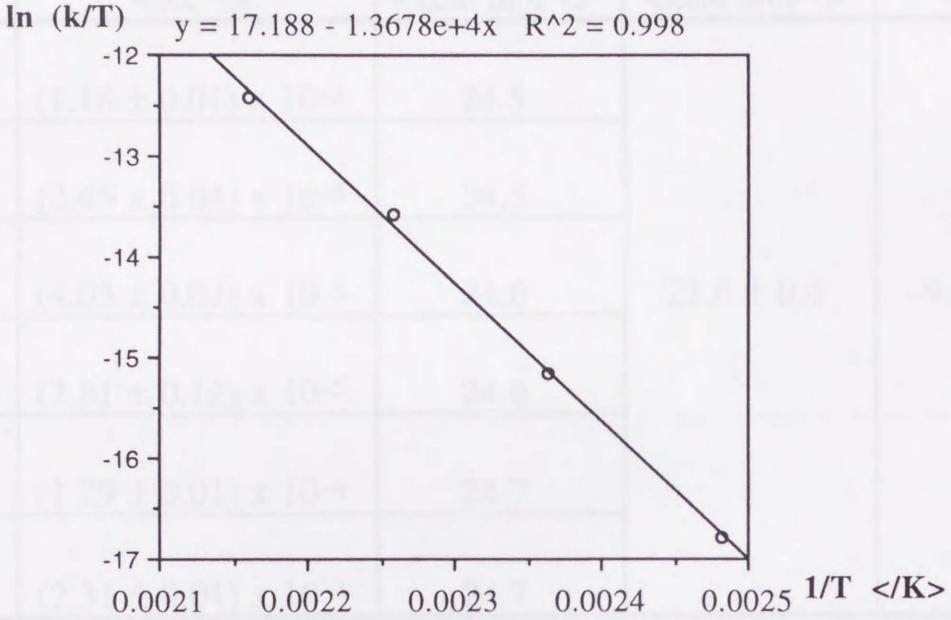

Table 3-6. Kinetic Parameters

8 in toluene-d_8

T <K>	k <sec^{-1}>	$\Delta G^{\ddagger}$ <kcal mol^{-1}>	$\Delta H^{\ddagger}$ <kcal mol^{-1}>	$\Delta S^{\ddagger}$ <eu>
302	(1.18 ± 0.01) x 10^{-5}	24.5		
308	(2.45 ± 0.04) x 10^{-5}	24.5		
313	(4.03 ± 0.07) x 10^{-5}	24.6	21.8 ± 0.4	–9.0 ± 1.2
318	(7.61 ± 0.12) x 10^{-5}	24.6		
323	(1.29 ± 0.01) x 10^{-4}	24.7		
328	(2.31 ± 0.01) x 10^{-4}	24.7		

8 in EtOH

T <K>	k <sec^{-1}>	$\Delta G^{\ddagger}$ <kcal mol^{-1}>	$\Delta H^{\ddagger}$ <kcal mol^{-1}>	$\Delta S^{\ddagger}$ <eu>
313	(3.44 ± 0.03) x 10^{-5}	24.7		
318	(6.56 ± 0.05) x 10^{-5}	24.7	23.1 ± 0.5	–5.3 ± 1.5
323	(1.16 ± 0.03) x 10^{-4}	24.8		
328	(1.97 ± 0.02) x 10^{-4}	24.8		

Table 3-6. Continued (1)

9 in 4-*t*-butyltoluene

T <K>	k <sec^{-1}>	$\Delta G^{\ddagger}$ <kcal mol^{-1}>	$\Delta H^{\ddagger}$ <kcal mol^{-1}>	$\Delta S^{\ddagger}$ <eu>
403	$(6.73 \pm 0.10) \times 10^{-6}$	33.4		
423	$(3.89 \pm 0.02) \times 10^{-5}$	33.5	27.2 ± 0.8	-13.1 ± 1.8
443	$(2.15 \pm 0.04) \times 10^{-4}$	33.7		
463	$(7.62 \pm 0.02) \times 10^{-4}$	34.1		

Kinetic Measurements of the Pseudorotation of 10-*exo* and 10-*endo*.

Samples of **10-*exo*** or **10-*endo*** (ca. 20 mg) dissolved in freshly distilled solvents (0.5–0.6 mL) were sealed in NMR tubes under N_2. For the observation of the pseudorotation between **10-*exo*** and **10-*endo*** ^{19}F NMR spectra were measured on a JEOL EX-400 at rt after heating samples at maintained temperatures for arbitrary periods of time. The specified temperatures were maintained with a silicon oil bath (error within ± 2 °C). The change in the diastereomers was monitored by integration of ^{19}F NMR signals. The data were analyzed by assuming reversible first-order kinetics using the equation $\ln [(x_e - x_0)/(x_e - x)] = k\,(K + 1)\,t$, in which x_e = ratio at equilibrium , x_0 = ratio observed at $t = 0$, x = ratio observed at arbitrary intervals, k = rate constant to be determined (k_+; **10-*exo*** to **10-*endo***: k_-; **10-*endo*** to **10-*exo***), and K = equilibrium ratio. The equilibrium ratios were determined after heating the measured samples in a silicon oil bath at the specified temperature (± 2 °C) for at least 5 lifetimes.

Figure 3-7. Plot of ln $[(x_e - x_0) / (x_e - x)]$ vs. time. (x_e = ratio at equilibrium, x_0 = ratio observed at $t = 0$, x = observed ratio at arbitrary intervals).

10 in 4-*t*-butyltoluene

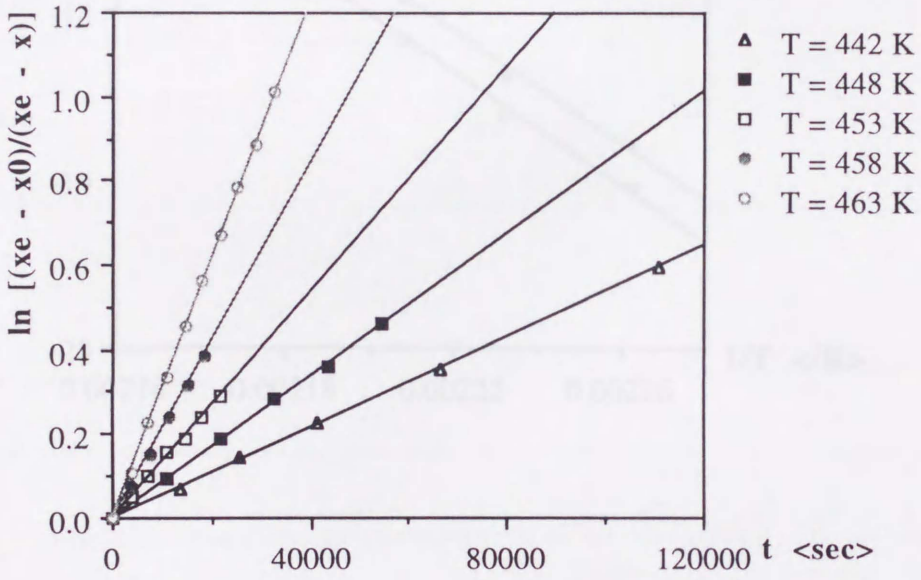

Figure 3-8. Eyring plot.

10 in 4-*t*-butyltoluene

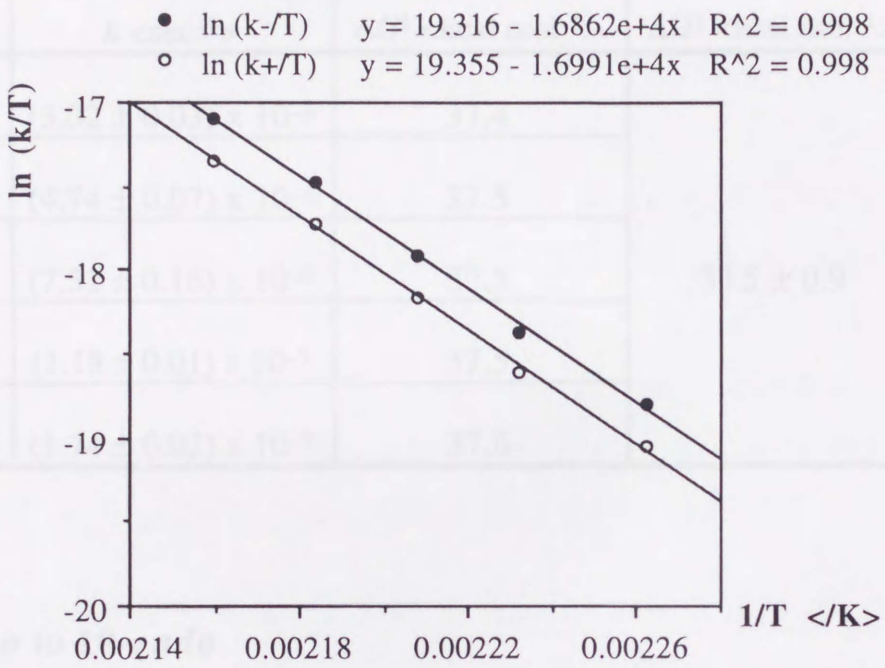

Table 3-7. Kinetic Parameters

10-*endo* to **10-*exo***

T <K>	k <sec^{-1}>	$\Delta G^{\ddagger}$ <kcal mol^{-1}>	$\Delta H^{\ddagger}$ <kcal mol^{-1}>	$\Delta S^{\ddagger}$ <eu>
442	$(3.02 \pm 0.03) \times 10^{-6}$	37.4		
448	$(4.74 \pm 0.07) \times 10^{-6}$	37.5		
453	$(7.52 \pm 0.16) \times 10^{-6}$	37.5	33.5 ± 0.9	-8.8 ± 1.9
458	$(1.18 \pm 0.01) \times 10^{-5}$	37.5		
463	$(1.74 \pm 0.02) \times 10^{-5}$	37.6		

10-*exo* to **10-*endo***

T <K>	k <sec^{-1}>	$\Delta G^{\ddagger}$ <kcal mol^{-1}>	$\Delta H^{\ddagger}$ <kcal mol^{-1}>	$\Delta S^{\ddagger}$ <eu>
442	$(2.34 \pm 0.03) \times 10^{-6}$	37.6		
448	$(3.68 \pm 0.06) \times 10^{-6}$	37.7		
453	$(5.83 \pm 0.12) \times 10^{-6}$	37.7	33.8 ± 0.9	-8.7 ± 1.9
458	$(9.18 \pm 0.09) \times 10^{-6}$	37.8		
463	$(1.35 \pm 0.02) \times 10^{-5}$	37.8		

D. References

(1) (a) Pimentel, G. C. *J. Chem. Phys.* **1951**, *19*, 446. (b) Hach, R. J.; Rundle, R. E. *J. Am. Chem. Soc.* **1951**, *73*, 4321.

(2) (a) Holmes, R. R. *Pentacoordinate Phosphorus-Structure and Spectroscopy*; ACS Monograph 175, 176; American Chemical Society: Washington, DC, 1980; Vols. I, II. (b) Trippett, S. *Phosphorus, Sulfur Silicon Relat. Elem.* **1976**, *1*, 89. (c) McDowell, R. S.; Streitwieser, A. *J. Am. Chem. Soc.* **1985**, *107*, 55. (d) Wang, P.; Zhang, Y.; Glaser, R.; Reed, A. E.; Schleyer, P. v. R.; Streitwieser, A. *J. Am. Chem. Soc.* **1991**, *113*, 55. (e) Thatcher, G. R. J.; Campbell, A. S. *J. Org. Chem.* **1993**, *58*, 2272. (f) Wasada, H.; Hirao, K. *J. Am. Chem. Soc.* **1992**, *114*, 16.

(3) (a) Granoth, I.; Martin, J. C. *J. Am. Chem. Soc.* **1979**, *101*, 4618. (b) Granoth, I.; Martin, J. C. *J. Am. Chem. Soc.* **1979**, *101*, 4623. (c) Kojima, S.; Kajiyama, K.; Akiba, K.-y. *Tetrahedron Lett.* **1994**, *35*, 7037. Kojima, S.; Kajiyama, K.; Akiba, K.-y. *Bull. Chem. Soc. Jpn.* **1995**, *68*, 1785. Kojima, S.; Nakamoto, M.; Kajiyama, K.; Akiba, K.-y. *Tetrahedron Lett.* **1995**, *36*, 22617.

(4) Berry, R. S. *J. Chem. Phys.* **1960**, *32*, 933.

(5) (a) Timosheva, N. V.; Prakasha, T. K.; Chandrasekaran, A.; Day, R. O.; Holmes, R. R. *Inorg. Chem.* **1995**, *34*, 4525. (b) Timosheva, N. V.; Chandrasekaran, A.; Prakasha, T. K.; Day, R. O.; Holmes, R. R. *Inorg. Chem.* **1996**, *35*, 6552.

(6) (a) Kawashima, T.; Kato, K.; Okazaki, R. *J. Am. Chem. Soc.* **1992**, *114*, 4008. (b) Kawashima, T.; Kato, K.; Okazaki, R. *Angew Chem., Int. Ed. Engl.* **1993**, *32*, 869.

(7) Kawashima, T.; Soda, T.; Kato, K.; Okazaki, R. *Phosphorus, Sulfur Silicon Relat. Elem.* **1996**, Vols. 109–110, 489.

(8) Kajiyama, K.; Kojima, S.; Akiba, K.-y. *Tetrahedron Lett.* **1996**, *37*, 8409.

(9) Furusaki, A. *Acta. Crystallogr.* **1979**, *A35*, 220.

(10) Katayama, C. *Acta. Crystallogr.* **1986**, *A42*, 19.

(11) Jackman, L. M.; Cotton, F. A. "*Dynamic Nuclear Magnetic Resonance Spectroscopy*", Academic Press, New York 1975.

(12) Wynne-Jones, W. F. K.; Eyring, H. *J. Chem. Phys.* **1935**, *3*, 492.

Chapter 4

Kinetic Studies

of Thermal Cyclization Reactions

of P–H (apical) Phosphoranes

Bearing a Hydroxy Group

A. Introduction

The heterolysis of element-carbon or element-hydrogen bonds which gives compounds bearing new element-heteroatom bonds with elimination of hydrocarbon or H_2 has been implicated to involve species of higher coordination number during the reaction.[1] As part of our continuous studies on hypervalent organic compounds, we have found that in the intramolecular cyclization reaction of a series of acyclic 8-Si-4[2] *o*-silylbenzyl alcohols (weak acids) **A** to 8-Si-4 cyclic alkoxysilanes **B** with elimination of hydrocarbons (eq 1), the selectivity of the eliminating hydrocarbon is highly dependent on the relative stabilities of isomeric 10-Si-5 transition states.[3] We have suggested that the reaction proceeded via transition states involving pentacoordinate species with a concerted four-membered ring formed by intramolecular coordination of the hydroxy oxygen to Si that the structural stability of the pentacoordinate species has a significant bearing on the selectivity of elimination. This showed the importance of participation of the hypervalent bond in the transition state besides acidity of the eliminating hydrocarbons.[4]

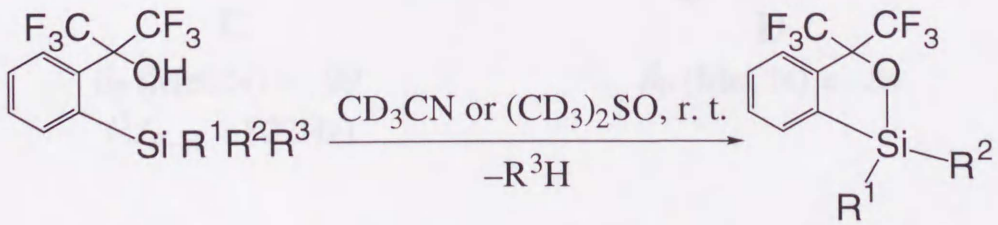

A **B** (1)

In analogous transformation of monocyclic 10-Bi-5 alcohols to bicyclic 10-Bi-5 bismuthanes the intermediacy of hexacoordinate 12-Bi-6 species could be verified.[5] We have also observed selectivity that does not parallel the acidities in hydrocarbon elimination from monocyclic 12-Sb-6 ate complexes upon hydrolysis.[6] In the case of phosphorus compounds this phenomenon is not usually seen for neutral ordinary valent compounds. Especially for hypervalent phosphorus compounds bearing P–H bonds we know of only a few examples. Hexacoordinate P–H phosphate **C** cyclized with elimination of hydrogen gas to give tricyclic hexacoordinate phosphate **D** (eq 2).[7] Monocyclic P–H phosphorane **F** was observed upon reacting **E** with cathecol, and **F** gradually transformed to **G** (eq 3).[8] However since hypervalent phosphorus compounds are usually very susceptible to moisture it has been rather difficult to carry out kinetic studies of this interesting process of dihydrogen elimination and there is no report that we are aware of.

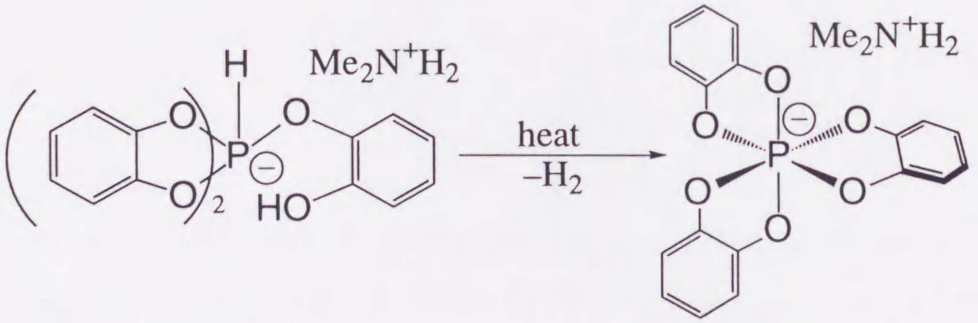

(2)

C

δ_P (MeCN) = –99

($^1J_{P-H}$ = 802Hz)

D

δ_P (MeCN) = –84

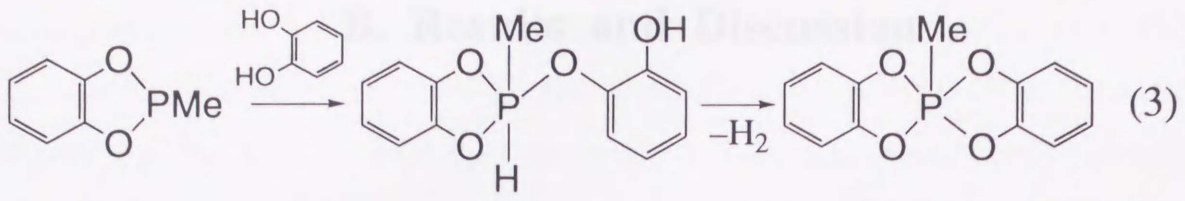

E **F** **G** (3)

As described in Chapter 3, monocyclic P–H (apical) phosphoranes **1–3** cyclized intramolecularly with elimination of hydrogen to form the coresponding [*TBPY*-5-11] spirophosphoranes **4–6** predominantly in nondonor solvents and the coresponding [*TBPY*-5-12] spirophosphoranes **8–10** predominantly in donor solvents on heating. In order to gain an understanding of the mechanism and the solvent effect of the thermal cyclization of **1–3**, we have carried out the kinetic studies on it. On the basis of these results we propose the mechanisms for the process for both in nondonor and donor solvents.

B. Results and Discussion

1. Kinetic Studies of Thermal Cyclization Reaction of P–H (Apical) Phosphoranes 2 and 3 Bearing a Hydroxyl Group in Nondonor Solvents.

Scheme 4-1

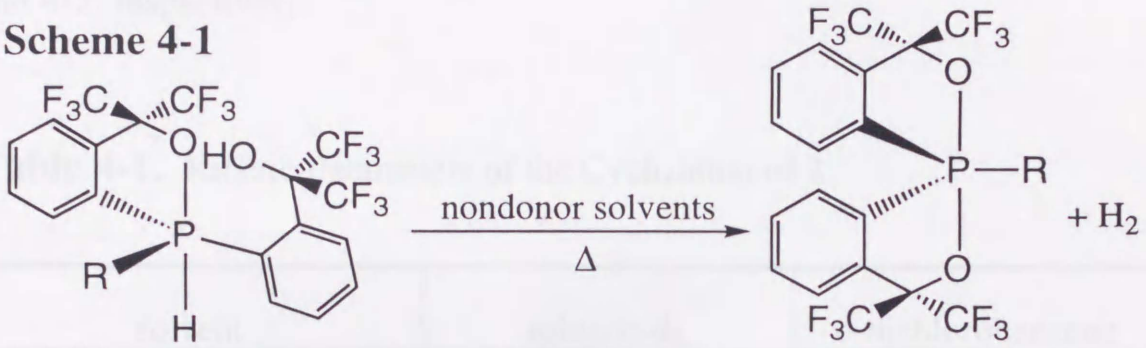

1; R = Me
2; R = *n*-Bu
3; R = *t*-Bu

4; R = Me
5; R = *n*-Bu
6; R = *t*-Bu
7; R = H

In nondonor solvents such as toluene, *p*-xylene, *o*-dichlorobenzene, monocyclic P–H (apical) phosphoranes **1–3** cyclized intramolecularly with elimination of hydrogen to form [*TBPY*-5-11] spirophosphoranes **4–6** on heating (Scheme 4-1). The cyclization of **1** (R = Me) to **4** was too fast to monitor. The rates of cyclization of **2** (R = *n*-Bu) to **5** were measured in toluene-d_8 (343–373 K) and *o*-dichlorobenzene (343–373 K) by monitoring ^{19}F NMR. In the case of cyclization of **3** to **6**, the rates in *p*-xylene (393–423K) and *o*-dichlorobenzene (393–423K) were measured by monitoring ^{31}P NMR because of the complexity of the ^{19}F NMR spectra. In the case of the cyclization of **3** in *o*-dichlorobenzene, [TBPY-5-11] P–H (equatorial)

spirophosphorane **7** [38 % (423 K)] also formed along with **6** [62 % (423 K)]. The cyclization of **3** to **7** could also be observed in *p*-xylene. However, in the range of 403–423 K **7** could only be detected in trace amounts compared with **6**. All the processes followed first-order kinetics quite satisfactorily. The Eyring plot of the rates also turned out to be linear thus implying the existence of only a single process for the cyclization. Representative rates and activation parameters of the cyclization of **2** and **3** are shown in Table 4-1 and 4-2, respectively.

Table 4-1. Kinetic Parameters of the Cyclization of **2**

solvent	toluene-d_8	*o*-dichlorobenzene
product	**5**	**5**
k <sec^{-1}> (373 K)	(1.46 ± 0.03) x 10^{-5}	(5.55 ± 0.05) x 10^{-5}
$\Delta G^{\ddagger}$ <kcal mol^{-1}> (373 K)	30.3	29.3
$\Delta H^{\ddagger}$ <kcal mol^{-1}>	17.3 ± 0.6	14.0 ± 0.2
$\Delta S^{\ddagger}$ <kcal mol^{-1}>	–34.7 ± 1.7	–41.0 ± 0.6

Table 4-2. Kinetic Parameters of the Cyclization of **3**

solvent	*p*-xylene	
product	**6**	**7**
k <sec^{-1}> (393 K)	(1.14 ± 0.02) x 10^{-6}	(8.10 ± 0.21) x 10^{-7}
$\Delta G^{\ddagger}$ <kcal mol^{-1}> (393 K)	33.9	34.2
$\Delta H^{\ddagger}$ <kcal mol^{-1}>	32.2 ± 1.1	—
$\Delta S^{\ddagger}$ <kcal mol^{-1}>	–4.29 ± 2.6	—

solvent	*o*-dichlorobenzene	
product	**6**	**7**
k <sec^{-1}> (393 K)	(2.06 ± 0.01) x 10^{-6}	(1.81 ± 0.02) x 10^{-6}
$\Delta G^{\ddagger}$ <kcal mol^{-1}> (393 K)	33.4	33.5
$\Delta H^{\ddagger}$ <kcal mol^{-1}>	29.5 ± 0.7	25.0 ± 1.0
$\Delta S^{\ddagger}$ <kcal mol^{-1}>	–9.9 ± 1.8	–21.8 ± 2.6

In nondonor solvents, the cyclization rates of phosphoranes **2** and **3** to [*TBPY*-5-11] spirophosphoranes **5**, **6** and **7** in *o*-dichlorobenzene (E_T^N = 0.225) as the polar solvent [**2** to **5**; k = (5.55 ± 0.05) x 10^{-5} sec^{-1} (373 K), **3** to **6**; k = (2.06 ± 0.01) x 10^{-6} sec^{-1} (393 K), **3** to **7**; k = (1.81 ± 0.02) x 10^{-6} sec^{-1} (393 K)] were faster than those in toluene-d_8 (E_T^N = 0.099) and *p*-xylene (E_T^N = 0.074) as the nonpolar solvents [**2** to **5**; k = (1.46 ± 0.03) x 10^{-5} sec^{-1} (373 K), **3** to **6**; k = (1.14 ± 0.02) x 10^{-6} sec^{-1} (393 K), **3** to **7**; k = (8.10 ±

0.21) x 10^{-7} sec^{-1} (393 K)]. The activation enthalpies in the polar solvent (**2**; $\Delta H^{\ddagger}$ = 14.0 ± 0.2 kcal mol^{-1}, **3**; $\Delta H^{\ddagger}$ = 29.5 ± 0.7 kcal mol^{-1}) were ca. 3 kcal mol^{-1} smaller than those in nonpolar solvents (**2**; $\Delta H^{\ddagger}$ = 17.3 ± 0.6 kcal mol^{-1}, **3**; $\Delta H^{\ddagger}$ = 32.2 ± 1.1 kcal mol^{-1}), while the difference in barriers between **2** and **3** was ca. 15 kcal/mol (= 32 – 17). The activation entropies of **2** were large negative values and those of **3** were negative but the magnitude was much smaller.

The fact that a solvent effect in terms of solvent polarity existed but the degree was small suggests that the intramolecular cyclization reactions of phosphoranes **1–3** with elimination of hydrogen gas proceed via slightly polarized, concerted four-membered transition states[3, 4] (**TS-A**), with the involvement of hexacoordinate phosphorus species which is considerably more congested than the pentacoordinate ground state to afford [TBPY-5-11] spirophosphoranes **4–6** as depicted in Scheme 4-2. **TS-A** and **TS-B** will result from pseudorotation and successive approach of the hydroxy oxygen to the lowest σ^* orbital; that of the P–O bond. Among nondonor solvents, the more polar solvent (*o*-dichlorobenzene) stabilizes the polarized transition state so that the rate of the intramolecular cyclization may be accelerated. The large difference in activation enthalpy between **2** and **3** probably reflects the reluctance for **3** to cyclize due to much larger steric hindrance. The large negative activation entropies values of **2** is in accord with the hindered enviropment about phosphorus upon assuming hexacoordination from pentacoordination in the transition state.[9] In the case of **3** to **6**, the ground state is probably already highly motionally hindered due to the back strain of the *t*-Bu group. That the magnitude of activation entropy of the formation of **7** is larger than that of **6** is probably because the *t*-butyl group itself participates in the bond transformation in the transition state (**TS-B**).

Scheme 4-2

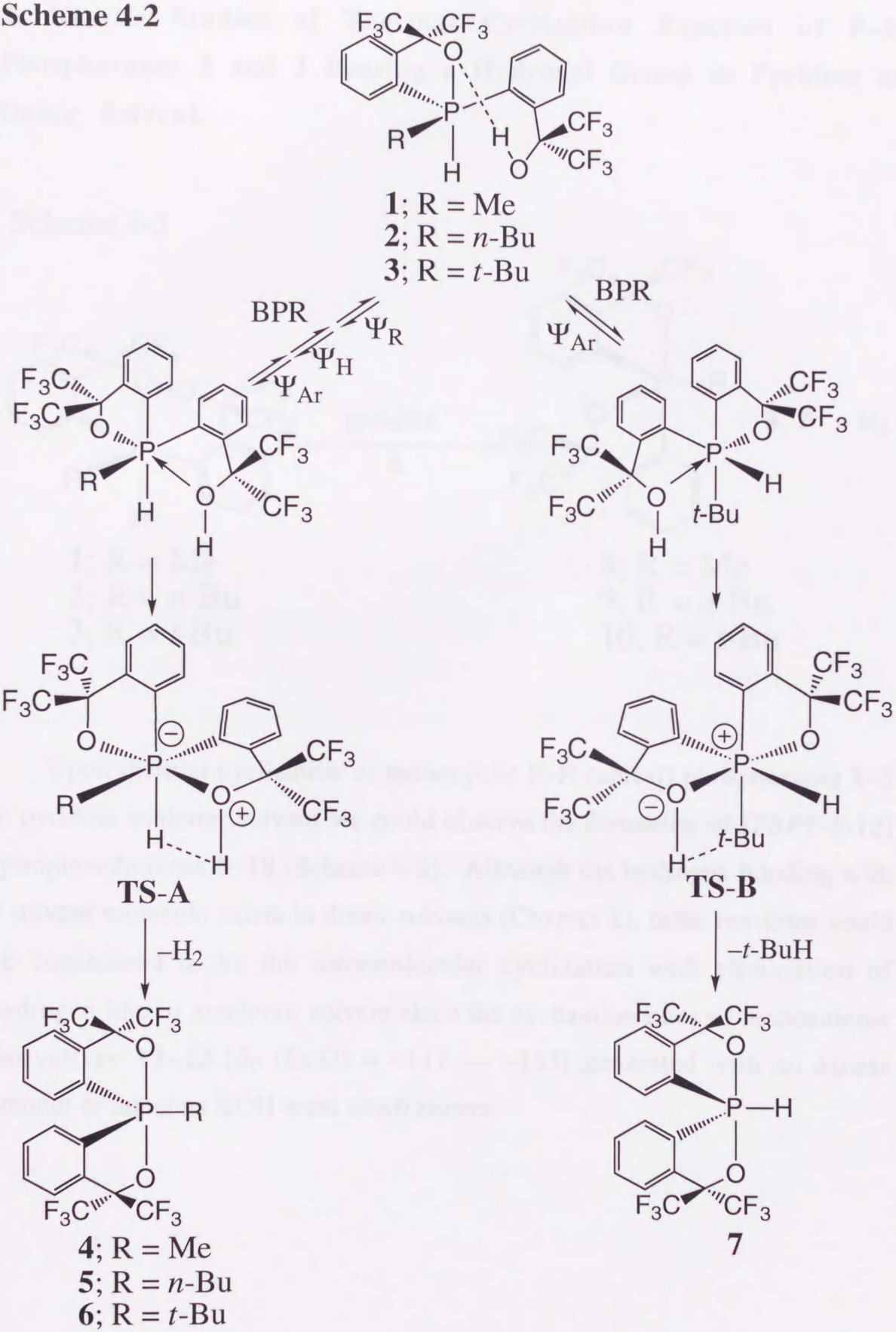

1; R = Me
2; R = *n*-Bu
3; R = *t*-Bu

4; R = Me
5; R = *n*-Bu
6; R = *t*-Bu

7

2. Kinetic Studies of Thermal Cyclization Reaction of P–H Phosphoranes 2 and 3 Bearing a Hydroxyl Group in Pyridine as Donor Solvent.

Scheme 4-3

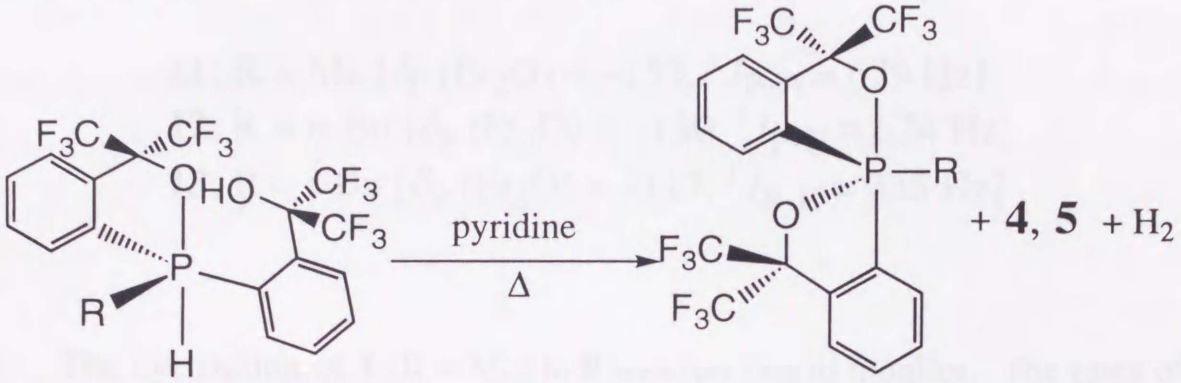

1; R = Me
2; R = *n*-Bu
3; R = *t*-Bu

8; R = Me
9; R = *n*-Bu
10; R = *t*-Bu

Upon thermal cyclization of monocyclic P–H (apical) phosphoranes **1–3** in pyridine as donor solvent we could observe the formation of [*TBPY*-5-12] spirophosphoranes **8–10** (Scheme 4-3). Although the hydrogen bonding with a solvent molecule exists in donor solvents (Chapter 2), these reactions could be considered to be the intramolecular cyclization with elimination of hydrogen like in nondonor solvent since the cyclization rates of monoanionic derivatives **11–13** [δ_P (Et_2O) = –117 — –153] generated with an excess amount of aqueous KOH were much slower.

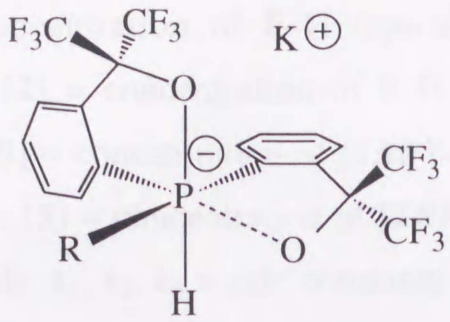

11; R = Me [δ_P (Et_2O) = –153, $^1J_{P-H}$ = 679 Hz]
12; R = *n*-Bu [δ_P (Et_2O) = –130, $^1J_{P-H}$ = 674 Hz]
13; R = *t*-Bu [δ_P (Et_2O) = –117, $^1J_{P-H}$ = 335 Hz]

The cyclization of **1** (R = Me) to **8** was too fast to monitor. The rates of cyclization of **2** (R = *n*-Bu) to **9** (308–323 K) and **3** (R = t-Bu) to **10** (333–363 K) were measured by monitoring ^{19}F NMR. In the case of **1** (R = Me) and **2** (R = *n*-Bu) the formation of [*TBPY*-5-11] spirophosphoranes **4** and **5**, respectively, was also observed even in the early reaction period. As mentioned in Chapter 3, since the pseudorotation of **9** to **5** occurred in this temperature range, the reaction of **2** in pyridine was assumed to involve a combination of competitive and consecutive reactions, and follow irreversible first-order kinetics (Scheme 4-4). The analysis was carried out by curve fitting (Fig. 4-1; T = 323 K) of the data to the following set of equations.

$$[\mathbf{2}] = [\mathbf{2}]_0 \exp\{-(k_1 + k_3)\, t\} \quad (1)$$

$$[\mathbf{9}] = \mathrm{K}\,[\mathbf{2}]_0 \exp\{-(k_1 + k_3)\, t\} - \mathrm{K}\,[\mathbf{2}]_0 \exp(-k_2\, t) \quad (2)$$

$$[\mathbf{5}] = [\mathbf{2}]_0 - (1 + \mathrm{K})\,[\mathbf{2}]_0 \exp\{-(k_1 + k_3)\, t\} + \mathrm{K}\,[\mathbf{2}]_0 \exp(-k_2\, t) \quad (3)$$

$$\mathrm{K} = k_1/\{k_2 - (k_1 + k_3)\}$$

in which $[\mathbf{2}]_0$ = concentration of P–H (apical) phosphorane **2** at $t = 0$ normalized to 100, [**2**] = concentration of P–H (apical) phosphorane **2** at arbitrary intervals, [**9**] = concentration of [*TBPY*-5-12] spirophosphorane **5** at arbitrary intervals, [**5**] = concentration of [*TBPY*-5-11] spirophosphorane **5** at arbitrary intervals, k_1, k_2, k_3 = rate constants to be determined. In order to attain maximum accuracy, equation (1), which corresponds to a first-order reaction was solved separately and $k_1 + k_3$ derived from this equation was used in the subsequent equations. Representative rates and activation parameters of the cyclization and pseudorotation of **2** are shown in Table 4-3.

Figure 4-1. Curve fitting (T = 323 K)

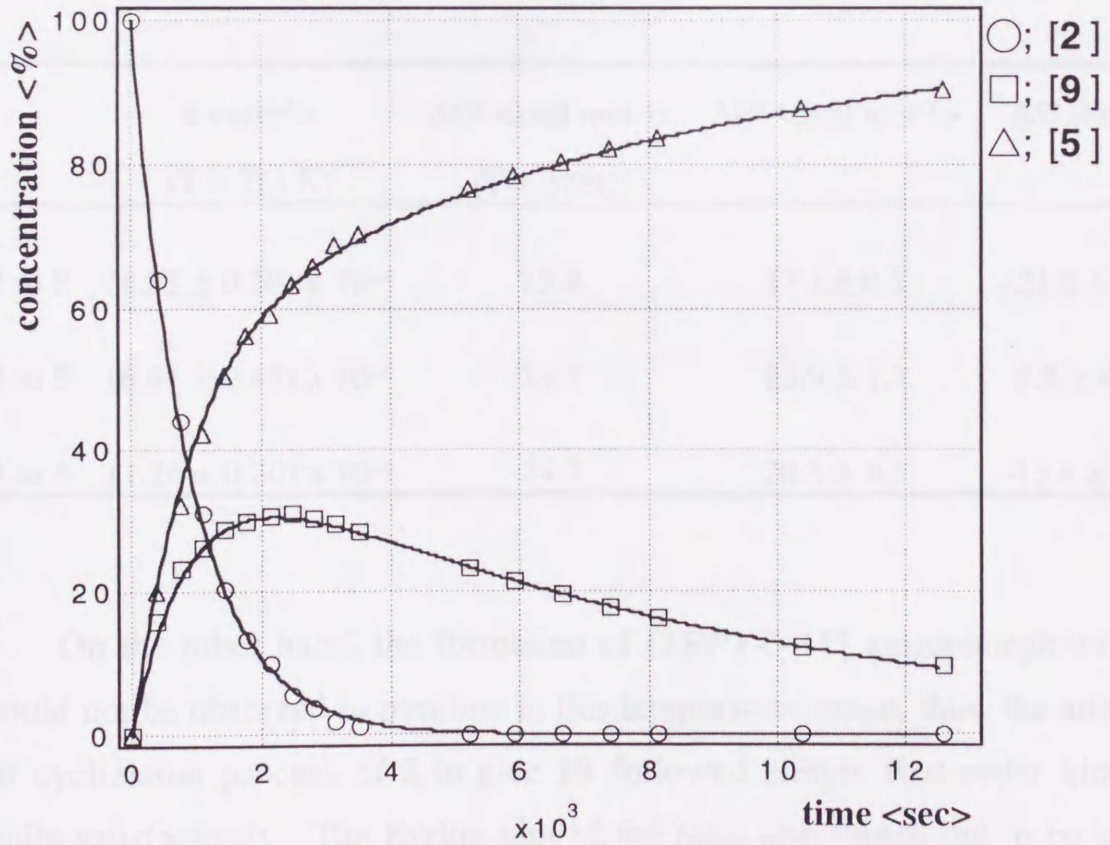

Scheme 4-4

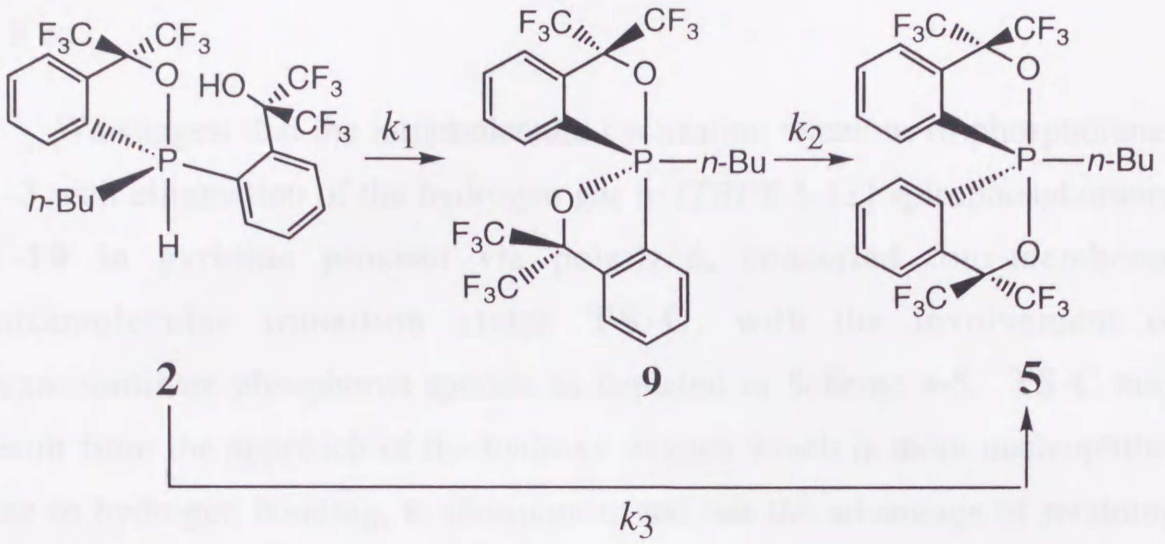

Table 4-3. Kinetic Parameters of the Cyclization and Pseudorotation of **2** in pyridine.

	k <sec^{-1}> (T = 323 K)	$\Delta G^{\ddagger}$ <kcal mol^{-1}> (T = 323K)	$\Delta H^{\ddagger}$ <kcal mol^{-1}>	$\Delta S^{\ddagger}$ <eu>
2 to **9**	$(4.52 \pm 0.20) \times 10^{-4}$	23.9	17.1 ± 0.3	-21.0 ± 1.1
2 to **5**	$(6.64 \pm 0.43) \times 10^{-4}$	23.7	23.9 ± 1.3	0.8 ± 4.2
9 to **5**	$(1.26 \pm 0.20) \times 10^{-4}$	24.7	20.3 ± 0.5	-13.8 ± 1.7

On the other hand, the formation of [*TBPY*-5-11] spirophosphorane **6** could not be observed in pyridine in this temperarure range, thus, the analysis of cyclization process of **3** to give **10** followed simple first-order kinetics quite satisfactorily. The Eyring plot of the rates also turned out to be linear thus implying the existence of only a single process for the cyclization and

gave the activation parameters $\Delta H^{\ddagger} = 22.3 \pm 0.6$kcal mol^{-1} and $\Delta S^{\ddagger} = -12.7 \pm 1.8$ eu..

We suggest that the intramolecular cyclization reactions of phosphoranes **1–3** with elimination of the hydrogen gas to [*TBPY*-5-12] spirophosphoranes **8–10** in pyridine proceed via polarized, concerted four-membered intramolecular transition states **TS-C**, with the involvement of hexacoordinate phosphorus species as depicted in Scheme 4-5. **TS-C** may result from the approach of the hydroxy oxygen which is more nucleophilic, due to hydrogen bonding, to phosphorus and has the advantage of retaining the structure of the ground state, thus allowing the formation of [*TBPY*-5-12] spirophosphoranes **8–10** in pyridine (donor solvent). The fact that the activation enthalpy was larger in pyridine than in toluene for the formation of **5** implies that solvation of **2** is stronger in pyridine leading to larger stabilization of the ground state. That the activation entropy of the cyclization of **2** to **5** was ca. 0 eu may be because the intermolecular hydrogen bonding with a solvent molecule in the ground state is lost in the transition state. The large negative value of entropy in the case of the cyclization of **2** to **9** could be an indication of a tighter transition state for product formation due to the higher lying σ^*_{P-C} compared with σ^*_{P-O}.

Scheme 4-5

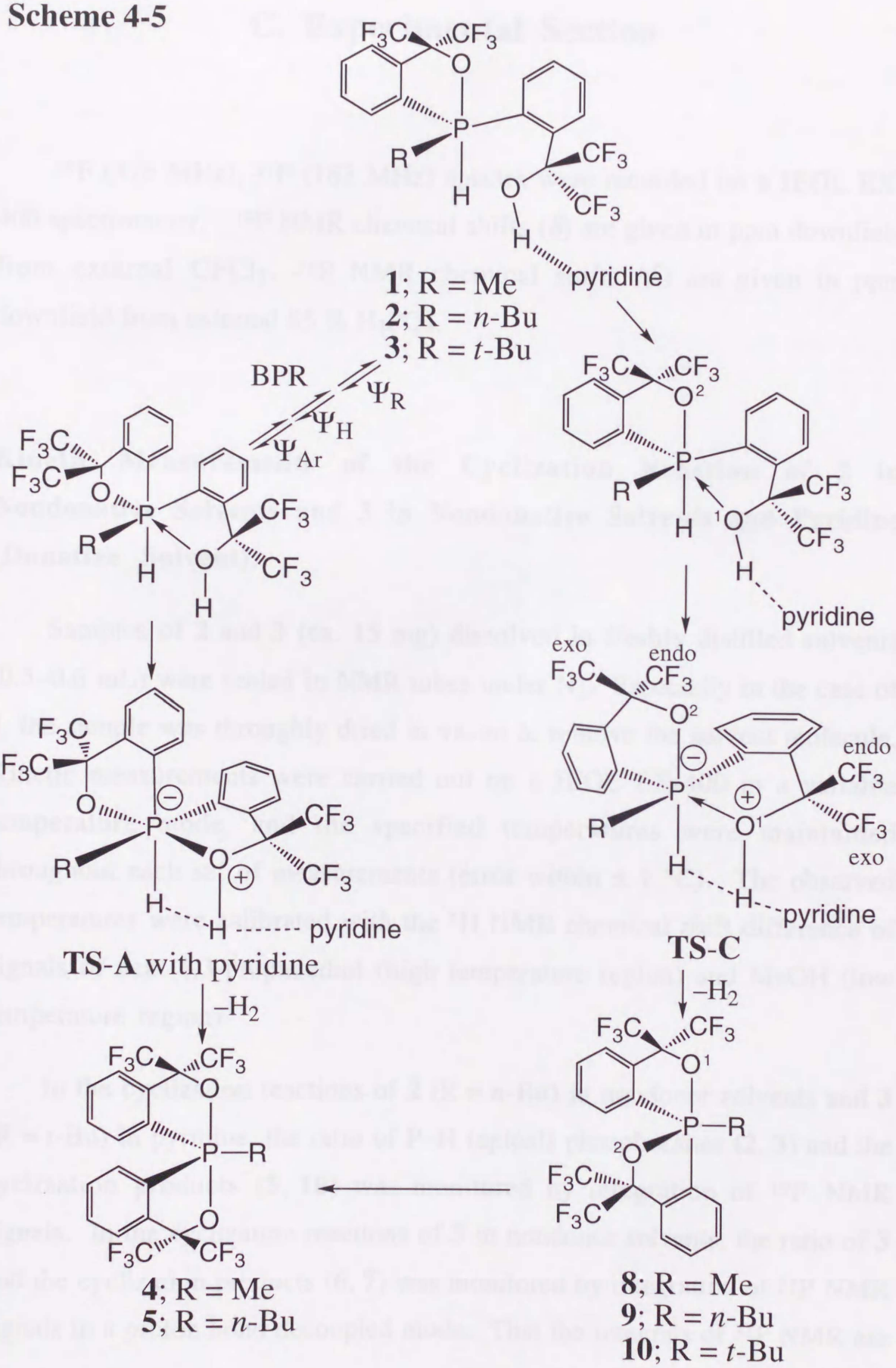
1; R = Me
2; R = n-Bu
3; R = t-Bu
pyridine
BPR
ΨR
ΨH
ΨAr
TS-A with pyridine
TS-C
–H2
4; R = Me
5; R = n-Bu
8; R = Me
9; R = n-Bu
10; R = t-Bu

C. Experimental Section

^{19}F (376 MHz), ^{31}P (162 MHz) spectra were recorded on a JEOL EX-400 spectrometer. ^{19}F NMR chemical shifts (δ) are given in ppm downfield from external $CFCl_3$. ^{31}P NMR chemical shifts (δ) are given in ppm downfield from external 85 % H_3PO_4.

Kinetic Measurements of the Cyclization Reaction of 2 in Nondonative Solvents and 3 in Nondonative Solvents and Pyridine (Donative Solvent).

Samples of **2** and **3** (ca. 15 mg) dissolved in freshly distilled solvents (0.5–0.6 mL) were sealed in NMR tubes under N_2. Especially in the case of 3, the sample was throughly dried in vacuo to remove the solvent molecule. Kinetic measurements were carried out on a JEOL EX-400 in a variable temperature mode, and the specified temperatures were maintained throughout each set of measurements (error within ± 1 °C). The observed temperatures were calibrated with the ^1H NMR chemical shift difference of signals of neat 1,3-propanediol (high temperature region) and MeOH (low temperature region).

In the cyclization reactions of **2** (R = *n*-Bu) in nondonor solvents and **3** (R = *t*-Bu) in pyridine, the ratio of P–H (apical) phosphoranes (**2**, **3**) and the cyclization products (**5**, **10**) was monitored by integration of ^{19}F NMR signals. In the cyclization reactions of **3** in nondonor solvents, the ratio of **3** and the cyclization products (**6**, **7**) was monitored by integration of ^{31}P NMR signals in a proton bond decoupled mode. That the integrals of ^{31}P NMR are

proportional to the compound was comfirmed by ^{19}F NMR. The data were analysed by assuming irreversible first-order kinetics using the equation ln $(c_0/c) = k\,T$, in which c_0 = concentration of P–H (apical) phosphoranes at t = 0, c = concentration of P–H (apical) phosphoranes at arbitrary intervals. Their graph are showed in Fig. 4-2.

The activation enthalpies and entropies were calculated according to the transition state theory of Eyring[10] by linear regression of the rate data using the following equation.[11]

$$\ln (k/T) = \Delta H^{\ddagger}/RT + \Delta S^{\ddagger} + \ln (k_B/h)$$

Plot of the measurements are showed in Fig. 4-3. Kinetic psrameters are listed in Table 4-4.

Figure 4-2. Plot of ln (c_0/c) vs time (c_0 = concentration of P–H (apical) phosphoranes at $t = 0$, c = concentration of P–H (apical) phosphoranes at arbitrary intervals)

2 in toluene-d_8; Product is **5**.

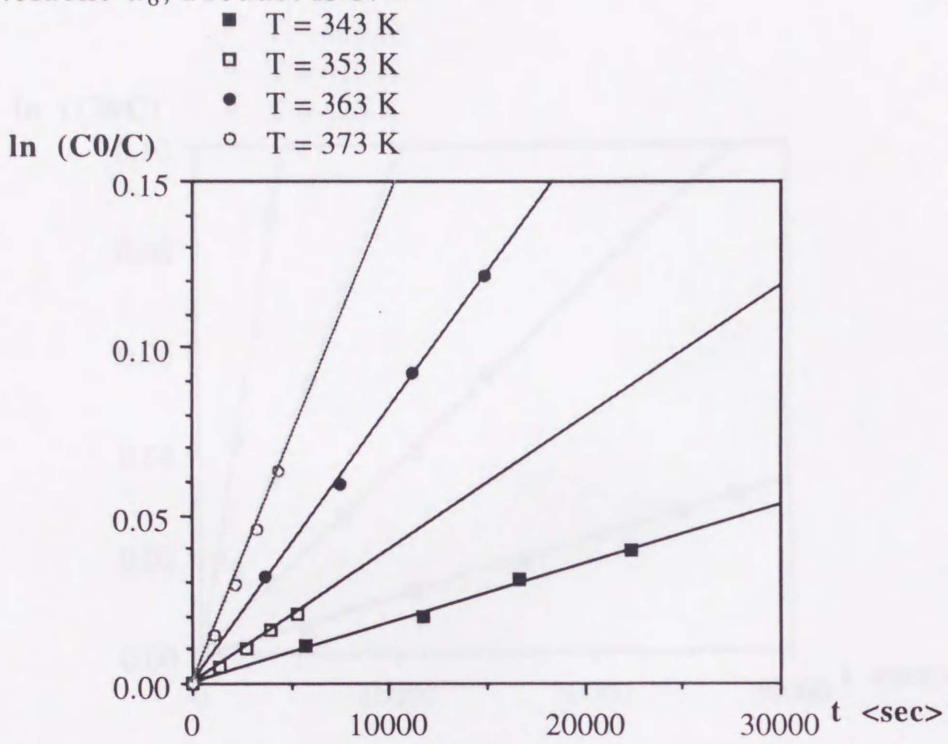

2 in *o*-dichlorobenzene; Product is **5**.

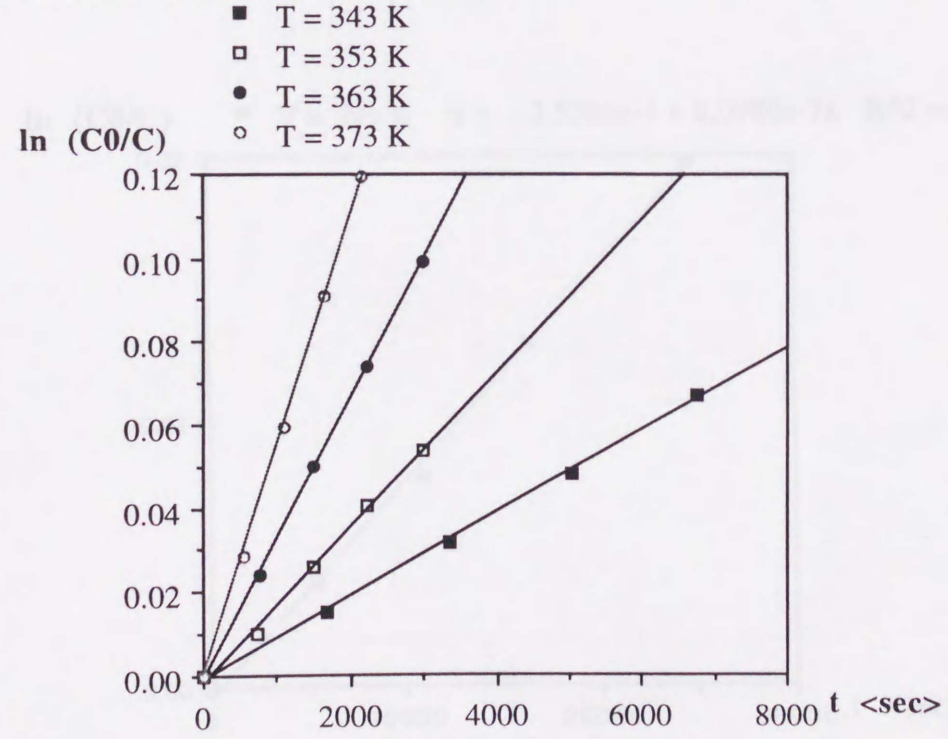

Figure 4-2. Continued (1)

3 in *p*-xylene; Product is **6**.

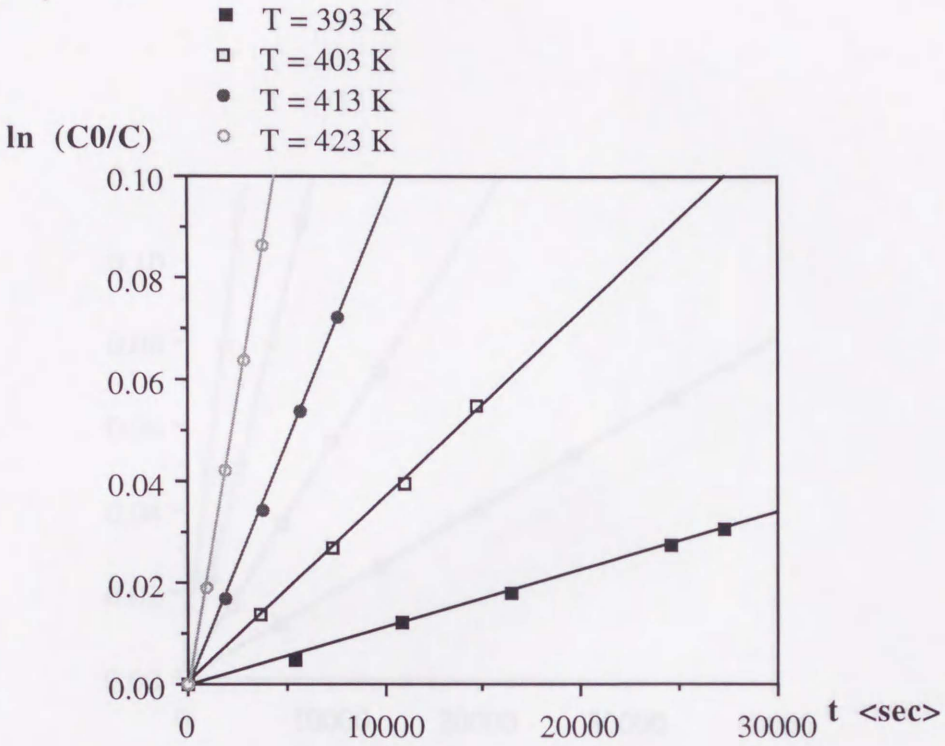

3 in *p*-xylene; Product is **7**.

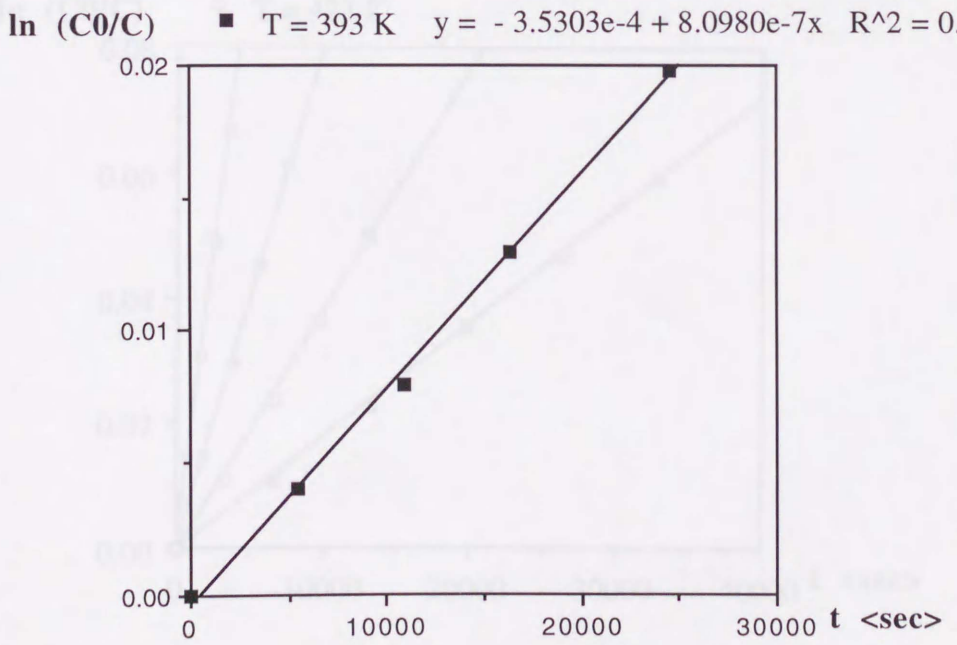

Figure 4-2. Continued (2)

3 in *o*-dichlorobenzene; Product is **6**.

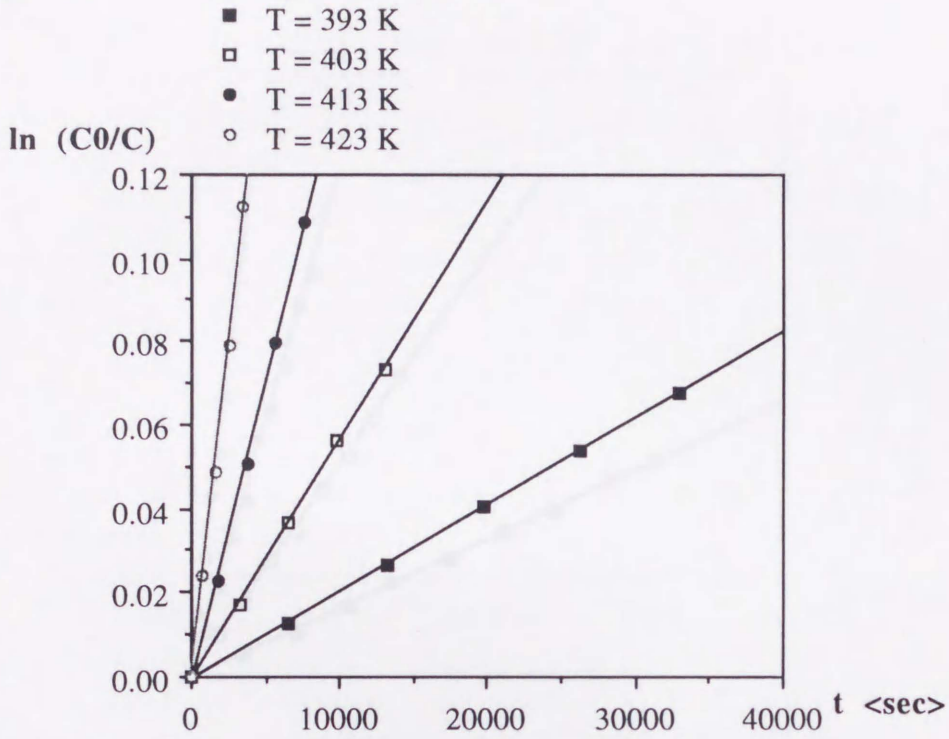

3 in *o*-dichlorobenzene; Product is **7**.

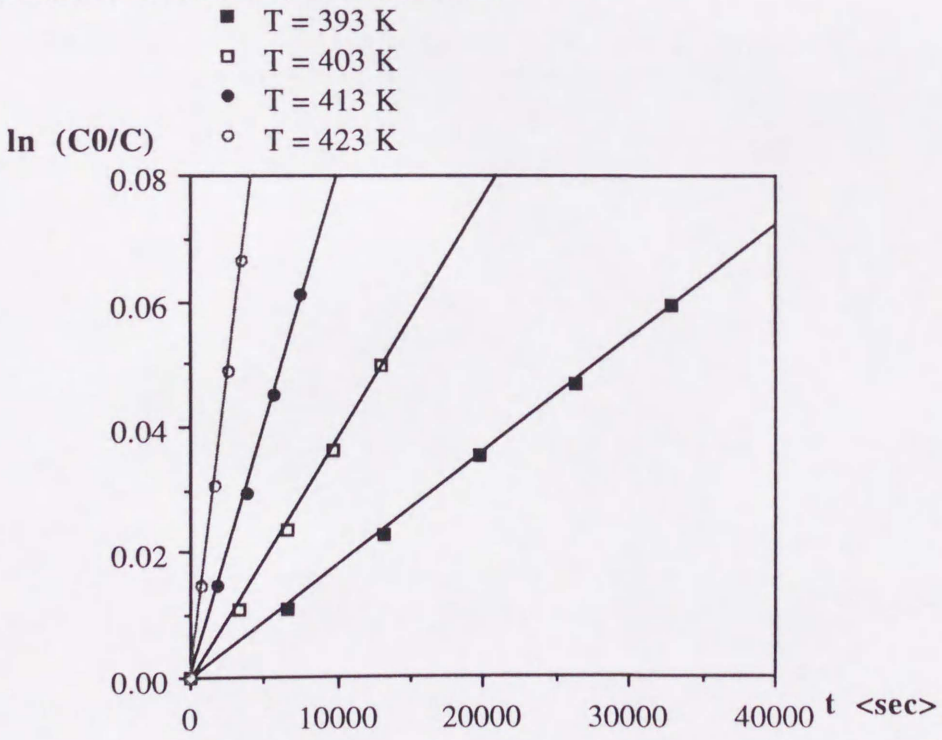

Figure 4-2. Continued (3)

3 in pyridine; Product is **10**.

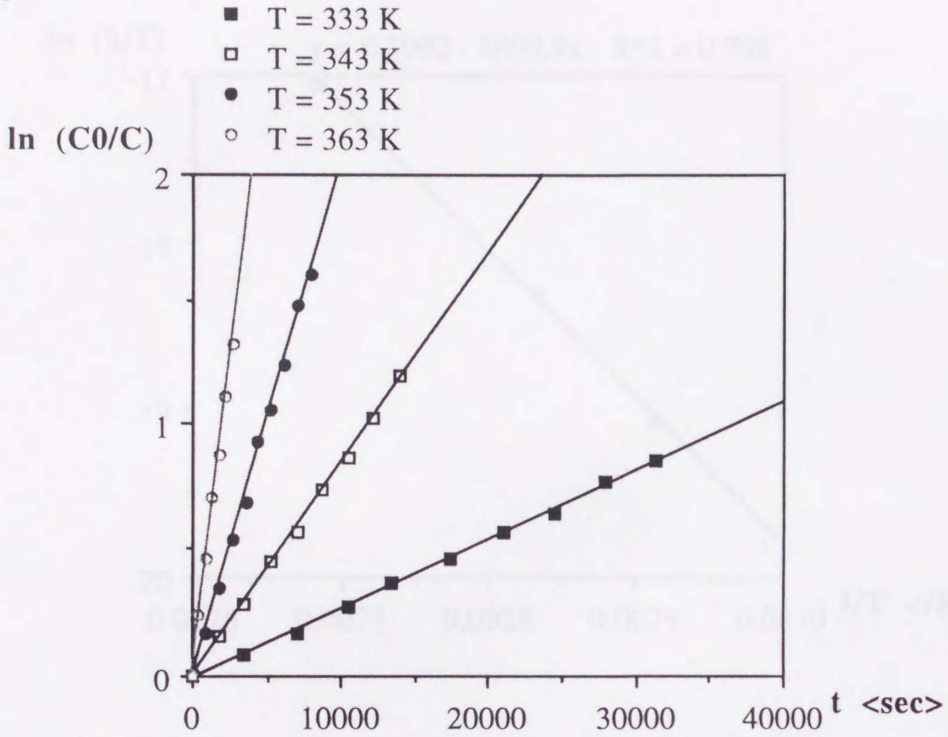

Figure 4-3. Eyring plot of the cyclization reaction of P–H (apical) phosphorane.

2 in toluene-d_8; Product is **5**.

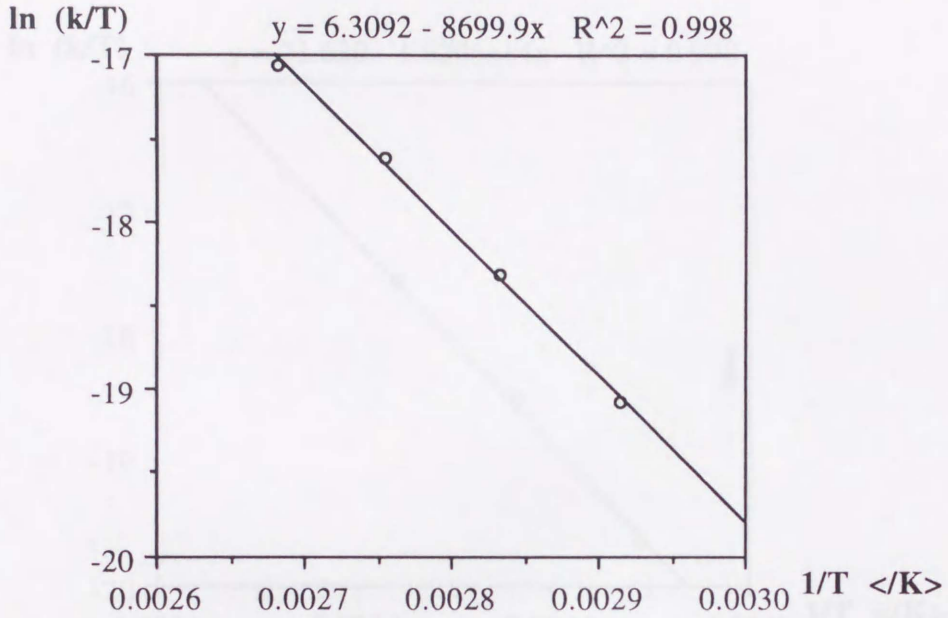

2 in *o*-dichlorobenzene; Product is **5**.

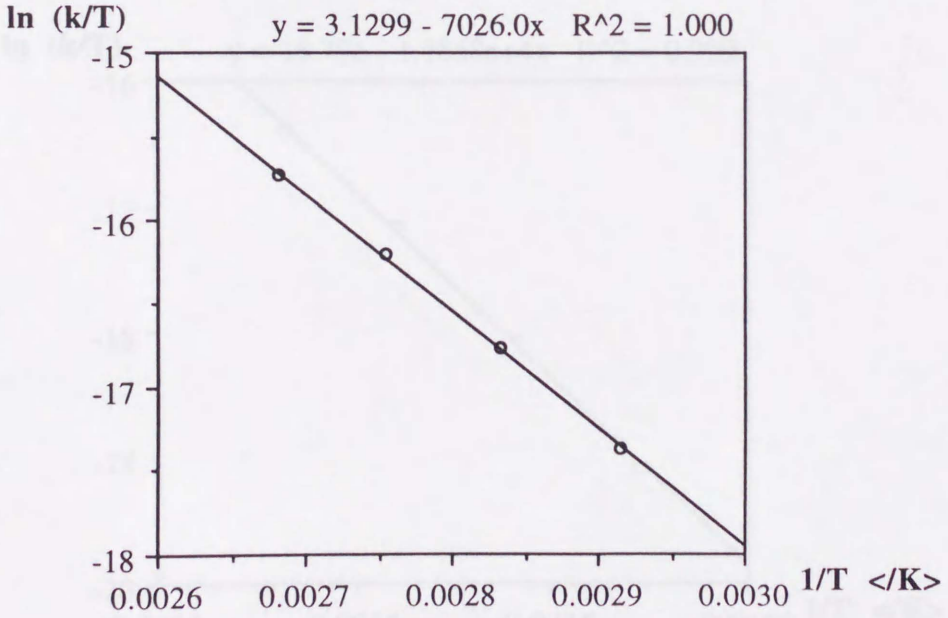

Figure 4-3. Continued (1)

3 in *p*-xylene; Product is **6**.

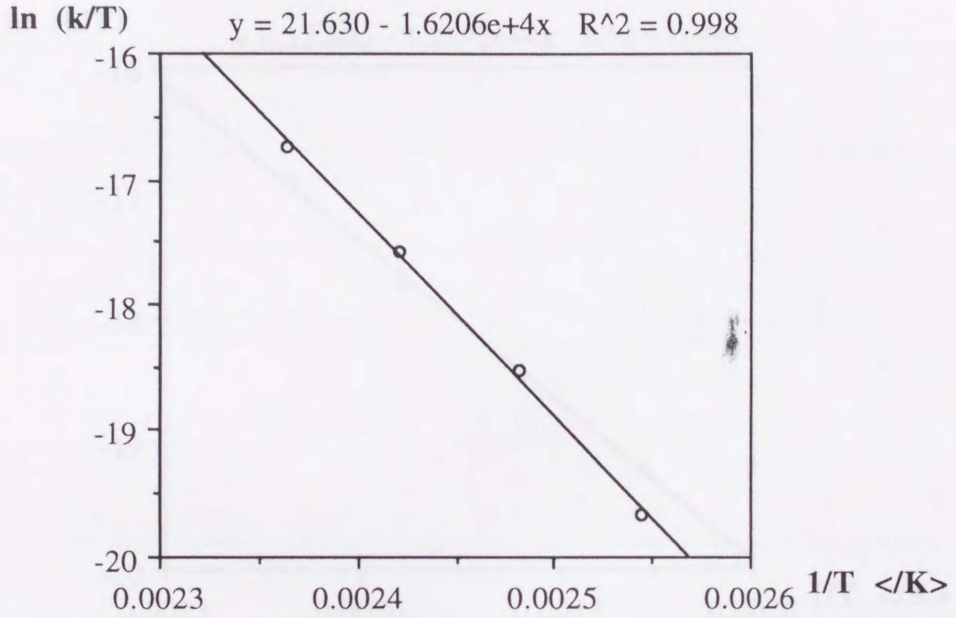

3 in *o*-dichlorobenzene; Product is **6**.

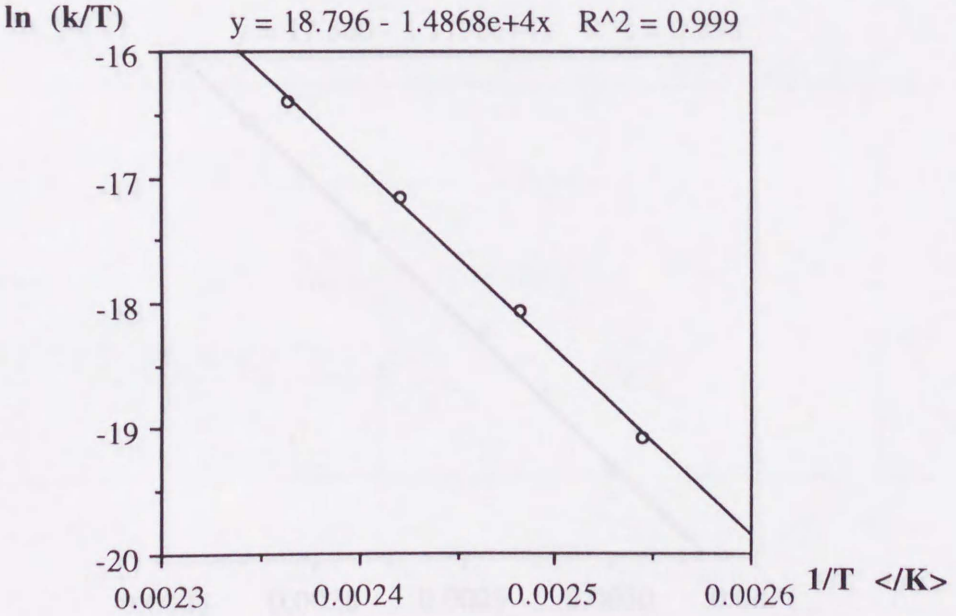

Figure 4-3. Continued (2)

3 in *o*-dichlorobenzene; Product is **7**.

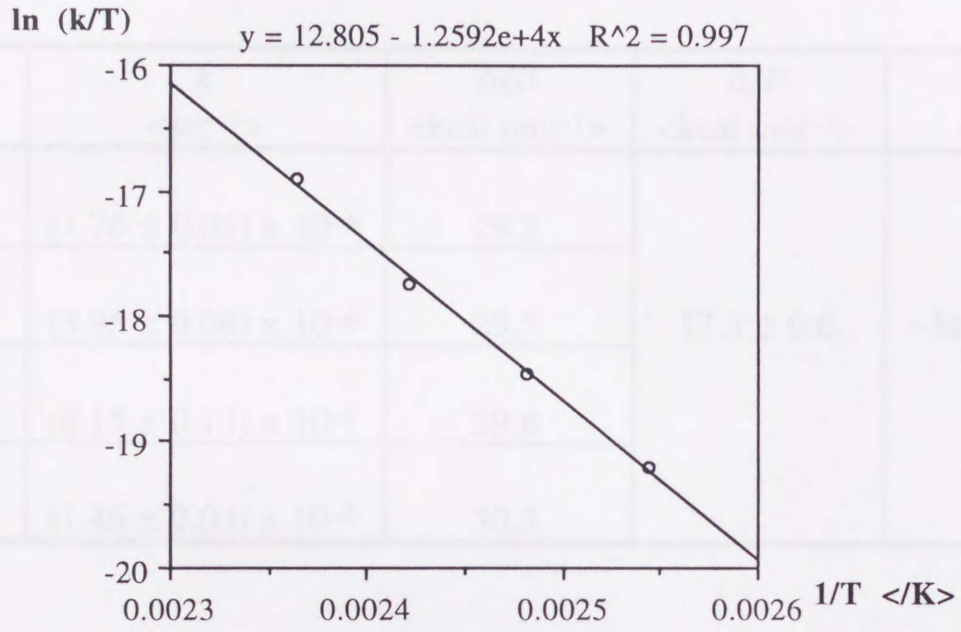

3 in pyridine; Product is **10**.

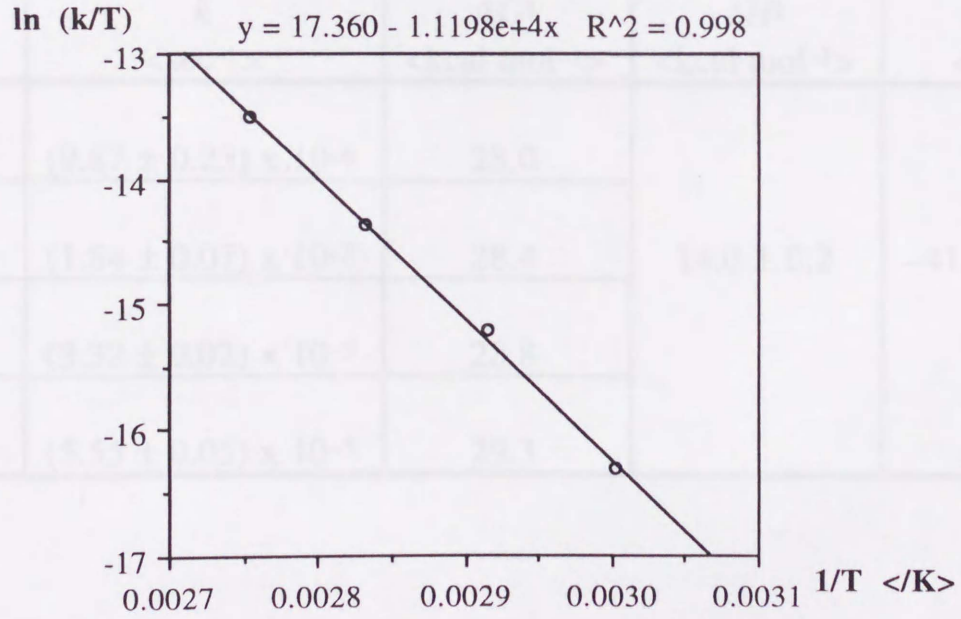

Table 4-4. Kinetic Parameters

2 in toluene-d_8; Product is **5**.

T <K>	k <sec^{-1}>	$\Delta G^{\ddagger}$ <kcal mol^{-1}>	$\Delta H^{\ddagger}$ <kcal mol^{-1}>	$\Delta S^{\ddagger}$ <eu>
343	(1.76 ± 0.05) x 10^{-6}	29.2		
353	(3.95 ± 0.08) x 10^{-6}	29.5	17.3 ± 0.6	–34.7 ± 1.7
363	(8.15 ± 0.12) x 10^{-6}	29.8		
373	(1.46 ± 0.03) x 10^{-5}	30.3		

2 in *o*-dichlorobenzene; Product is **5**.

T <K>	k <sec^{-1}>	$\Delta G^{\ddagger}$ <kcal mol^{-1}>	$\Delta H^{\ddagger}$ <kcal mol^{-1}>	$\Delta S^{\ddagger}$ <eu>
343	(9.87 ± 0.23) x 10^{-6}	28.0		
353	(1.84 ± 0.07) x 10^{-5}	28.4	14.0 ± 0.2	–41.0 ± 0.6
363	(3.32 ± 0.02) x 10^{-5}	28.8		
373	(5.55 ± 0.05) x 10^{-5}	29.3		

Table 4-4. Continued (1)

3 in *p*-xylene; Product is **6**.

T <K>	*k* <sec^{-1}>	$\Delta G^{\ddagger}$ <kcal mol^{-1}>	$\Delta H^{\ddagger}$ <kcal mol^{-1}>	$\Delta S^{\ddagger}$ <eu>
393	$(1.14 \pm 0.02) \times 10^{-6}$	33.9		
403	$(3.66 \pm 0.07) \times 10^{-6}$	33.9	32.2 ± 1.1	-4.2 ± 2.6
413	$(9.58 \pm 0.01) \times 10^{-5}$	33.9		
423	$(2.30 \pm 0.04) \times 10^{-5}$	34.0		

3 in *o*-dichlorobenzene; Product is **6**.

T <K>	*k* <sec^{-1}>	$\Delta G^{\ddagger}$ <kcal mol^{-1}>	$\Delta H^{\ddagger}$ <kcal mol^{-1}>	$\Delta S^{\ddagger}$ <eu>
393	$(2.06 \pm 0.01) \times 10^{-6}$	33.4		
403	$(5.73 \pm 0.10) \times 10^{-6}$	33.5	29.5 ± 0.7	-9.9 ± 1.8
413	$(1.45 \pm 0.04) \times 10^{-5}$	33.6		
423	$(3.22 \pm 0.07) \times 10^{-5}$	33.7		

Table 4-4. Continued (2)

3 in *o*-dichlorobenzene; Product is **7**.

T <K>	k <sec^{-1}>	$\Delta G^{\ddagger}$ <kcal mol^{-1}>	$\Delta H^{\ddagger}$ <kcal mol^{-1}>	$\Delta S^{\ddagger}$ <eu>
393	$(1.81 \pm 0.02) \times 10^{-6}$	33.5		
403	$(3.84 \pm 0.08) \times 10^{-6}$	33.8	25.0 ± 1.0	-21.8 ± 2.6
413	$(8.06 \pm 0.09) \times 10^{-6}$	34.1		
423	$(1.92 \pm 0.03) \times 10^{-5}$	34.2		

3 in pyridine; Product is **10**.

T <K>	k <sec^{-1}>	$\Delta G^{\ddagger}$ <kcal mol^{-1}>	$\Delta H^{\ddagger}$ <kcal mol^{-1}>	$\Delta S^{\ddagger}$ <eu>
333	$(2.75 \pm 0.03) \times 10^{-5}$	26.5		
343	$(8.43 \pm 0.11) \times 10^{-5}$	26.6	22.3 ± 0.6	-12.7 ± 1.8
353	$(2.04 \pm 0.03) \times 10^{-4}$	26.7		
363	$(4.93 \pm 0.08) \times 10^{-4}$	26.9		

Kinetic Measurements of the Cyclization Reaction of 2 in Pyridine (Donative Solvent)

Samples of **2** (ca. 15 mg) dissolved in freshly distilled solvents (0.5–0.6 mL) were sealed in NMR tubes under N_2. ^{19}F NMR spectra were measured on a JEOL EX-400 in a variable temperature mode, and the specified temperatures were maintained throughout each set of measurements (error within ± 1 °C). The observed temperatures were calibrated with the ^{1}H NMR chemical shift difference of signals of neat 1,3-propanediol (high temperature region) and MeOH (low temperature region).

The ratio of **2** and the cyclization products (**5**, **8**) was monitored by integration of ^{19}F NMR signals. The reaction was assumed to involve a combination of competitive and consequtive reactions and follow irreversible first-order kinetics. The analysis was carried out curve fitting of the data to the following set of equations.

$$[\mathbf{2}] = [\mathbf{2}]_0 \exp\{-(k_1 + k_2)\, t\} \quad (1)$$

$$[\mathbf{5}] = \mathrm{K}\,[\mathbf{2}]_0 \exp\{-(k_1 + k_2)\, t\} - \mathrm{K}\,[\mathbf{2}]_0 \exp(-k_2\, t) \quad (2)$$

$$[\mathbf{8}] = [\mathbf{2}]_0 - (1 + \mathrm{K})\,[\mathbf{2}]_0 \exp\{-(k_1 + k_2)\, t\} + \mathrm{K}\,[\mathbf{2}]_0 \exp(-k_2\, t) \quad (3)$$

$$\mathrm{K} = k_1/\{k_2 - (k_1 + k_3)\}$$

in which $[\mathbf{2}]_0$ = concentration of P–H (apical) phosphorane **2** at $t = 0$ normalized to 100, [**2**] = concentration of P–H (apical) phosphorane **2** at arbitrary intervals, [**5**] = concentration of [*TBPY*-5-12] (*O*-cis) spirophosphorane **5** at arbitrary intervals, [**8**] = concentration of [*TBPY*-5-11] (*O*-trans) spirophosphorane **8** at arbitrary intervals, k_1, k_2, k_3 = rate

constants to be determined. In order to attain maximum accurary, equation (1), which corresponds to a first-order (Fig. 4-4).

The activation enthalpies and entropies were calculated according to the transition state theory of Eyring using the following equation. Plot of the measurements are showed in Fig. 4-5.

$$\ln (k/T) = \Delta H^{\ddagger}/RT + \Delta S^{\ddagger} + \ln (k_B/h)$$

The kinetic parameters are listed in Table 4-5.

Figure 4-4. Curve fit

T = 308 K

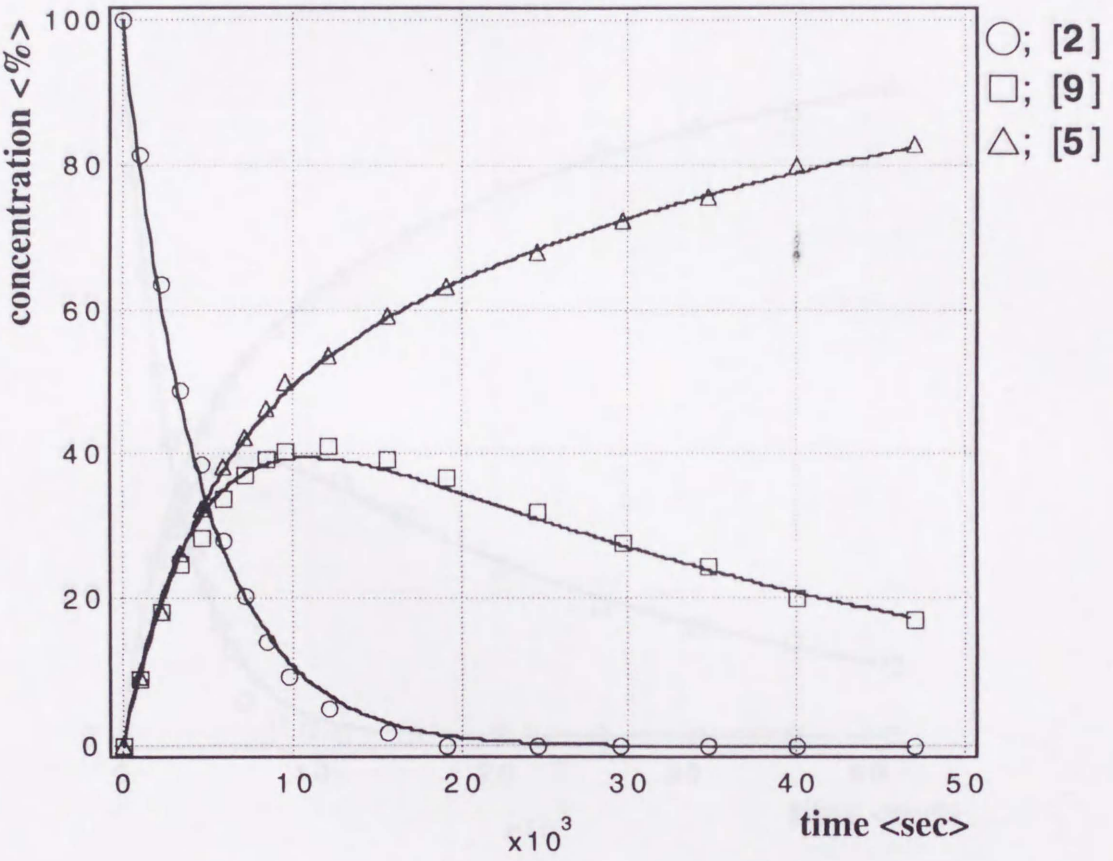

[**2**] = 100 exp (–2.2010 x 10^{-4} t)

[**9**] = –60.091 exp (–2.2010 x 10^{-4} t) + 60.091 exp (–2.6314 x 10^{-5} t)

[**5**] = 100 – 39.909 exp (–2.2010 x 10^{-4} t) –60.091 exp (–2.6314 x 10^{-5} t)

$k_1 + k_3 = (2.2010 \pm 0.07) \times 10^{-4}$

K $[\mathbf{2}]_0 = k_1 [\mathbf{2}]_0/\{k_2 - (k_1 + k_3)\} = -60.091 \pm 1.14$

$k_2 = (2.6314 \pm 0.08) \times 10^{-5}$

Figure 4-4. Continued (1)

T = 313 K

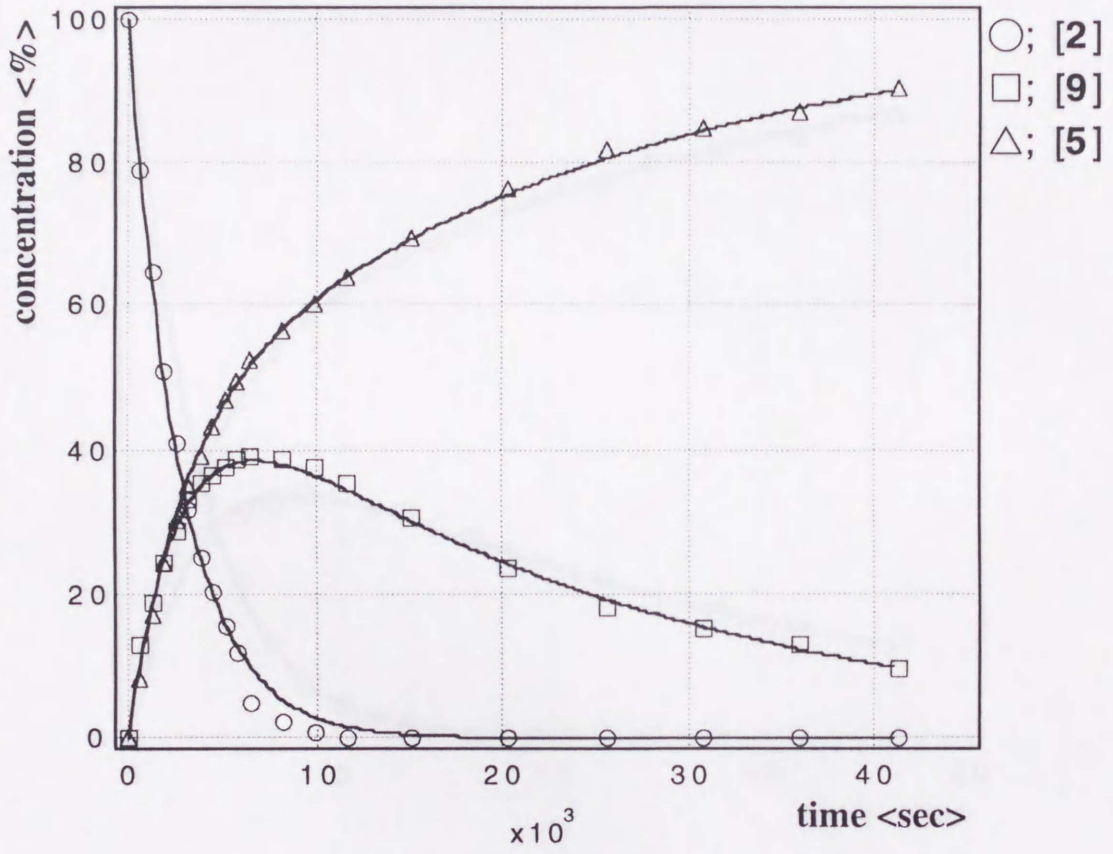

[**2**] = 100 exp (–3.5748 x 10^{-4} t)

[**9**] = –58.898 exp (–3.5748 x 10^{-4} t) + 58.898 exp (–4.3611 x 10^{-5} t)

[**5**] = 100 – 41.102 exp (–3.5748 x 10^{-4} t) –58.898 exp (–4.3611 x 10^{-5} t)

$k_1 + k_3 = (3.5748 \pm 0.04) \times 10^{-4}$

K $[\mathbf{2}]_0 = k_1 [\mathbf{2}]_0/\{k_2 - (k_1 + k_3)\} = -58.898 \pm 0.76$

$k_2 = (4.3611 \pm 0.11) \times 10^{-5}$

Figure 4-4. Continued (2)

T = 318 K

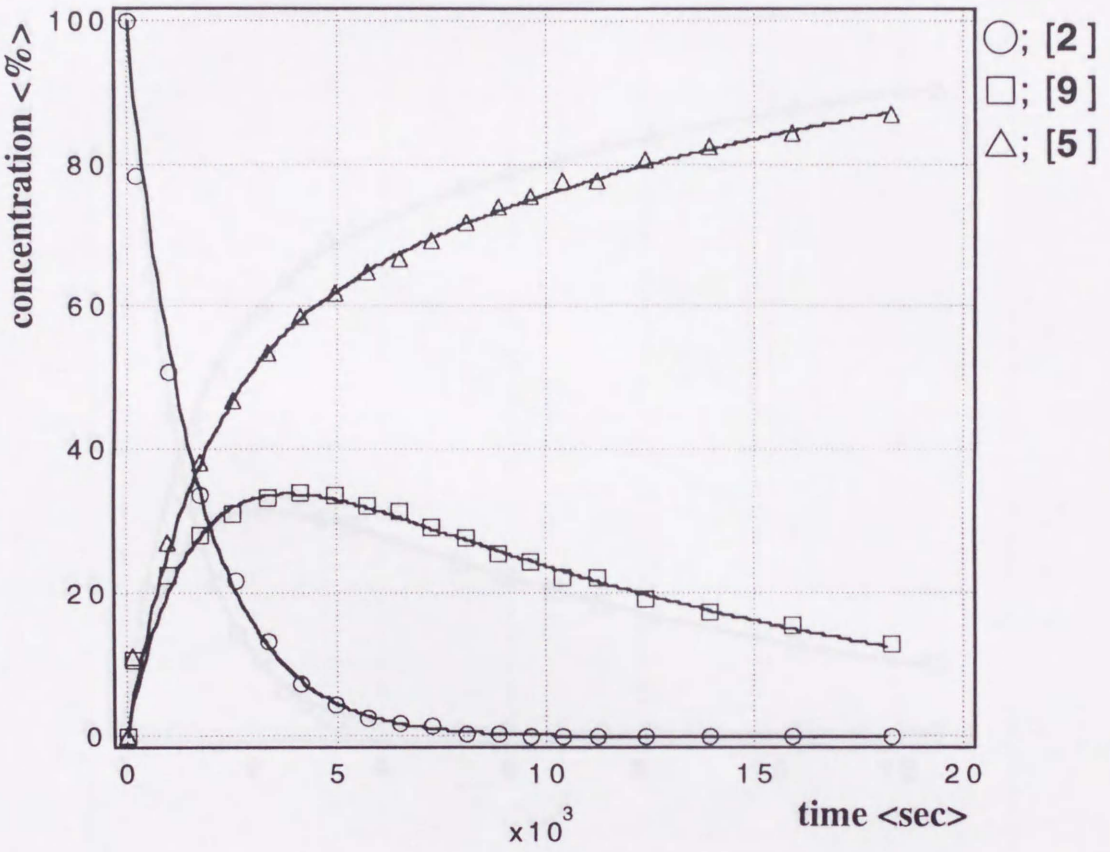

[**2**] = 100 exp (–6.1475 x 10^{-4} t)

[**9**] = –52.485 exp (–6.1475 x 10^{-4} t) + 52.485 exp (–7.8271 x 10^{-5} t)

[**5**] = 100 – 47.515 exp (–6.1475 x 10^{-4} t) –52.485 exp (–7.8271 x 10^{-5} t)

$k_1 + k_3 = (6.1475 \pm 0.15) \times 10^{-4}$

K $[\mathbf{2}]_0 = k_1 [\mathbf{2}]_0/\{k_2 - (k_1 + k_3)\} = -52.485 \pm 3.05$

$k_2 = (7.8271 \pm 0.38) \times 10^{-5}$

Figure 4-4. Continued (3)

T = 323 K

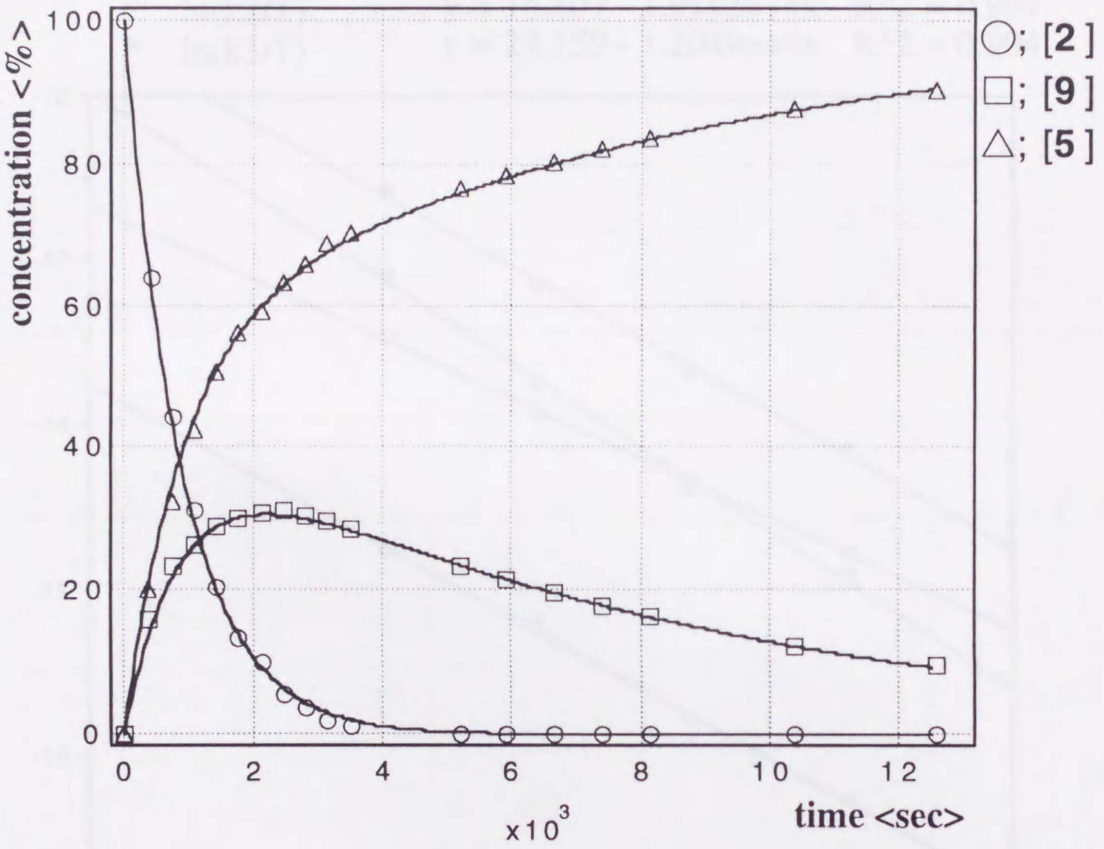

[**2**] = 100 exp (–1.1153 x 10^{-3} t)

[**9**] = –45.646 exp (–1.1153 x 10^{-3} t) + 45.646 exp (–1.2589 x 10^{-4} t)

[**5**] = 100 – 54.354 exp (–1.1153 x 10^{-3} t) –45.646 exp (–1.2589 x 10^{-4} t)

$k_1 + k_3 = (1.1153 \pm 0.02) \times 10^{-3}$

K $[\mathbf{2}]_0 = k_1 [\mathbf{2}]_0/\{k_2 - (k_1 + k_3)\} = -45.646 \pm 0.80$

$k_2 = (1.2589 \pm 0.04) \times 10^{-4}$

Figure 4-5. Eyring plot

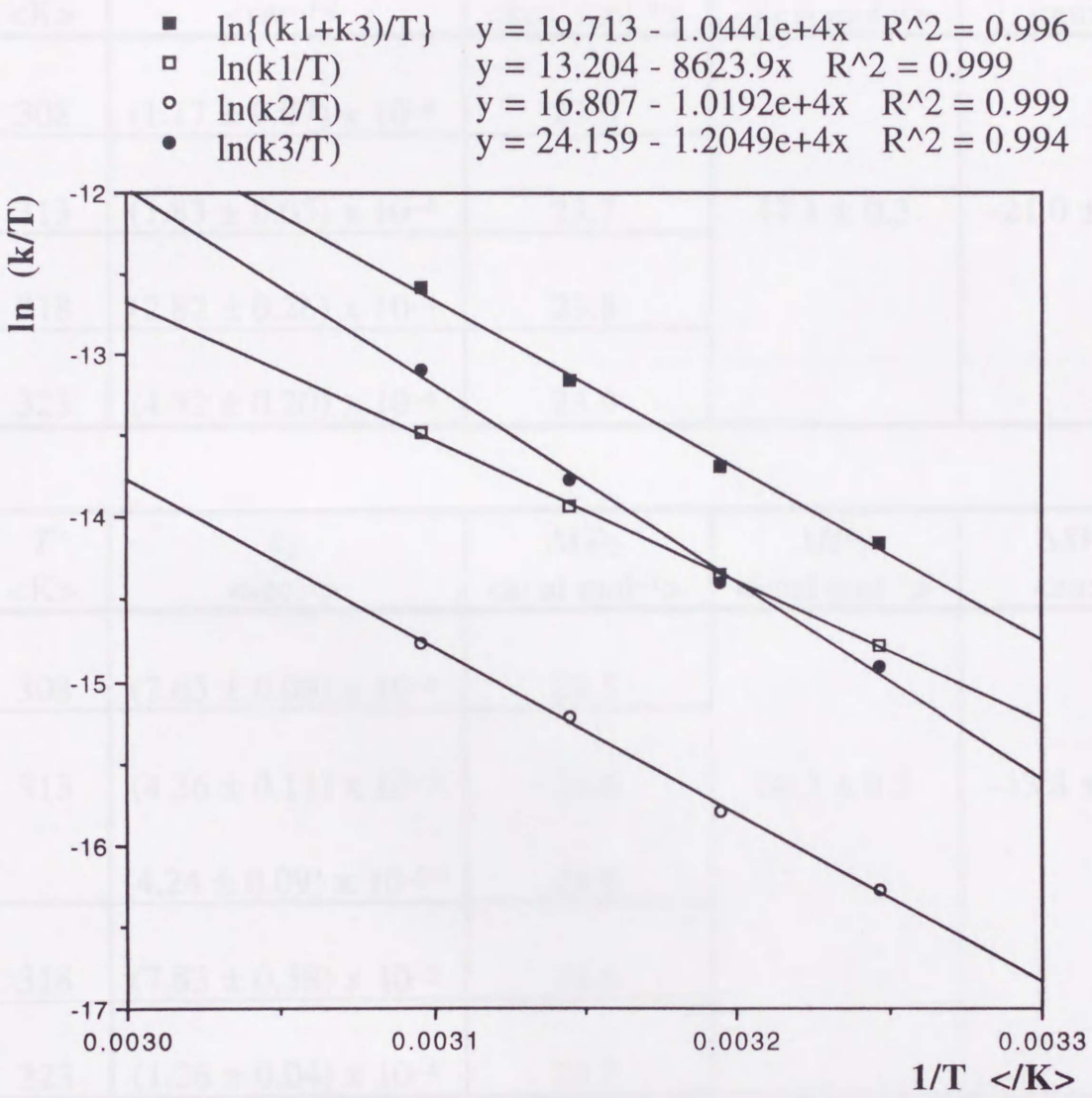

Table 4-5. Kinetic Parameters of the Cyclization Reaction of **2** in Pyridine

T <K>	k_1 <sec^{-1}>	$\Delta G^{\ddagger}_1$ <kcal mol^{-1}>	$\Delta H^{\ddagger}_1$ <kcal mol^{-1}>	$\Delta S^{\ddagger}_1$ <eu>
308	$(1.17 \pm 0.07) \times 10^{-4}$	23.6		
313	$(1.83 \pm 0.05) \times 10^{-4}$	23.7	17.1 ± 0.3	-21.0 ± 1.1
318	$(2.82 \pm 0.26) \times 10^{-4}$	23.8		
323	$(4.52 \pm 0.20) \times 10^{-4}$	23.9		

T <K>	k_2 <sec^{-1}>	$\Delta G^{\ddagger}_2$ <kcal mol^{-1}>	$\Delta H^{\ddagger}_2$ <kcal mol^{-1}>	$\Delta S^{\ddagger}_2$ <eu>
308	$(2.63 \pm 0.08) \times 10^{-5}$	24.5		
313	$(4.36 \pm 0.11) \times 10^{-5}$	24.6	20.3 ± 0.5	-13.8 ± 1.7
	$(4.24 \pm 0.09) \times 10^{-5}$*	24.6		
318	$(7.83 \pm 0.38) \times 10^{-5}$	24.6		
323	$(1.26 \pm 0.04) \times 10^{-4}$	24.7		

* The rate was measured from **9** by monitoring ^{19}F NMR.

T <K>	k_3 <sec^{-1}>	$\Delta G^{\ddagger}_3$ <kcal mol^{-1}>	$\Delta H^{\ddagger}_3$ <kcal mol^{-1}>	$\Delta S^{\ddagger}_3$ <eu>
308	$(1.04 \pm 0.14) \times 10^{-4}$	23.7		
313	$(1.74 \pm 0.09) \times 10^{-4}$	23.7	23.9 ± 1.3	$+0.79 \pm 4.2$
318	$(3.33 \pm 0.41) \times 10^{-4}$	23.7		
323	$(6.64 \pm 0.43) \times 10^{-4}$	23.7		

D. References

(1) For example: Abraham, M. H.; Grellier, P. L. *In the Chemistry of the Metal-Carbon Bond*; Hartley, F.; Patai, S., Eds. John Wiley and Sons: New York, 1985; Vol. 2, Chapter 2.

(1) For designation: Perkins, C. W.; Martin, J. C.; Arduengo, A. J.; Lau, W.; Alegria, A.; Kochi, J. K. *J. Am. Chem. Soc.* **1980**, *102*, 7753.

(3) Yamamoto, Y.; Takeda, Y.; Akiba, K.-y. *Tetrahedron Lett.* **1989**, *30*, 725.

(4) (a) Depuy, C.H.; Bierbaum, L.W.; Damrauer, R. *J. Am. Chem. Soc.* **1984**, *106*, 4051. (b) Depuy, C.H.; Damrauer, R.; Bowie, J. H.; Sheldon, J. C. *Acc. Chem. Res.* **1987**, *20*, 127. (c) Davis, L.P.; Burggraf, L.W.; Gordon, M.S. *J. Am. Chem. Soc.* **1988**, *110*, 3056. (d) Taylor, W. S.; Babcock, L. M. *J. Am. Chem. Soc.* **1995**, *117*, 6497.

(5) Yamamoto, Y.; Ohdoi, K.; Chen, X.; Kitano, M.; Akiba, K.-y. *Organometallics* **1993**, *12*, 3297.

(6) Yamamoto, Y.; Fujikawa, H.; Fujishima, H.; Akiba, K.-y. *J. Am. Chem. Soc.* **1989**, *111*, 2276.

(7) Lopez, L.; Boisdon, M. T.; Barrans, J. *Acad. Sci., Ser. C*, **1972**, *275*, 295.

(8) Malavaud, C.; Barrans, J. *Tetrahedron Lett.* **1975**, *35*, 3077.

(9) (a) Rothwell, L. I. *Acc. Chem. Res.* **1988**, *21*, 153. (b) Li, L.; Hung, M.; Xue, Z. *J. Am. Chem. Soc.* **1995**, *117*, 12746.

(10) Wynne-Jones, W. F. K.; Eyring, H. *J. Chem. Phys.* **1935**, *3*, 492.

(11) Jackman, L. M.; Cotton, F. A. "*Dynamic Nuclear Magnetic Resonance Spectroscopy*", Academic Press, New York 1975.

Acknowledgment

The author expresses his sincere gratitude to Professor Kin-ya Akiba of Hiroshima University for his relevant guidance, advice, encouragement, and full support of this work.

The author is especially grateful to Research Associate Satoshi Kojima of Hiroshima University for his relevant guidance, discussion, encouragement, and full support of this work.

The author is grateful to Professor Katsuo Ohkata, Associate Professor Yamamoto Yohsuke, and Research Associate Mao Minoura of Hiroshima University for their advice, discussion and encouragement.

The author appreciates Mr Masaaki Nakamoto for his assistance and discussion, Miss Natsuko Shimizu for the theoretical calculations, and all the members of Professor K.-y. Akiba's Laboratory and fellows for their help.

Last but not least, the author is deeply grateful to his family for their support and encouragement all through his graduate study.

List of Publications

(1) Characterization of an Optically Active Pentacoordinate Phosphorane with Asymmetry Only at Phosphorus.

Kojima, S.; Kajiyama, K.; Akiba, K.-y. *Tetrahedron Lett.* **1994**, *35*, 7037–7040.

(2) Non-dissociative Permutation of a Stable Hydrophosphorane and Retention of Stereochemistry of the Electrophilic Reaction of Its Conjugate Phosphoranide Base.

Kojima, S.; Nakamoto, M.; Kajiyama, K.; Akiba, K.-y. *Tetrahedron Lett.* **1995**, *36*, 2261–2264.

(3) Characterization of Enantiomeric Pairs of Optically Active 10-P-5 Phosphoranes with Asymmetry Only at Phosphorus.

Kojima, S.; Kajiyama, K.; Akiba, K.-y. *Bull. Chem. Soc. Jpn.* **1995**, *68*, 1785–1797.

*(4) Synthesis and Characterization of Intra- and Intermolecular Hydrogen Bonding Isomers of P–H (apical) Phosphoranes Bearing a Hydroxyl Group and Their Thermal Cyclization.

Kajiyama, K.; Kojima, S.; Akiba, K.-y. *Tetrahedron Lett.* **1996**, *37*, 8409–8412.

*(5) First Characterization of a 10-P-5 Spirophosphorane with an Apical Carbon-Equatorial Oxygen Ring. Kinetic Studies on Pseudorotation of Stereoisomers.

Kojima, S.; Kajiyama, K.; Nakamoto, M.; Akiba, K.-y. *J. Am. Chem. Soc.* **1996**, *118*, 12866–12867.

*これらは主論文の基礎となった原著論文である。

No. 1, 2, 3は参考論文である。